Czech Technical University in Prague

Faculty of Nuclear Sciences and Physical Engineering

Generation and application of supercontinuum for high power laser systems

This dissertation is submitted for the degree of

Doctor of Philosophy

Prague 2023

Lukáš Indra

DECLARATION

I hereby declare that except where specific reference is made to the work of others, the contents of this dissertation are original and have not been submitted in whole or in part for consideration for any other degree or qualification in this, or any other university. This dissertation is my own work and contains nothing which is the outcome of work done in collaboration with others, except as specified in the text and Acknowledgements.

Lukáš Indra

March 2023

Bibliographic Entry

Author:	**Ing. Lukáš Indra** Czech Technical University in Prague Faculty of Nuclear Sciences and Physical Engineering Department of Physical Electronics
Title of Dissertation:	Generation and application of supercontinuum for high power laser systems
Degree Programme:	Applications of Natural Sciences
Field of study:	Physical Engineering
Supervisor:	Doc. Ing. Miroslav Čech, CSc. Department of Physical Electronics, FNSPE CTU
Supervisor Specialist:	Ing. Pavel Bakule, DPhil. ELI Beamlines
Academic Year:	2022/2023
Number of Pages:	103
Keywords:	Supercontinuum, Nonlinear optics, Regenerative amplifier, OPCPA, DPSSL, Pump laser, Self-focusing, Filamentation

Bibliografický záznam

Autor: **Ing. Lukáš Indra**
České vysoké učení technické
Fakulta jaderná a fyzikálně inženýrská
Katedra fyzikální elektroniky

Název práce: Generace a aplikace superkontinua pro vysokovýkonové Laserové systémy

Studijní program: Aplikace přírodních věd

Studijní obor: Fyzikální inženýrství

Školitel: Doc. Ing. Miroslav Čech, CSc.
Katedra fyzikální elektroniky, FJFI ČVUT

Školitel specialista: Ing. Pavel Bakule, DPhil.
ELI Beamlines

Akademický rok: 2022/2023

Počet stran: 103

Klíčová slova: Supercontinuum, Nelineární optika, Regenerativní zesilovač, OPCPA, Diodově buzené pevnolátkové lasery, Čerpací laser, Autofokusace, Filamentace

Acknowledgements

This work would not be possible without the support and help of many people.

First of all, I would like to thank to Petr Hříbek, who introduced me to supercontinuum generation. He provided me with an endless amount of new ideas, problems to think about, experiments to perform, but also explanations to a variety of issues I was struggling with. Our discussions many times helped me very much with my understanding of supercontinuum generation.

I would like to thank my supervisor specialist at ELI-Beamlines Pavel Bakule who gave me the opportunity to work here in the first place and was always supportive and available even despite his very busy schedule. I also want to thank my supervisor Miroslav Čech from CTU.

I would like to thank Tyler Green, the leader of the L2 team, who provided a huge amount of help and consultations during creation of this work. Without his proof-reading, the reading of this work would be a significantly worse experience. It has been great to work with Tyler, he is always willing to give advice or help you as much as necessary to finish the task at hand.

Special thanks to Alexandr Špaček who spend the last years with me in the L2 lab, building the front end portion of the laser system. His numerical simulations often provided new insights into the supercontinuum process, which would otherwise have remained hidden.

I would like to thank Jakub Novák. He was an infinite well of knowledge during our endless struggles with the pump laser and also to thank Zbyněk Hubka who constructed the initial version of this time eating machine.

Many to thanks to my colleagues Emily Erdman, Roman Antipenkov, František Batysta, Robert Boge and Václav Šobr, for their willingness to help and the friendly atmosphere they helped to create in the L1 team. I also want to thank to the other members of L1 team, L2 team and control system team who assisted with overall development of the L1 and L2 systems.

I would like to thank my parents Petra and Karel, my brother Michal and my girlfriend Simona for their support during all this time.

The author also acknowledges the following grants:

- European Regional Development Fund
  (ADONIS, CZ.02.1.01/0.0/0.0/16-019/0000789)
- Ministry of Education, Youth and Sports of the Czech Republic
  (ProjectNo. LM2018141)
- Ministry of Education, Youth and Sports of the Czech Republic
  (CZ.1.07/2.3.00/20.0091, LQ1606, RVO68407700)

Abstract

This thesis explores the possibility of generating the broadband supercontinuum with picosecond pulses as a seed for high power OPCPA. Currently, the most common source of broadband light for seeding OPCPA are Ti:sapphire oscillators. However, having two separate laser sources for OPCPA seed and pump often requires sophisticated synchronization mechanisms, increasing the complexity of the system. This is the architecture used in the L1 laser system at ELI-beamlines, where the regenerative amplifier produces picosecond pump pulses and the Ti:sapphire oscillator serves as a seed source. The possibility to generate a sufficiently broadband pulse directly using the optical pulses from the pump laser can potentially simplify an existing laser system, as well as future projects.

The supercontinuum generation is a result of multiple nonlinear effects. This effect is manifested by focusing a sufficiently strong beam into nonlinear medium, which initiates the process of filamentation and subsequently spectral broadening, which can produce new optical frquencies spanning from near ultraviolet to the mid infrared region. This thesis summarizes the nonlinear effects leading to supercontinuum generation, such as:self-focusing, self-phase modulation, material ionization, plasma defocusing, pulse splitting and self-steepening. The supercontinuum discussed in this work was generated in loose focus setup inside a long (13 cm) YAG crystal to prevent optical damage to the material. Multiple experimental schemes and different pump laser parameters were investigated in order to generate a stable broadband supercontinuum. It is shown that, with properly chosen configuration, the pulse-to-pulse stability of generated supercontinuum can be better than that of the pump pulse.

The generated supercontinuum was amplified in two stages of OPCPA and compressed close to the Fourier limit in a prism compressor, demonstrating its possible application as a seed for high power OPCPA systems. As a result, the picosecond supercontinuum was chosen as a source of broadband pulses to seed two new high power OPCPA systems, which are currently being developed at ELI-Beamlines and are described in the final part of this thesis.

Abstract (česky)

Tato disertační práce se zabývá možností generace širokospektrálního superkontinua za využití pikosekundových pulsů za účelem seedování vysokovýkonných OPCPA systémů. V této době nejběžnější zdroj širospektrálních pulsů pro seedování OPCPA představují Ti:safírové oscillatory. Existence dvou oddělených zdrojů laserového záření pro OPCPA často vyžaduje implementaci sofistikovaných synchronizačních metod, což vede ke zvýšení complexity systému. Na této architektuře je aktuálně postavený laserový system L1 v ELI-Beamlines, kde regenerativní zesilovač produkuje pikosekundové čerpací pulsy a Ti:safírový oscillator zajišťuje seedování. Možnost generace dostatečně širokospektrálních pulsů za pomoci čerpacího záření může potenciálně vést ke zjednodušení existujícího laserového systému i budoucích projektů.

Generace supercontinuua je důsledkem řady nelineárních jevů, fokusace dostatečně silného svazku do nelineárního materiálu vede k filamentaci a značnému spektrálnímů rozšiřování, které může produkovat spektrum sahající od blízké ultrafialové až po střední infračervenou oblast. Tato disertační práce shrnuje nelineární efekty vedoucí ke generaci superkontinua: auto-fokusace, auto-modulace fáze, ionizace, defokusace plasmatem, štěpení pulsu a self-steepening. Aby se předešlo optickému poškození materiálu, superkontinuum bylo generováno v uspořádání s dlouhým fokusem za využití dlouhého (13 cm) YAG krystalu. K dosažení generace stabilního, širokospektrálního superkontinuua byla vyzkoušena řada experimentálních uspořádání a různých parametrů čerpacího laseru. V práci je ukázáno že, při vhodně zvolené konfiguraci, stabilita generovaného superkontinuua může překonat stabilitu čerpacího pulsu.

Vygenerované superkontinuum bylo zesíleno ve dvou OPCPA stupních a zkomprimováno za použití hranolového kompresoru, čímž bylo ukázáno, že superkontinuum generované pikosekundovými pulsy může být využito jako zdroj seedovacích pulsů pro vysokovýkonové OPCPA. Na základě dosažených experimentálních poznatků bylo superkontinuum zvoleno jako zdroj širokospektrálních pulsů pro dva nové vysokovýkonové systémy, které jsou aktuálně vyvýjeny v ELI-Beamlines a jsou popsány ve finální části této práce.

Table of Contents

List of Symbols and acronyms

Symbols

Δn	Change in refractive index	[-]
c	Speed of light in vacuum	[m/s]
d	Beam diameter	[m]
E	Laser pulse energy	[J]
e	Euler’s number $\simeq 2.71828\ldots$	[-]
e	Electron charge	[C]
E_{cr}	Threshold critical energy for self-focusing	[J]
E_g	Bandgap energy	[eV]
f	Focal length	[m]
$\hbar$	Reduced Planck constant	[J s]
I	Laser beam intensity	[W m^{-2}]
J	Bessel function	[-]
k	Wavenumber	[rad/m]
L_c	Nonlinear focus	[m]
l_{coh}	Coherent length	[m]
L_R	Rayleigh length	[m]
L_{SF}	The characteristic length for self-focusing	[m]
M^2	Beam quality factor	[-]
m_e	Mass of electron	[kg]
n	Refractive index	[-]
n_0	Linear refractive index	[-]
n_2	Nonlinear refractive index	[-]
P	Power	[W]
P_{cr}	Threshold critical power for self-focusing	[W]
tp	Pulse duration	[s]
U_i	Ionization potential	[eV]
γ	Keldysh parameter	[-]
$\Delta\lambda$	Spectral bandwidth	[m]
$\delta\omega(t)$	frequency change	[rad/s]
ϵ_0	Permittivity of the vacuum	[F m^{-1}]
λ	Wavelength	[m]
π	$\simeq 3.1415\ldots$	[-]
ρ	Free-electron density	[m^{-3}]
ρ_c	Critical plasma density	[m^{-3}]
$\varphi_{\mathrm{nl}}(\mathrm{t})$	Nonlinear phase	[-]
$\chi^{(3)}$	The third-order (Kerr) nonlinearity coefficient	[-]
ω	Angular frequency	[rad/s]
ω_0	Central angular frequency	[rad/s]

Acronyms and abbreviations

AP	Aperture
BBFE	Broadband front end
BBO	Beta-barium borate (β–BaB_2O_4)
BiBo	Bismut borate (BiB_3O_6)
BS	Beamsplitter
CAM	Camera
CCD	Charge-coupled device
CEP	Carrier-envelope phase
CFBG	Chirped fiber Bragg grating
CMP	Compressor
DAZZLER	Acousto-optic programmable dispersive filter
DFG	Different frequency generation
DPSSL	Diode pumped solid state laser
DUMP	Beamdump
ELI	Extreme Light Infrastructure
ETS	Electronic timing system
FC	Fiber collimator
FE	Front end
FROG	Frequency resolved optical gating
F-SYNC	Femtosecond Synchronization project
FWHM	Full width at half maximum
GDD	Group delay dispersion
GR	Grating
GVD	Group velocity dispersion
HEAD	Thin disc laser head
IBA	Inverse Bremsstrahlung absorption
IR	Infrared
ISO	Isolator
KD*P	Potassium dideuterium phosphate (KD_2PO_4)
LBO	Lithium triborate (LiB_3O_5)
LiF	Lithium fluoride
LWFA	Laser wakefeeld acceleration
MLD	Multi-layer dielectric
MPI	Multiphoton ionization
OCT	Optical Coherence Tomography
OPA	Optical parametric amplification
OPCPA	Optical parametric chirped pulse amplification
PC	Pockels cell
PM	Piezo actuated mirror
PP	Pulse picker
RA	Regenerative amplifier
RF	Radio-frequency

RMS	Root mean square
ROT	Rotator
RT	Round trip
SC	Supercontinuum
SCG	Supercontinuum generation
SHG	Second harmonic generation
TFP	Thin film polarizer
TI	Tunnelling ionization
Ti:sapphire	Titanium doped sapphire ($Ti^{3+}:Al_2O_3$)
TOD	Third order dispersion
UV	Ultraviolet
XFEL	X-ray free electron laser
YAG	Yttrium aluminium garnet ($Y_3Al_2O_3$)
Yb:YAG	Ytterbium doped yttrium aluminium garnet ($Y^{3+}:Y_3Al_2O_3$)
$\lambda/2$	Half-wave
$\lambda/4$	Quarter-wave

Introduction

Propagation of intense short laser pulses in bulk transparent nonlinear media can lead to the formation of a filament. This process produces very significant spectral broadening of the initial pulse, called white-light continuum or, supercontinuum (SC). The generation of supercontinuum with femtosecond pulses already proved to be a compact and efficient technique for the generation of very broadband coherent pulses. The wavelength range of light generated in this way can cover a significant part of the optical spectra from near ultraviolet to mid-infrared.

Coherent ultra-broadband light sources are in demand for a variety of applications. A direct application is the broadband characterization of the non-linear absorption spectra [1], [2]. Various other applications include femtosecond laser-induced nonlinear spectroscopy for remote sensing [3], multi-octave absorption spectroscopy [4], frequency combs in the visible to mid-infrared region [5], pump-probe spectroscopy to study ultrafast molecular dynamics and processes with femtosecond time resolution [6], [7]. For our applications, we are interested in coherent broadband radiation that has a bandwidth to support femtosecond compression. Short pulses in the time domain allow us to reach high peak intensities, which is a prerequisite for strong-field experiments.

The first wide-spread light sources capable of generating broadband pulses were dye lasers. However, due to the toxicity and instability of dyes, these lasers are rarely used anymore and were mostly replaced by other sources. Currently, the most common sources off broadband radiation are solid state lasers using Ti:sapphire as the active medium, offering broadband spectrum, which allows for the generation of pulses with a time duration of less than 10 fs. Another light source capable of producing very broadband pulses is supercontinuum generation.

The first reported measurements of frequency broadening in the solid material was done by Alfano and Saphiro in 1970 during early years of nonlinear optics [8]. This was achieved by focusing 5 mJ, 4 ps long pulses into a borosilicate glass, producing a spectrum in the visible range from 400 to 700 nm. Soon after this discovery, the spectral broadening was also observed in various crystals and glasses, which confirmed the universal nature of this phenomenon [9].

The following early development of supercontinua was motivated mainly by the need for a high power broadband light source for Raman absorption spectroscopy. This was initially achieved in silica fibres. in 1976, a 1 kW of nanosecond supercontinuum with 180 nm bandwidth centered around 530 nm was generated [10]. Just two years later, a supercontinuum generated again in silica fiber, but with a spectrum stretching from 0.7 to 2.1 µm and providing up to 12 kW of power was reported [11]. Since the late 1970s, a variety of experiments was done, generating supercontinuum not only in various fibers, but also solid bulk materials, liquids and gasses with different pump sources. A significant example among these was a study conducted in 1983 by Fork *et al.* [12], who were the first to generate and report the supercontinuum generation with femtosecond pulses. This was achieved by focusing an 80 fs, 627 nm pulses into a jet of ethylene glycol, showing that the generation of supercontinuum with femtosecond pulses was easier, more reliable and repeatable.

It is interesting to note that up till this point the dramatic spectral broadening of pulses caused by supercontinuum generation was not theoretically explained. While it was believed that the main factor behind the spectral broadening was the self-phase modulation, the actual generated spectra were much wider than what was predicted by theory. The first paper providing a complete model of the supercontinuum generated with femtosecond pulses in fibres (in the regime of anomalous dispersion) was published in 1992 [13].

The realization and availability of Ti:sapphire oscillators, which are able to generate very short laser pulses and provided better performance than dye lasers, lead to further advance in supercontinuum generation with femtosecond pulses. The SC generation was intensively studied in a variety of wide-bandgap solid-state media with femtosecond pulses [14], [15]. It was shown that the broadest supercontinuum generation can be achieved by pumping in the anomalous dispersion regime. However, it was difficult to make use of this regime, since anomalous dispersion region of many materials falls into mid infrared portion of spectra and suitable pump sources were not common. This regime of operation became much more available with the development of femtosecond parametric amplifiers, which resulted in the generation of ultrabroadband, several octave spanning spectra generated with ultrashort near and mid infrared pulses [16], [17]. It was also shown that the filamentation of femtosecond laser pulses in solid state media can be safely performed by choosing a proper, low numerical aperture focusing configuration, which is a condition to mitigate material damage [18].

The pumping with femtosecond pulses became the dominant method of supercontinuum generation It was shown, that the supercontinuum can be generated in various solid state media for a wide range of pump wavelengths. One of the prominent materials used for SC generation are Alkali metal fluorides, which have an intrinsically large bandgap and have extremely broad transparency window, and produce the most ultraviolet-shifted supercontinuum of all materials. The shortest supercontinuum wavelength was obtained with lithium fluoride (LiF) pumped by the third harmonic of a Ti:sapphire oscillator (262 nm) and reached all the way to 200 nm [19]. The supercontinuum in the mid infrared region spanning even beyond 5 µm can be generated in various materials, including alkaline metals, glasses or laser hosts if the pump beam wavelength falls into anomalous dispersion regime of the given material [20], [21], [22].

While the femtosecond supercontinuum is proven to be a well working mechanism, the supercontinuum generation with picosecond pulses in solid state media is considered to be a difficult task and poses high requirements for the nonlinear medium, such as high optical damage threshold, polishing and crystalline quality. The supercontinuum generation with picosecond laser pulses has been performed successfully in liquids and gasses, where no permanent optical damage occurs [23]. Because the supercontinuum generation with picosecond pulses requires significantly more energy in the pump pulse than with femtosecond pulses, the main limiting factors are the optical degradation, damage and permanent modification of the material [24]. Because of these requirements, the laser host crystals possessing a good crystalline quality, high nonlinearity and a high optical damage threshold seems to be a good choice for generation of picosecond supercontinuum in solid state media. The first stable and repeatable supercontinuum with 1 ps long pulses was achieved with YAG (Yttrium aluminium garnet) crystal [25].

Motivation and Aims of the thesis

ELI-Beamlines is a large scale facility providing high peak power and high average power lasers and secondary sources of radiation for user-driven fundamental and applied research, including the acceleration of electrons and ions, plasma physics experiments, ultra-high intensity laser-matter interactions, bio and material applications or various X-ray generation sources. The ELI-Beamlines facility consist of four laser systems providing different pulse energies, repetition rates, pulse duration and are based on different amplification technologies.

The motivation for this work initially comes from the L1 Allegra laser, which is an OPCPA based system designed to provide 100 mJ pulses at 1 kHz with a pulse duration under 15 fs [26]. The broadband seed pulses for the OPCPA are provided by a Ti:Sapphire oscillator and stretched to ≈ 3 ps in order to match the length of pump pulses, which are generated by multiple regenerative amplifiers. The precise temporal overlap of the seed and pump pulse is ensured by an in-house developed active pulse synchronization system based on balanced optical cross correlation [27].

The broad spectrum of the SC makes it an ideal candidate for seeding ultrafast amplifiers. While mode-locked lasers are often used to seed high energy OPA systems due to their exceptional stability, [28], [29] the separate seed and pump lasers add complexity to a OPCPA laser system and typically require sophisticated synchronization schemes to actively maintain temporal overlap of the pump and seed envelopes, which ensures stable long term amplification [30]. Using a SC generated by a single pump laser to seed an OPA system would greatly simplify such laser systems by eliminating the need for a separate mode-locked seed laser and timing jitter stabilization schemes [31].

This work investigates the possibility to use the supercontinuum generated with ≈ 3 ps long pulses at 1030 nm as a seed for high power OPCPA. These pump pulses are generated by Yb:YAG thin disk regenerative amplifiers, which are used as pump lasers for the OPCPA system within the L1-Allegra laser at ELI-Beamlines [29], [32], [33]. The possibility to use these pump lasers to directly generate the seed pulses for the OPCPA instead of relying on a separate seed source have the potential to significantly simplify existing laser systems, as well as any future projects.

In order for the generated supercontinuum to be usable as a seed for a high power OPCPA system, such as the L1 Allegra laser, it needs to meet some necessary requirements. The spectrum of the SC has to be sufficiently broad and stable and the energy stability needs to be comparable or even exceeding the stability of the pump pulses. The continuous generation must not be introducing any optical damage or modification to the material even after prolonged laser operation. The supercontinuum also must be coherent and the portion of the spectra amplified in the OPCPA needs to be compressible close to the Fourier limit.

The supercontinuum is generated in a loose focus setup, using the lens with long focal length for focusing into the long (13 cm) YAG crystal to prevent optical damage to the material. The performance of the generated supercontinuum is investigated for a variety of experimental setups, as well as different parameters of the pump pulses, such as pulse energy, length, chirp, *B*-integral. We show that it is possible to generate broadband supercontinuum with pulse-to-pulse energy stability exceeding that of the pump laser if the right configuration is chosen. Furthermore, the possibility to use the generated SC as a seed for the OPCPA is demonstrated by amplifying it in two OPCPA stages and compressing it close to the Fourier limit.

Thanks to these results, the picosecond supercontinuum was chosen as a source of broadband pulses to seed two new high power OPCPA systems which are now being built at ELI-Beamlines as a part of ADONIS project. The F-SYNC system will provide a synchronized auxiliary 1 kHz, 10 mJ femtosecond pulse train to the existing 1 kHz L1-Allegra laser. L2-DUHA system is intended to be a high repetition rate, 100 TW-class laser system whose primary purpose is to serve as a driver for a laser wakefeeld acceleration. Both systems utilize the supercontinuum in similar fashion, where the picosecond output of the pump laser system (regenerative amplifier and grating compressor) serves as a pump for the SC seed and as a pump for the OPCPA, which is seeded by the SC.

Theoretical part

1 Theoretical introduction

Supercontinuum generation is the result of a series of linear and nonlinear effects. A laser pulse is focused via nonlinear self-focusing, reaching an intensity high enough to ionize the medium and create a plasma, which reduces the effective refractive index of material, causing the defocusing of the beam. Combined effect of a beam self-focusing and plasma defocusing leads to a propagation regime where the beam travels over long distance without change in its diameter, creating a filament. The high intensity beam propagating through the material with normal GVD experiences beam splitting, where each of new sub-pulses contains different spectral frequencies. These sub-pulses, propagating over long distance along the filament, are reaching very high peak powers and are responsible for generation of new spectral components due to self-phase modulation and self-steepening, dramatically broadening the pulse. Individual effects leading to filament creation and following generation of broadband supercontinuum are described in this section.

1.1 Self-focusing

The refractive index of an optical medium n in the presence of an intense electromagnetic field depends not only on its frequency, but also on its intensity, which is spatially and temporally dependent $I(r,t)$. The resulting refractive index is then given as:

$$n = n_0 + n_2 I(r,t). \tag{1}$$

Here n_0 is the linear refractive index and n_2 is the nonlinear Kerr refractive index which is related to the third order susceptibility $\chi^{(3)}$ by [34]:

$$\chi^{(3)} = \frac{4\epsilon_0 c n_2 n_0^2}{3}, \tag{2}$$

where ϵ_0 represents the permittivity of the vacuum. The coefficient n_2 is usually positive and thus leads to an increase in the refractive index in presence of high intensity laser beam. For a Gaussian beam, the intensity is highest at the centre of the beam, so the nonlinear refractive index leads to wavefront curvature similar to that of a converging lens. This effect is cumulative and can, in the absence of other saturating effects, leads to a catastrophic collapse of the beam on itself and destruction of material.

The characteristic length L_{SF} for self-focusing is defined as the length over which the accumulated nonlinear phase, measured by the B-integral ($B = k_0 \int_0^z n_2 I dz$), varies by a factor of one. It is expressed as a function of the peak intensity I_0 [34]:

$$L_{SF} = \frac{1}{n_2 k_0 I_0}. \tag{3}$$

The significant parameter for self-focusing is the initial power P_{in} of the beam and not the initial intensity. The beam will overcome diffraction and will lead to collapse due to self-focusing if the input power P_{in} exceeds a critical threshold given by equation [35]:

$$P_{cr} = \frac{3.72\lambda_0^2}{8\pi n_0 n_2}. \tag{4}$$

When the critical input power value is reached, the beam diffraction is precisely compensated by self-focusing. Equation (4) is valid for specific beam shape, sometimes called the Townes beam [36]. For beams with different shape the critical power is usually higher. The beam shape in our experimental setup is Gaussian, because of that in all calculations in this work, the coefficient 3.72 in Equation (4) will be replaced by 3.77 to obtain the critical power corresponding to a Gaussian beam [37].

For supercontinuum generation we are using a pump laser with wavelength of 1030 nm and mainly YAG crystal. The refractive index n_0 of YAG at 1030 nm is 1.8153 [38] and nonlinear refractive index n_2 is 6.13×10^{-16} cm^2/W [39]. By putting these values into the equation (4) we can calculate the critical power for our specific case as $P_{cr} = 1.43\times10^6$ W. If we multiply the critical power by the length of a laser pulse, which in our case is typically 3 ps, we get a critical energy for self-focusing $E_{cr} = 4.29\times10^{-6}$ J.

This value is an important parameter when planning an experimental setup for supercontinuum generation. Self-focusing is the first and necessary step in the process of supercontinuum generation. Without self-focusing it isn't possible to achieve the high intensities inside the crystal required for photo-ionization generating plasma and all following effects. Because of that we know for certain that the energy of our pump pulses need to be larger than E_{cr}.

While critical power for self-focusing is only dependent on wavelength and material, the energy needed increases linearly with pulse length. With longer pulses we are getting closer to laser induced damage threshold of our material, creating another problem which we need to be aware of. Because of that, femtosecond pulses are often used for supercontinuum generation, decreasing energy needed by multiple orders, keeping it well under damage threshold.

Although whether the beam will be undergoing self-focusing or not is given only by its power and is completely independent on its size, it is still an important parameter determining how fast the self-focusing of the beam will happen. The propagation length, L_c of a Gaussian beam with power exceeding the critical power to the point where it collapses is well approximated by a semi-empirical formula [40]:

$$L_c = \frac{0{,}367 L_R}{\sqrt{\left[\left(P_{in}/P_{cr}\right)^{1/2} - 0{,}852\right]^2 - 0{,}0219}}, \qquad (5)$$

Where L_R is the Rayleigh length of the beam which is the distance from the beam waist where the beam radius is increased by a factor of the square root of 2. For Gaussian beams it is determined by the waist radius w_0 and the wavelength λ: $L_R = \frac{\pi w_0^2}{\lambda}$. The nonlinear focus L_c, like the Rayleigh length L_R varies with the square of the diameter of the laser beam. This means that beams with a larger initial diameter will need to travel a longer distance before they collapse due to self-focusing.

To generate a supercontinuum the propagation length L_c needs to be short enough that the beam collapse due to self-focusing happens before it leaves the material. A laser beam with a power of $2\times P_{cr}$ and diameter of 3 mm (which is the approximate diameter of our beam after compressor) will, according to equation (5), have a propagation length L_c of 23.01 m. This means that, in order to speed up the self-focusing process, the beam needs to be focused to significantly smaller diameter. If we focus the beam with same power to a diameter of 200 µm, the propagation length will be 23 cm. To further decrease L_c we need to either decrease the beam diameter or increase power, both of these options are increasing the energy density of pump laser, bringing us closer to material damage threshold. For example, if we would like L_c to be equal to 1 mm the beam diameter would need to be around 7 µm, increasing energy density to 5.5 J/cm^2.

One other approach to ensuring L_c is smaller than the length of material is to simply increase the length of the material. The disadvantage of this is, of course, the higher price of the required material and the limitations of manufacturers, as the maximum length of crystals is typically given by their equipment and cannot be increased without limit. In this work we use a 13 cm long undoped YAG crystal which gives us more options when designing a pump geometry. With this crystal we can use pump pulses with power of $2.5\times Pcr$ and diameter of 200 µm, which will lead to propagation length L_c 7.6 cm and energy density 0.034 J/cm^2.

The required beam diameter of 200 µm can be achieved by focusing an initially collimated beam with a 3mm diameter. For a Gaussian beam, the desired focal length f of lens can be calculated as: $f = w_0\pi d/2M^2\boldsymbol{\lambda}$, where d is beam diameter at lens and M^2 is beam quality parameter, which for this case is considered as 1, resulting in focal length $f = 457$ mm.

According to these considerations, if we focus a 3 mm beam, with a pulse energy of $E = 2.5\times E_{cr} \approx 17$ µJ, using lens with a 400 mm focal length into our 13 cm long YAG crystal, we can expect the beam to collapse due to self-focusing leading to supercontinuum generation after approximately 7 cm of propagation through material. While this consideration is taking into account just the self-focusing of laser the beam, it can give us some useful information when designing an experimental setup for supercontinuum generation regarding pump beam parameters and geometrical arrangement.

1.2 Photo-ionization

When the beam size is reduced due to the self-focusing effect, the beam becomes intense enough, that it starts to ionize the material through which it propagates.

There are two photo-ionization processes which can take place: multiphoton ionization (MPI) and tunnelling ionization (TI). Multi photon ionization occurs when the electron simultaneously absorbs multiple photons, providing it with enough energy to overcome the ionization potential U_i. The energy of the laser photons, which are being used for supercontinuum generation, needs to be significantly smaller than the ionization potential of the medium. If the ionization potential would be too small ($U_i < 3\hbar\omega$), the attenuation of the pump pulse due to two and three photon absorption will be too significant and the generation of the supercontinuum will not be possible [34]. The energy of photons at 1030 nm, which are used as our pump, is $\hbar\omega \approx 1.2$ eV. Therefore, to overcome the ionization potential of the

YAG crystal U_i = 6.5 eV, 6 photons need to be absorbed, so the MPI rate will scale as I^6. The necessary condition for supercontinuum generation $3\hbar\omega < U_i$ is fulfilled as well, but in some cases, especially for generation using lower wavelength photons, it can be a limiting factor for some materials. As the ionization potential U_i increases, the nonlinear refractive index n_2, which is defining the strength of nonlinear effects as self-focusing and self-phase modulation, typically decreases [41].

Tunnelling ionization occurs at higher intensities and can be described as the escape of an electron from the Coulomb potential of the nucleus, which is highly perturbed by the external electromagnetic field. The concept of multiphoton and tunnelling ionization is shown in Figure 1. Both ionization processes require very high field/intensity, and therefore only occur when the beam is focused, either by external focusing or self-focusing. Ionization steps in very abruptly because its probability strongly depends on the light intensity.

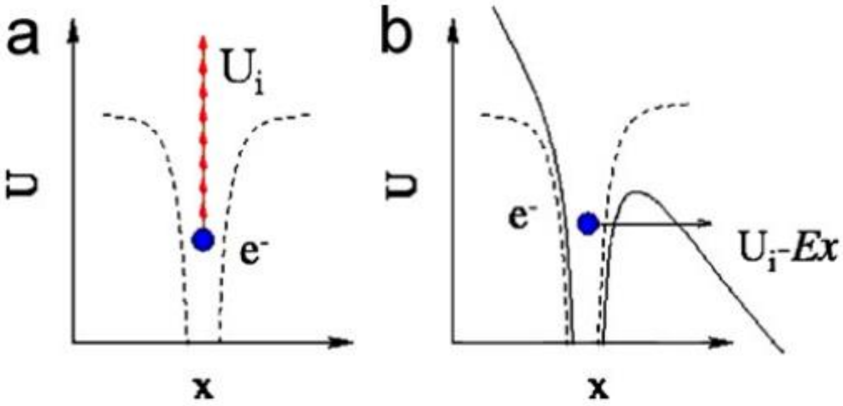

Figure 1: Schematic diagram of: (a) multiphoton ionization and (b) tunnel ionization [34].

To decide whether the MPI or TI is taking place in our case, we can calculate the Keldysh parameter γ:

$$\gamma = \frac{\omega}{e}\sqrt{\frac{m_e U_i n_0 c \varepsilon_0}{I}}, \qquad (6)$$

Where ω is the laser angular frequency, m_e and e the mass and charge of an electron respectively. c is the speed of light in vacuum and ε_0 is the permittivity of free space [42]. If $\gamma \gg 1$ MPI is dominating factor, while tunnelling ionization dominates if $\gamma \ll 1$.

If we take our laser parameters of 17 μJ energy, 1030 nm wavelength and 3 ps pulse length in focal point of 400 mm lens with 200 μm diameter we obtain the Keldysh parameter

$\gamma = 1.046$. However, the diameter of pulse can decrease to ≈ 10 μm [43], [44] due to self-focusing, which leads to a Keldysh parameter of $\gamma = 0.05$. This means that initially the ionization effect is caused by combination of MPI and TI and when the intensity increases due to self-focusing, the TI starts to be more dominant. Because we operate in a regime close to $\gamma \approx 1$ we cannot reliably decide whether MPI or TI is solely the cause of ionization and while there are studies describing behaviour in this regime [45], both MPI and TI should be taken into consideration when computing the plasma density. Free electrons generated through MPI and TI continue to interact with optical field and acquire extra energy through inverse Bremsstrahlung absorption (IBA). IBA is efficient absorption mechanism, in which an electron absorbs a photon while colliding with another particle. The electron which acquired an extra energy can transfer energy to the other electrons through collisions, resulting in the formation of more electrons. This form of ionization, requiring an already ionized medium, is called avalanche ionization. The free-electron density development in time can be described by equation [46]:

$$\partial_t \rho(r,z,t) = \frac{\sigma}{n_b^2 E_g}\rho I + \frac{\beta^{(K)}}{K\hbar\omega_0} I^K - a\rho^2. \tag{7}$$

The first term on the right-hand side describes avalanche ionization with σ being the cross-section for inverse bremsstrahlung, $\beta^{(K)}$is MPI coefficient and E_g is the band gap energy. The second term accounts for electron generation via MPI, and the third term describes recombination. The exact value of free-electron density in specific space and time needs to be calculated using numerical simulation and several articles address this problem either as part of supercontinuum generation simulation or separately [42], [44], [45], [46], [24], [47].

1.3 Plasma defocusing

The combined effect of multiphoton, tunnelling and avalanche ionization creates plasma which introduces local reduction in the refraction index, according to [48]:

$$n \cong n_0 - \frac{\rho(r,t)}{2\rho_c}, \tag{8}$$

where $\rho(r,t)$ is the density of free electrons and ρ_c denotes the value of the critical plasma density above which the plasma becomes opaque.

$$\rho_c = \varepsilon_0 m_e \, \omega_0^2 / e^2, \qquad (9)$$

m_e and e denote the electron mass and charge. For light with wavelength of 1030 nm, which corresponds to our pump beam, $\rho_c = 1.05 \times 10^{-27} m^{-3}$. The generated plasma reduces the refractive index of the material and acts as a divergent lens, preventing the complete collapse of the beam on itself. The electron plasma is generated by the forward part of pulse which in turn defocuses mainly the trailing part of the pulse. In addition to the spatial aspect, plasma defocusing acts locally in time and leads to a strong asymmetry in the pulse temporal profile, which is partly at the origin of the dynamics in filamentation and temporal compression effects [34]. Electron plasma generated in the wake of the pulse also contributes to a spectral broadening, shift towards blue in the leading part of the pulse, and can modify the dispersive properties of the medium [49], [50].

1.4 Refocusing cycles

A pulse with peak power above P_{cr} should undergo a collapse due to self-focusing. However, the beam cannot focus without limit; the beam collapse at the nonlinear focus is arrested by multiphoton absorption and ionization, producing an energy loss and generating free electron plasma, which further absorbs and defocuses the beam. The ionization properties of the medium ensure that the maximum intensity in the crystal changes very little with respect to the input energy. This effect is called intensity clamping and is positively affecting the stability of supercontinuum [44].

Once the beam defocuses because of ionization loses and plasma defocusing it may still contain the critical power for self-focusing and undergo another focusing-defocusing cycle. This scenario can repeat multiple times and sustain a long range, self-guided propagation in the form of a filament. The recurrence of these cycles depends mainly on the peak power of the input pulse. The interplay between self-focusing, and ionization is therefore a highly dynamic process, with recurrent, aperiodic strings or spikes of ionization surging whenever the beam starts collapsing again, schematically shown in Figure 2 [34].

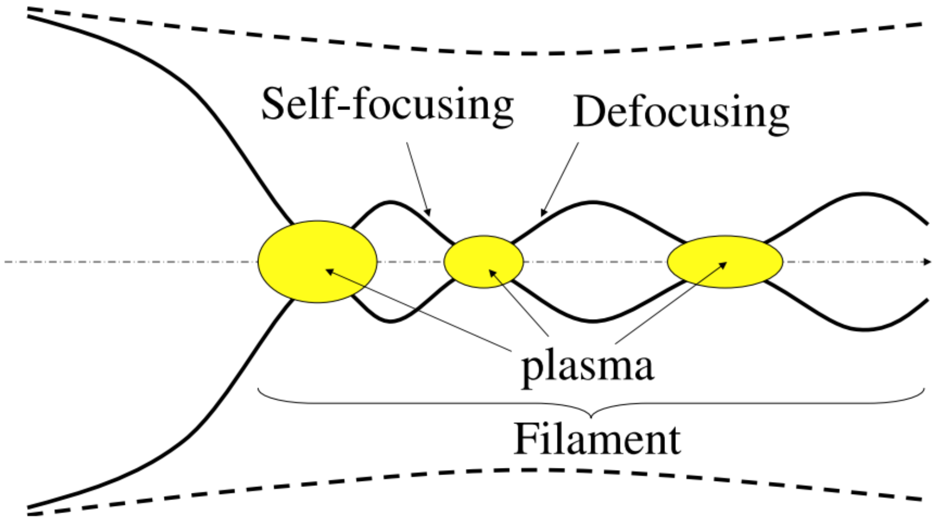

Figure 2: Schematic representation of the focusing–defocusing cycles undergone by the intense core of the beam. The solid curves indicate the diameter of the intense core. The filamentation length is the distance covered by these cycles. The dashed line indicates the root mean square radius of the full beam [34].

Figure 3 shows a photo of a filament generated inside a 13 cm long YAG crystal pumped by 1030 nm beam (the pump beam is coming from the right side of the picture) at four different energies. Figure 3 (a) shows the filament formed without refocusing and by increasing the energy of the pump beam, the first refocusing cycle appears (b). With a further increase in pump energy, the first refocusing cycle moves closer to the initial focusing position and 2 more refocusing cycles are generated further back inside the crystal (c). The filament generated with an even stronger pump beam in Figure 3 (d) consist of many refocusing cycles, many of these are very close together in the first, very bright, portion of filament and cannot be distinguished anymore.

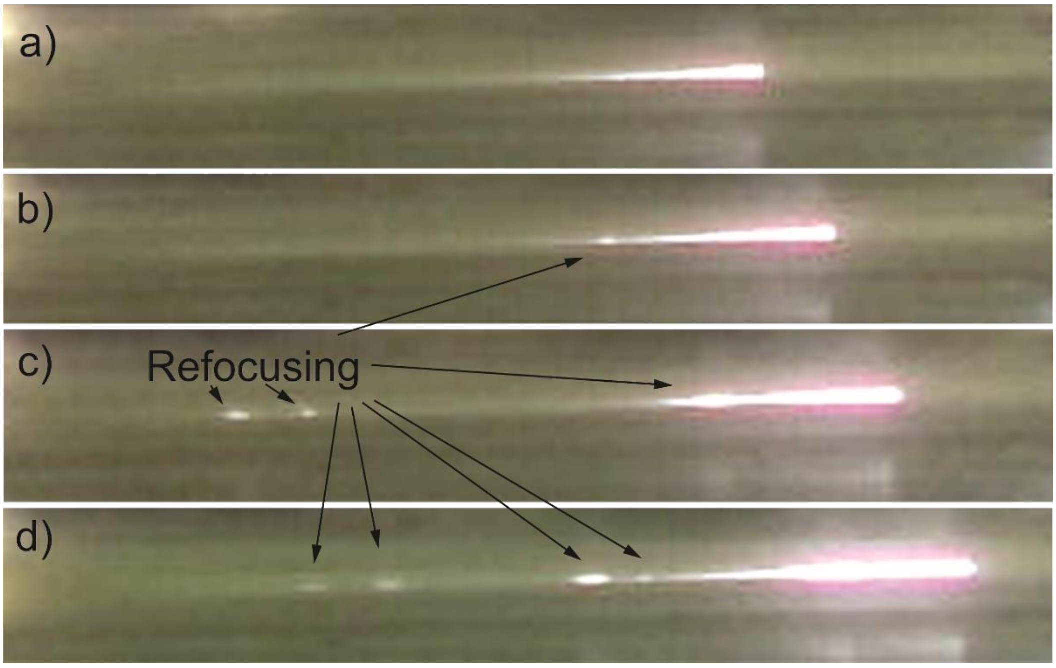

Figure 3: Generation of filament inside the YAG crystal without refocusing (a) and with refocusing due to increase in pump power (b), (c) and (d).

1.5 Self-phase modulation

While the spatial dependence of the refractive index results in self-focusing of the beam, the time dependence manifests as self-phase modulation. In the time domain, the time-varying refractive index imparts a nonlinear change in the phase of the pulse

$$\phi_{nl}(t) = -\frac{\omega_0}{c} n_2 I(t) z, \tag{10}$$

where ω_0 is the carrier frequency and z is the propagation distance, which produces the frequency change

$$\delta\omega(t) = \frac{\mathrm{d}}{\mathrm{d}t} \phi_{nl}(t). \tag{11}$$

This frequency change results in the time-varying instantaneous frequency

$$\omega(t) = \omega_0 + \delta\omega(t). \tag{12}$$

This leads to spectral broadening of the pulse. For a Gaussian pulse with the pulse duration of t_p, the variation of the instantaneous frequency is expressed as:

$$\delta\omega(t) = -2\frac{\omega_0}{ct_p^2}n_2 I_0 \exp(-\frac{t^2}{t_p^2})tz. \qquad (13)$$

This effect is called self-phase modulation and causes spectral broadening of the pulse by inducing a negative shift of the instantaneous frequency at the leading (ascending) front of the pulse and a positive shift of the instantaneous frequency at the trailing (descending) front of the pulse, as schematically illustrated in Figure 4.

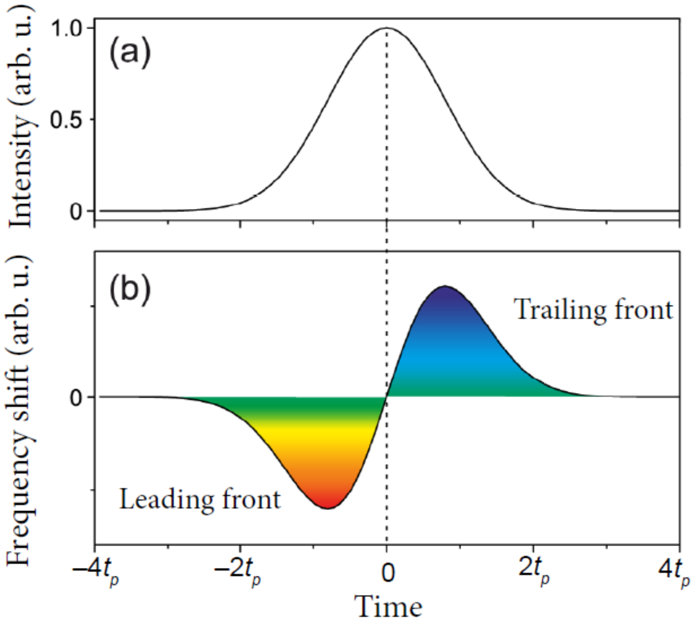

Figure 4: Self-phase modulation of the Gaussian pulse shown in (a), which produces a variation of the instantaneous frequency shown in (b) [24].

1.6 Pulse splitting and chromatic dispersion

Chromatic dispersion is an important aspect of supercontinuum generation, it determines the shape and width of the supercontinuum spectrum [51]. The sign of group velocity dispersion (GVD) defines the dynamics of a filament creation and also the temporal and spectral content of supercontinuum [52]. We distinguish three separate regimes, depending on the sign of the GVD coefficient, which is defined as:

$$k_0^{"} = \frac{\partial^2 k}{\partial \omega^2}, \qquad (14)$$

where $k = \omega_0 n_0 / c$ is the wavenumber. The first is the region of normal GVD ($k_0^{"} > 0$), where the red-shifted frequencies travel faster than blue-shifted ones. The opposite is true in the region of anomalous GVD ($k_0^{"} < 0$), where blue-shifted frequencies are faster. The last regime is called zero GVD ($k_0^{"} = 0$) and frequencies at this regime travel at the same speed.

Normal GVD

The normal GVD of wide-bandgap dielectric materials typically lies in the wavelength range from the UV to the near IR. The pump pulses we use for the supercontinuum generation have a wavelength of 1030 nm and fit into the normal GVD region of the YAG which spans up to 1.6 µm [38]. In the region of normal GVD of dielectric media, the main effect determining the dynamics of pulse propagation at and beyond the nonlinear focus, such as self-focusing and spectral broadening, is the pulse splitting [24].

The initial pump pulse is broadened by self-phase modulation, producing nonlinear frequency modulation (chirp), where the red-shifted frequencies are generated at leading parts of the pulse and blue-shifted frequencies at the trailing parts of the pulse. The leading and trailing part of the pulse are traveling at different velocities which divides the pulse into two sub-pulses with shifted carrier frequencies, this effect is called pulse splitting [53]. Because these pulses are propagating at different velocities, the sub-pulses move in opposite directions in the frame of the input pulse [44]. After pulse splitting these two distinct temporal pulses compress sharply to much higher intensities as they self-focus.

These dynamics have been previously modelled numerically [53]. Numerically modelled development of pulse propagating through nonlinear medium with normal dispersion is shown in Figure 5. Here we can observe, how an initially Gaussian pulse (a) is first slightly shortened due to self-focusing pulse-compression effect (b). Afterwards pulse is split into two temporally separated pulses which are reaching intensities much higher than initial pulse. The distance between these two pulses increases as they propagate through medium. Figure 6 shows continuous development of peak power during propagation. After pulse splitting, the intensity of split pulses (solid curve) grows sharply, while original pulse gets weaker.

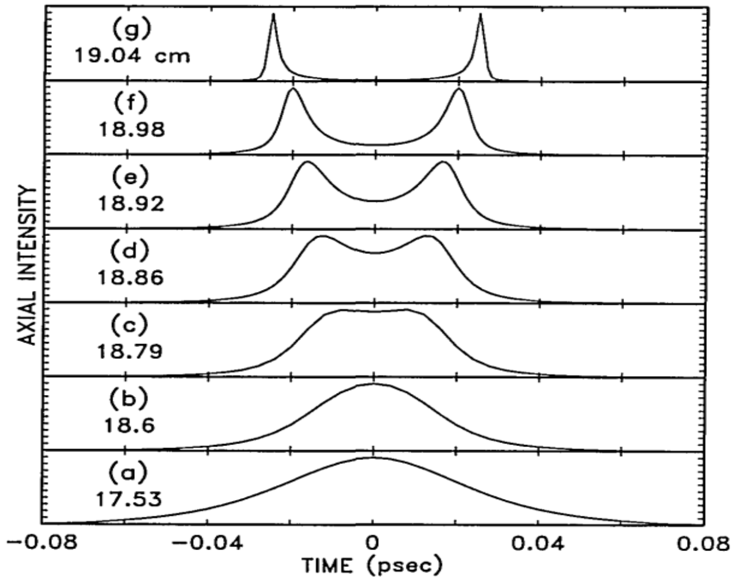

Figure 5: Calculated intensity on axis versus time of a self-focusing pulse at the propagation distance indicated. The peak intensity ($\times 10^{12}$ W/cm^2) at each distance is (a) 0.85, (b) 6.3, (c) 11, (d) 14, (e) 20, (f) 34, and (g) 150 [53].

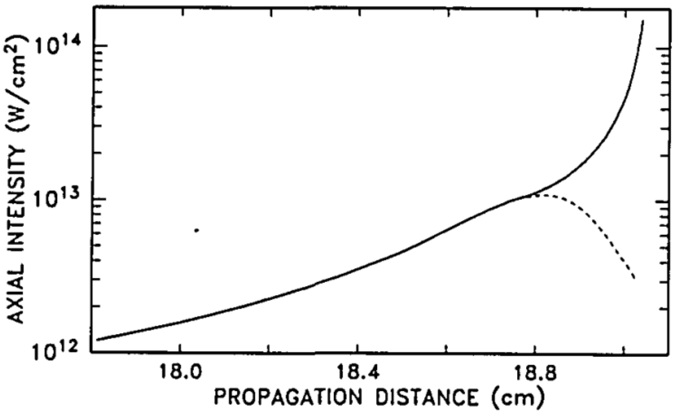

Figure 6: Peak axial intensity of the split pulses (solid curve) and the axial intensity at the original pulse centre (dashed curve) versus the propagation distance [53].

This phenomenon was also observed experimentally [54]. Figure 7 shows experimentally measured temporal and spectral profiles of pulses undergoing self-focusing through 1-inch thick BK7 glass sample for different input powers. While pulse with power under self-focusing threshold passes material unchanged (a) and (a’), pulse with power of $P/P_{cr} = 1.7$ shows signs of pulse splitting and spectra broadening (b) and (b’). At higher power $P/P_{cr} = 2.7$, clear evidence of pulse splitting is observed, and spectrum is significantly broadened.

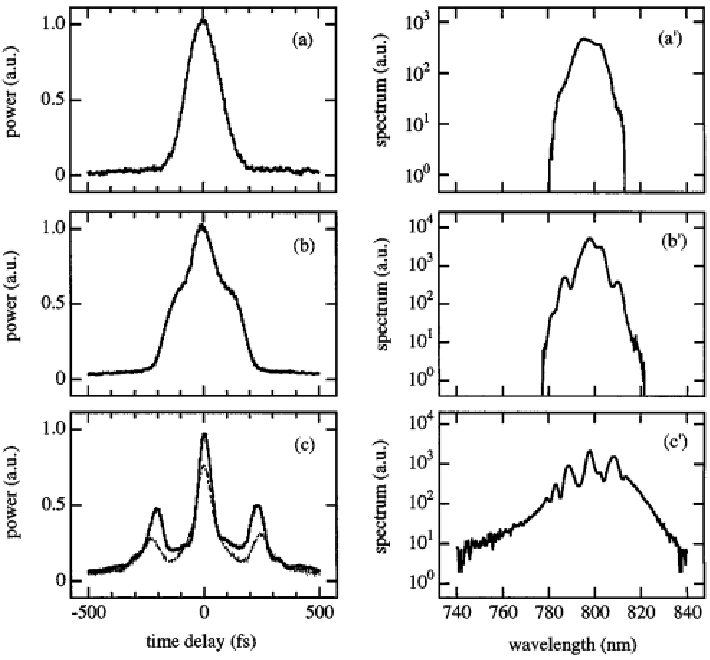

Figure 7: Experimentally measured temporal autocorrelations (a)–(c) and power spectra (a')–(c') of the pulses transmitted through a BK7 glass sample as the input power is increased [54].

These sub-pulses reaching very high peak powers are responsible for the generation of new spectral components due to self-phase modulation and self-steepening, which will be described in the next chapter. Split sub-pulses experience different self-steepening. In the near-infrared spectral range a very steep edge is formed at the trailing front of the trailing sub-pulse, creating a broad, blue-shifted pedestal in the SC spectrum. On the other hand, self-steepening of the leading front of the leading sub-pulse is much less significant, resulting in a smaller, red-shifted spectral broadening [24]. Chirping the initial pulse can strongly increase the achievable peak intensity by competing with the splitting of the pulse in the time domain [55]. This may affect the process of supercontinuum generation with differently chirped pulses and will be experimentally tested.

A numerical simulation written in house by Alexandr Špaček illustrating the splitting of the pulse as it propagates through the YAG crystal during the supercontinuum generation for different energies of the pump pulse is shown in Figure 8 [44]. The simulation was performed for a 100 mm long YAG crystal pumped by a 1030 nm beam focused by a lens with 400 mm focal length, corresponding well with the setup used during experiments described in the following sections of this work. The top row shows the on-axis temporal envelope as the filament propagates in the YAG crystal where the temporal splitting can be observed. The bottom row shows the spatially averaged spectrum for the same energy. Figure 8 (a) and (b) corresponds to 4 µJ, which is just above the threshold for SC generation, (c) and (d) to 5 µJ, and (f) to 6.5 µJ which is high enough for the beam to refocus in the crystal resulting in a second pulse, as described in section 1.4.

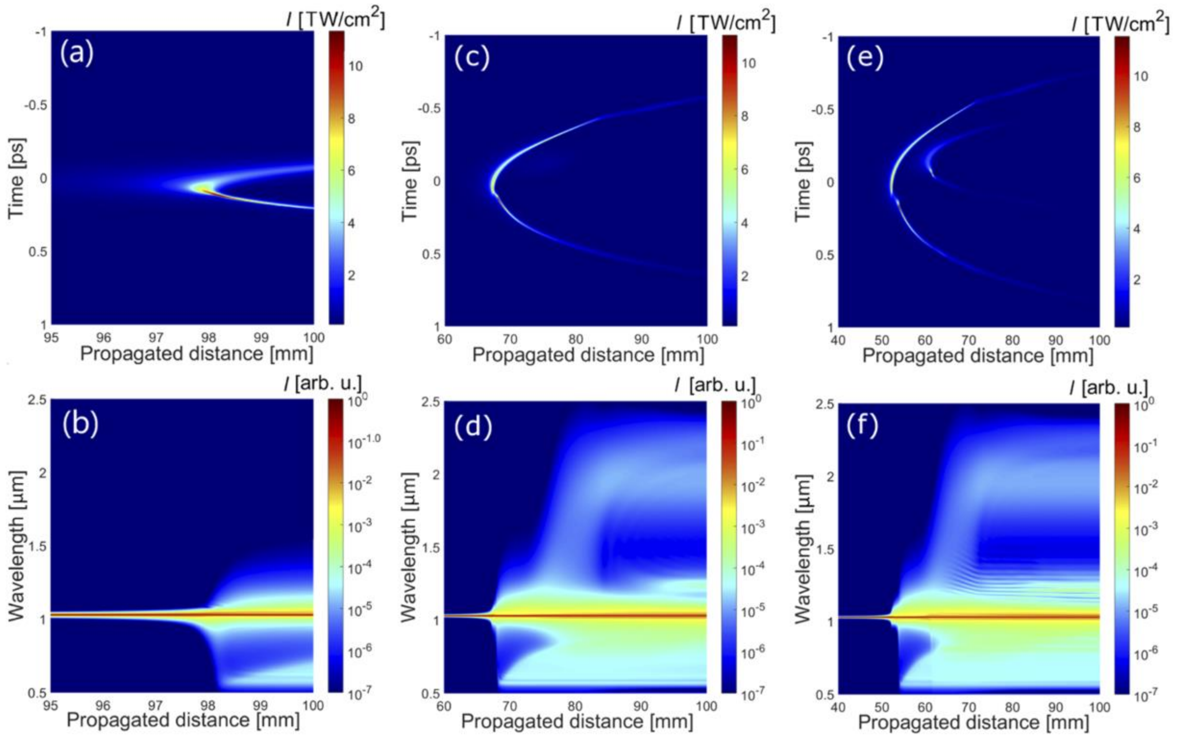

Figure 8: Evolution of the on-axis temporal envelope (top row) and the averaged spectrum (bottom row) during filamentation in YAG for three different energies. (a) and (b) correspond to 4 µJ, (c) and (d) to 5 µJ, € and (f) to 6.5 µJ [44].

Anomalous GVD

The situation changes significantly for anomalous GVD. The new red-shifted and blue-shifted frequencies generated by the self-phase modulation on the ascending (leading) and descending (trailing) parts of the pulse are swept back to the peak of the pulse, instead of being dispersed as in the case of normal GVD. The combined effect of diffraction, anomalous dispersion, and nonlinear refraction, can cause an optical pulse to collapse simultaneously in time and space. Such a collapse can yield short pulses with extremely large optical fields and possibly create light bullets – pulses that propagate without change in space or time [56].

Figure 9 (c) shows a numerically modelled example illustrating formation and propagation dynamics of such light bullet in a sapphire crystal. This is accompanied by the generation of an ultrabroadband supercontinuum (f) in comparison to pulse-splitting occurring in cases of normal and zero GVD (a), (b) [24].

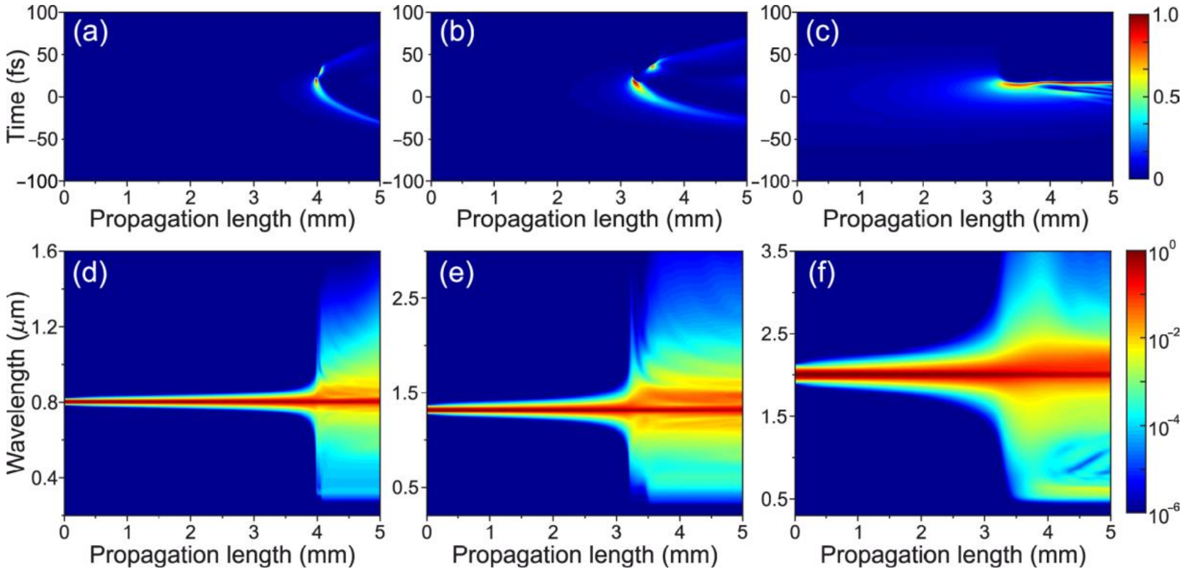

Figure 9: Top row: numerically simulated temporal dynamics of 100 fs laser pulses propagating in a sapphire crystal with the input wavelengths of (a) 800 nm, (b) 1.3 µm and (c) 2.0 µm, representing the filamentation regimes of normal, zero and anomalous GVD, respectively. Bottom row shows the corresponding spectral dynamics [24].

Zero GVD

The zero GVD wavelengths of commonly used wide-bandgap dielectric materials typically falls into the infrared spectral range, typically in the interval between 1 and 2 µm. In the zero GVD region, the input pulse undergoes the splitting at nonlinear focus in the time domain, as shown in Figure 9 (b). The dynamics of propagating pulse are similar to that observed in the case of normal GVD shown in Figure 9 (a). It was experimentally shown that pulse splitting prevails even in the case of weak anomalous GVD [57]. The pulse development in near-zero GVD regime to some extent combines properties of both normal and anomalous GVD and produces a more symmetric spectral broadening than in two previous regimes [52]. The spectral broadening in the regimes of normal and zero GVD is associated with the pulse splitting, and the spectral broadening in the regime of anomalous GVD is associated with pulse self-compression.

1.7 Self–steepening

Self-steepening, together with self-phase modulation are the main reasons for broadening of the pulse after pulse splitting. Laser pulse self-steepening changes the temporal shape of the pulse and occurs because the velocity of the peak intensity of the pulse is smaller than that of the trailing edge of the pulse, due to the intensity dependent change of refractive index $\Delta n = n_2 I$. If the nonlinearity leads to increase in the refractive index, which can be caused, for example, by Kerr effect, the trailing edge of the pulse steepens until its trailing edge is as sharp as the dispersion will allow. Steepening occurs on the trailing part of the pulse in materials where the velocity of the peak of the pulse is slower than that of the wings and because of that the trailing part of the pulse catches up with the peak. The formation of a steep edge in the trailing part of the pulse due self-steepening is shown in Figure 10.

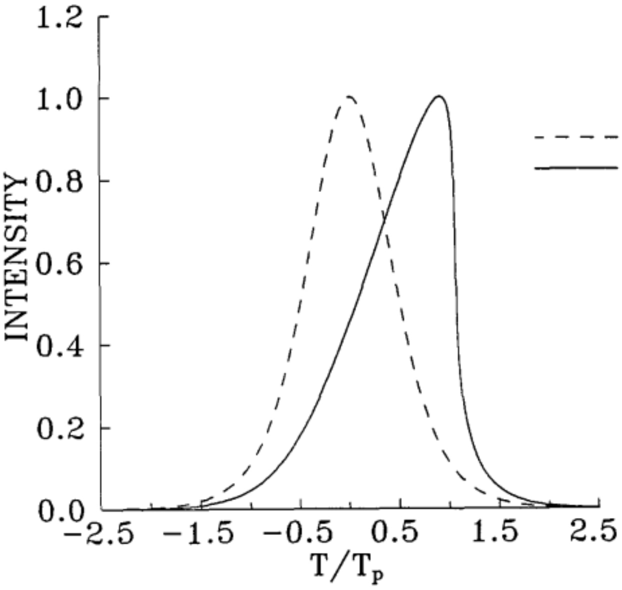

Figure 10: The effect of self-steepening on an initially Gaussian pulse propagating through a dispersive media. [58].

The development of an infinitely sharp trailing edge is prevented by dispersion, which also limits the Fourier spectrum of the pulse from spreading indefinitely [59]. This effect leads to a faster self-focusing of the trailing part of the pulse (in comparison with the leading part) and to an increase of the bluer frequencies generated in the steep trailing part. Self-steepening also leads to asymmetric pulse splitting [60]. A numerical simulation showing combined effect of self-steepening and self-focusing on a pulse propagating in a normally dispersive media is shown in Figure 11.

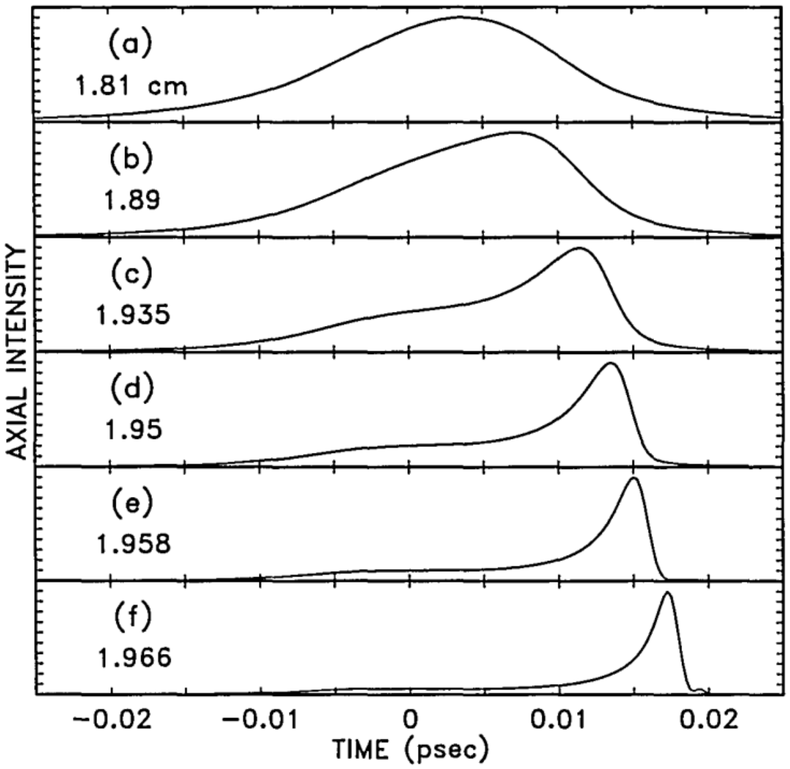

Figure 11: Calculated intensity on axis (normalized units) as a function of time for a self-focusing and self-steepening of a pulse propagating in a normally dispersive medium [61].

Experimental part

2 Pump laser generation and parameters

The parameters of the pump pulses are the most important factor in supercontinuum generation. As will be shown later, the energy, spectrum, and stability of the generated supercontinuum is heavily dependent on the characteristics of the pump laser. In order to be able to generate a stable supercontinuum usable for further amplification in OPA, we need to ensure adequate stability of energy, length, chirp, profile and pointing of pump pulses. Here is described how the pump pulses are amplified to the desired energy and what mechanism are used for stabilization.

We have produced supercontinuum using three different pump sources, each of which have a very similar design and produce laser pulses with nearly identical parameters. For this reason, only one of them will be described in detail in this chapter. This pump system is being built within DUHA project (described in detail later in this work), which will be using SC pulses as a seed for high power OPCPA and I was heavily involved in the implementation of this system.

The scheme of the pump laser setup used to generate the pump pulses for the supercontinuum and subsequent OPCPA stages is shown in Figure 12. The initial seed pulse with a repetition rate of 80 MHz and 80 mW of power is generated by fiber oscillator called “Origami”. These pulses are then stretched using a CFBG (chirped fiber Bragg grating), amplified with fiber amplifier back to sufficient power and are used to seed a regenerative amplifier. The pulses are amplified up to 85 W at 2 kHz and are compressed using a grating compressor to 3 ps. The regenerative amplifier is synchronized in time with the Origami using an electronic timing system. Individual parts of this system will be described in detail in following chapters.

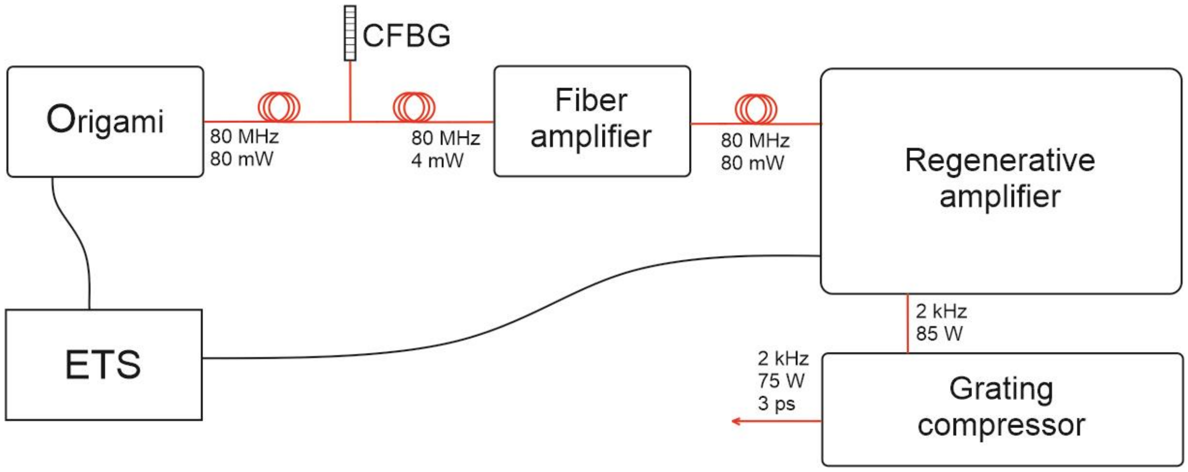

Figure 12: Simplified scheme of pump laser setup. Origami: fiber laser oscillator, CFBG (chirped fiber brag grating): fiber stretcher, ETS: electronic timing system.

2.1 Seed

The starting point for the entire laser system is a fiber soliton-based laser oscillator “Origami” from NKT Photonics. This oscillator produces linearly polarized pulses at 1030 nm with a repetition rate of 80 MHz and other key parameters are summarized in table 1. Figure 13 is photo of the Origami laser oscillator and Figure 14 shows the generated spectra directly at the output and after propagating through 3 m of single mode, polarization maintaining fiber.

Measured element	**Value**	**Units**
Average output power	82	mW
Pulse energy	1.02	nJ
Pulse repetition rate	80.051933	MHz
Pulse duration	635	fs
Center wavelength	1032.4	nm
Spectral width (FWHM)	18.7	nm
Time-bandwidth product	2.01	
Polarization extinction ration	24.8	dB

Table 1: Parameters of Origami oscillator provided by manufacturer.

Figure 13: Photo of Origami laser oscillator consisting of control unit (right) and fiber oscillator itself (left).

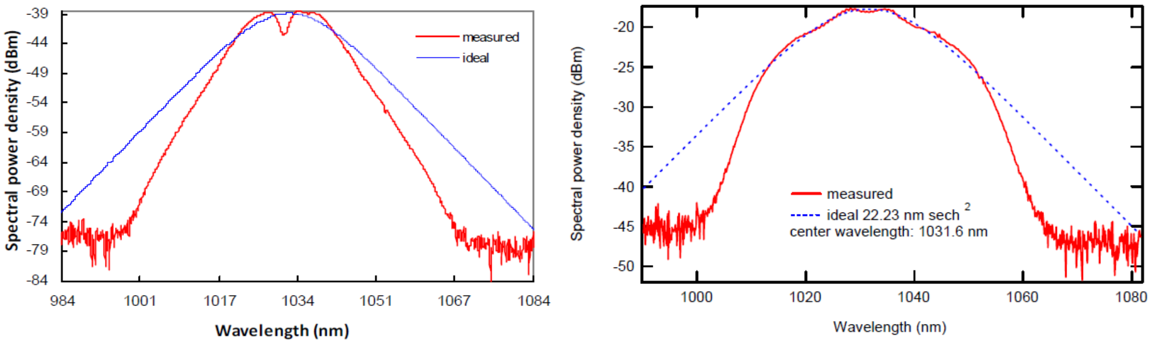

Figure 14:Spectrum of Origami oscilator provided by manufacturer directly at output (left) and after propagating through 3m of single mode, polarization maintaining fiber Panda PM980 (right)

The output of the Origami is coupled to a single mode polarization maintaining fiber (Panda PM980) via an FC/APC connection. Before amplifying, the seed pulses need to be stretched to the proper pulse length. This is achieved using chirped fiber bragg grating (CFBG) with a stretching factor of 350 ps/nm. The generated laser pulses go through a fiber isolator (to prevent reflections back into the oscillator) and a fiber circulator into the CFBG which reflects different wavelengths of light at different position, chirping the pulse. The reflected light goes back through the fiber circulator and another isolator into an Yb-doped fiber amplifier (OneFive GmbH) which compensates the loses of CFBG, FC/APC connectors and other components and amplifies the seed pulses back to 80 mW. The Output of the fiber amplifier is then delivered by polarization maintaining optical fiber to the regenerative amplifier. The scheme of the seed distribution setup is shown on Figure 15. Most of the fiber components are placed inside a single rack mounted box, photo of the box is shown in Figure 16.

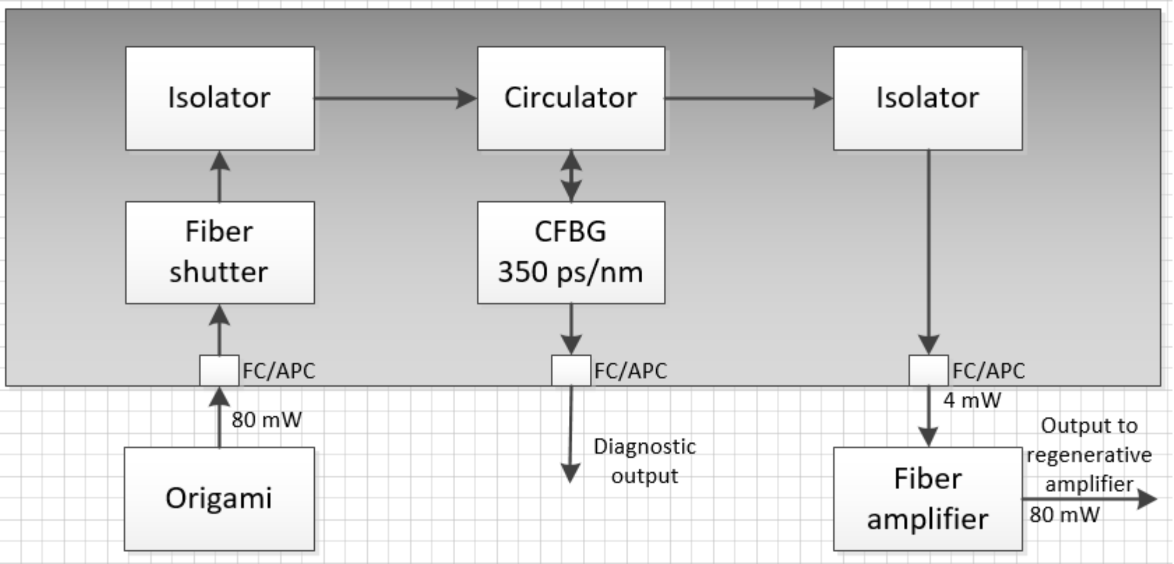

Figure 15: Scheme of seed distribution, stretching pulses generated in Origami oscillator using CFBG (chirped fiber brag grating) and then amplifying them, before sending them to regenerative amplifier.

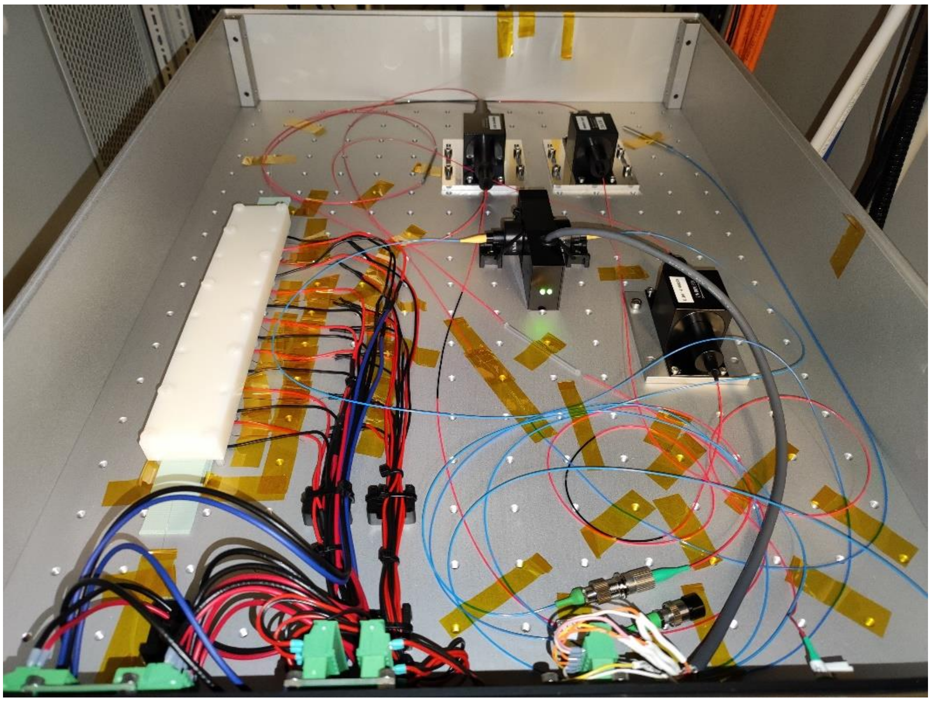

Figure 16: Photo of fiber seed distribution box consisting of CFBG, circulator, two isolators and fiber shuter.

As shown in Figure 15, by going through the seed distribution setup, we lose about 95% of power. Around 90% of these loses are caused by CFBG itself because the spectrum of light reflected by CFBG (4 nm reflectivity bandwidth) is narrower than the spectrum generated by the Origami. The remaining loses are caused by the fiber shutter and FC/APC fiber connectors which have a loss of about 1 dB per connection. Light, which does not get reflected by the CFBG is transmitted and can be used as diagnostic beam, for example to monitor the Origami power level. The CFBG itself is very temperature sensitive and must be carefully temperature stabilized to ensure high quality pulse compression over long periods of time. Constant temperature is achieved by seven Peltier units placed under the stretcher over its entire length, while stretcher itself is surrounded by thermally conductive foam ensuring proper temperature distribution and safety of the actual fiber. A thermometer and stabilization loop is allocated to each Peltier ensuring that the chosen temperature will not change. While the high temperature sensitivity may initially seem to be a disadvantage, this sensitivity can be used to precisely control the GDD and TOD of the stretcher by the application of temperature gradients [62]. This mechanism is already used in the fiber-based front end of the L1 laser [63].

The Origami also provides an RF signal, which is output of an internal photodiode. This signal is used as reference for timing system, allowing proper time synchronization of entire laser system. This requires an uninterrupted operation of Origami, even when the seed itself is not needed. For this reason, the first component after Origami in Figure 15 is fiber shutter, allowing us to contain laser beam inside fiber and operate room in safe laser regime even when the oscillator is still on and providing synchronization signal.

2.2 Regenerative amplifier

The main part of the system generating the pump pulses is a regenerative amplifier (RA), whose simplified optical scheme is shown in Figure 17 and photo in Figure 18. The arriving seed pulse with a repetition rate of 80 MHz and 1 nJ energy goes through a λ/2 waveplate into a pulse picker (PP). The pulse picker consists of a power source, providing high voltage onto a KD*P crystal, which is placed inside a water cooled holder with copper electrodes. When the half wave voltage of 7.8 kV is applied to the KD*P crystal, the polarization of passing laser pulses is rotated by 90°, changing it from vertical to horizontal polarization.

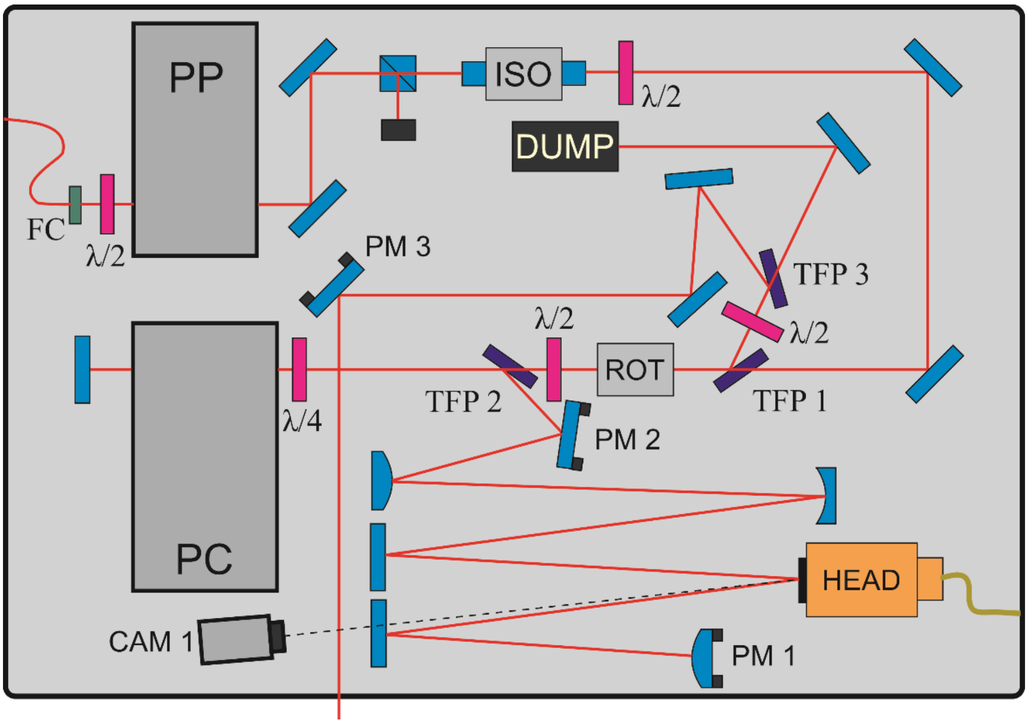

Figure 17: Simplified optical scheme of regenerative amplifier. PP - pulse picker, PC – Pockels cell, ISO – isolator, ROT – rotator, DUMP – beamdump, PM – piezo actuated mirror, HEAD – Thin disk laser head, FC - fiber collimator, TFP – thin film polarizer.

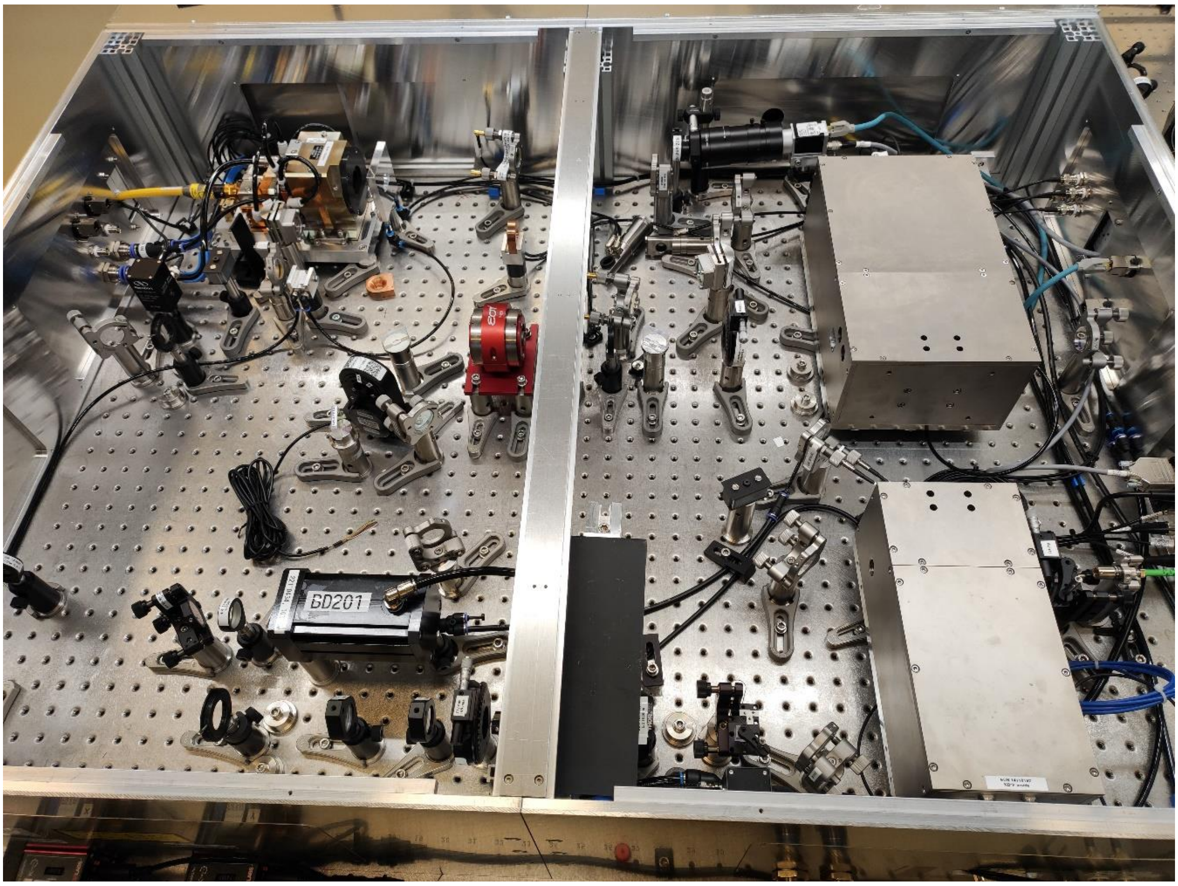

Figure 18: The photo of regenerative amplifier used for generation and further amplification of supercontinuum.

Using the pulse picker, we pick pulses with repetition rate of 2 kHz. In order to pick to pulses correctly, the pulse picker needs to be synchronized with Origami. Nanosecond timing precision is sufficient to pick seed pulses for the RA. This is achieved by electronic timing system (ETS), which has its internal clock synchronized with the Origami oscillator and then provides us with multiple trigger outputs which all are synchronized. A polarizing beam splitter cube is placed after the pulse picker, which is reflecting all vertically polarized (non-rotated) pulses and transmits our picked pulses with 2 kHz repetition rate.

The next element is an optical isolator, consisting of a Faraday rotator and two polarization dependent beam splitter cubes mutually rotated by 45°, which protects the stretcher and oscillator from back reflected amplified pulses. The polarization of the seed is then rotated to vertical using a λ/2 waveplate and its size is adjusted using a three lens telescope to be same size as mode size supported by resonator. Before entering the cavity, the beam passes through a rotator and polarizer which are used for output coupling. The seed passes through a TFP (thin film polarizer) and then a Faraday rotator which rotates the polarization by 45 degrees, λ/2 waveplate (rotates polarization by another 45° to obtain horizontal polarization) and then enters laser cavity through second TFP which works as input and output mirror of cavity.

After entering cavity, the beam goes through a λ/4 waveplate, Pockels cell, with no applied voltage, is reflected by the end mirror back through the Pockels cell and L/4 waveplate. The beam is unaffected by the Pockels cell and by passing through the λ/4 waveplate twice its polarization is rotated from horizontal to vertical, ensuring that it gets reflected by the cavity TFP inside cavity. At this point the Pockels cell is turned on. The round trip time of the cavity is 25 ns and the rise time of the L/4 voltage across the BBO crystal is 3 ns, so when the pulse returns the Pockels cell now provides a L/4 rotation to the polarization. This, with the L/4 waveplate, maintain vertical polarization keeping laser beam inside cavity until Pockels cell is turned off.

The Pockels cell, similar to pulse picker, consists of high voltage power supply and water cooled 12x 12x 20 mm BBO crystal. It is timed precisely that it gets turned on after first pulse passes through and turned off only when pulse inside cavity reaches saturation. The amplifying medium of the regenerative amplifier is a TruMicro series 5000 laser head from TRUMPF Scientific Laser GmbH. The head is based around an Yb:YAG thin disk which is glued onto a water cooled diamond substrate. The disc has a diameter of 9 mm and thickness of 100 µm, which, together with the excellent thermal conductivity of diamond, ensures proper heat extraction and minimizes thermal lensing.

The cavity itself consists of a flat end mirror, convex mirror (r = 5 m), concave mirror (r = -1.5 m), laser head (r = 2.1 m) and convex end mirror (r = -1 m). The expected mode radius inside cavity is shown in Figure 19, which was created with reZonator software. The cavity is designed in a way that the beam passing through the Pockels cell, is as big as possible to reduce the accumulation of *B*-integral. The beam radius at the laser head is around 1.6 mm, which is approximately 80% of the size of the pump spot on the disk to achieve ideal power conversion from pump to seed. The beam size on the disk can be fine-tuned by moving the end mirror closer or further from the laser head to optimize output power.

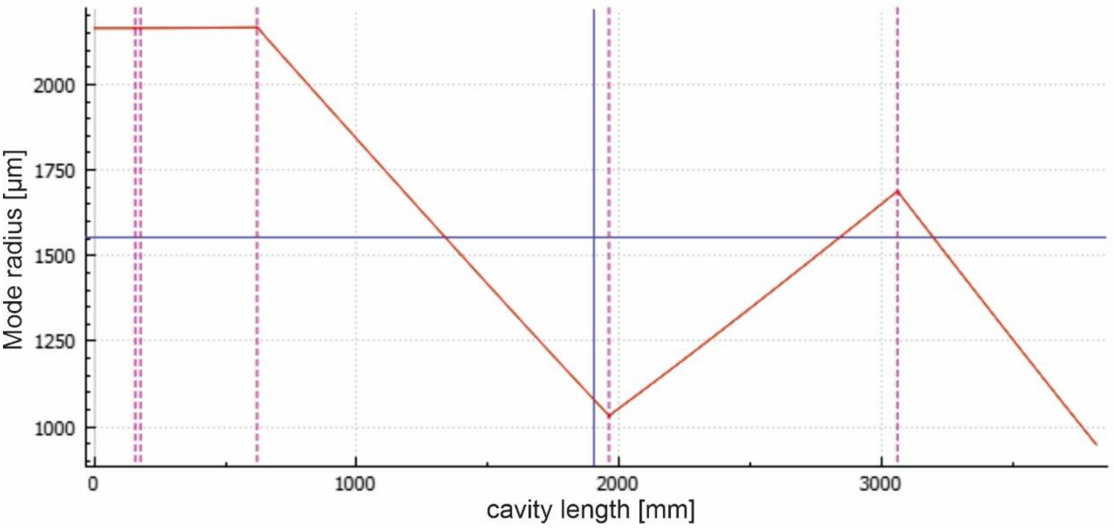

Figure 19: Mode radius inside cavity of regenerative amplifier modeled using reZonator software.

The entire cavity length is nearly 4 m and one round trip (RT) takes around 25 ns. During each roundtrip, the pulse passes two times through laser head which amplifies pulse with each pass, until saturation is reached, where further roundtrips does not add any more energy to pulse. In this case, around 100 roundtrips are needed to reach saturation, which means that our pulse travels nearly 800 m inside cavity. Because of this significant distance, output beam is very sensitive to any instabilities, like air fluctuation, mechanical vibration, or thermal effects. To mitigate the influence of these effects, many of the components are water cooled (laser head, PP, PC, beamdump, camera and irises blocking the parasitic beams) and entire RA is enclosed in aluminium box.

The disc is pumped by a laser diode module from Dilas with a stabilized wavelength of 939 nm (3.3 nm line width), which can provide up to 600 W of continuous pump power with a wall plug efficiency of 50.1 %. The graph showing the dependence of output power and voltage on provided current is shown in Figure 20. The pump light is delivered to the head via fiber and, with help a parabolic mirror and prisms, is imaged 36-times on the disc, resulting in nearly complete absorption of the pump light. The scheme of the laser head is shown in Figure 21. The pump spot on the disk is slightly blurred to reduce the thermal gradient on the edges and to support a larger cavity mode size [64].

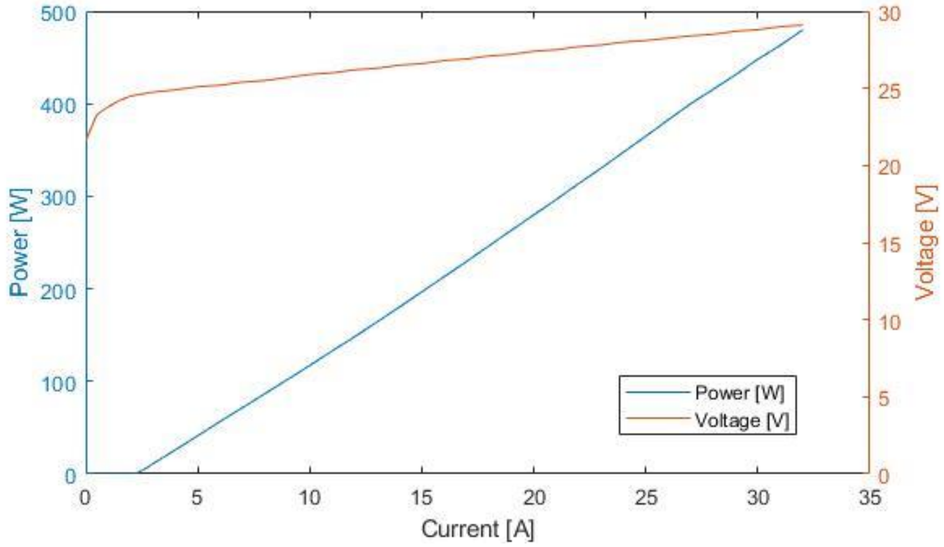

Figure 20: Graph showing the dependence of output power and voltage on provided current with Dilas pump diode module.

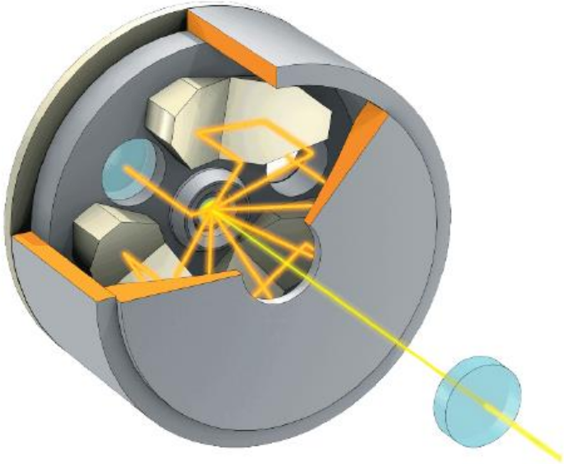

Figure 21: Scheme of laser head, showing pump beam being 36-times imaged onto the disc (courtesy of Trumpf Laser GmbH).

Once the beam reaches saturation, it leaves the cavity through TFP and then λ/2 waveplate which is mounted inside motorized holder. A final TFP is placed after the waveplate which either lets light pass through into water cooled beamdump or reflects it out of regenerative amplifier. By rotating the waveplate we can continuously adjust the amount of light getting out of the RA without having to decrease pump power, which would decrease laser stability (put the RA into a different operational regime with different nonlinearity and thermal load), as RA performs best when saturated. Because waveplate is placed inside the motorized holder, it can be adjusted without opening the laser enclosure, making the procedure very nondisruptive.

The maximum pulse energy generated by this regenerative amplifier is 42.5 mJ with a repetition rate of 2 kHz (85 W of average power). The output beam diameter is 4.5 mm and the wavelength is 1030 nm.

2.3 Grating compressor

Pulses coming out of the regenerative amplifier need to be compressed before they can be used for pumping of following systems. A Treacy compressor consisting of a multi-layer dielectric (MLD) grating pair (Plymouth Grating Laboratory) is used for compression. The gratings have a groove density of 1760 lines/mm, dimensions of 35(W) x 35(H) x 16(T) mm and 120(W) x 35(H) x 25(T) mm, and are separated by distance of 1.43 m with an incidence angle of 59°. The simplified scheme of grating compressor is shown in Figure 22 and photo in Figure 23.

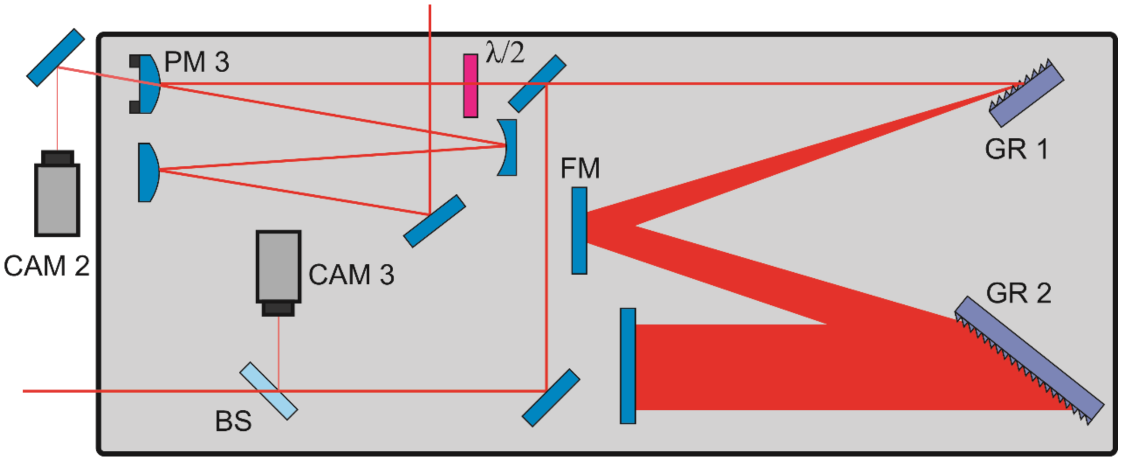

Figure 22: Simplified scheme of grating compressor. PM – piezo actuated mirror, GR – grating, FM – folding mirror, CAM – camera, BS – beamsplitter.

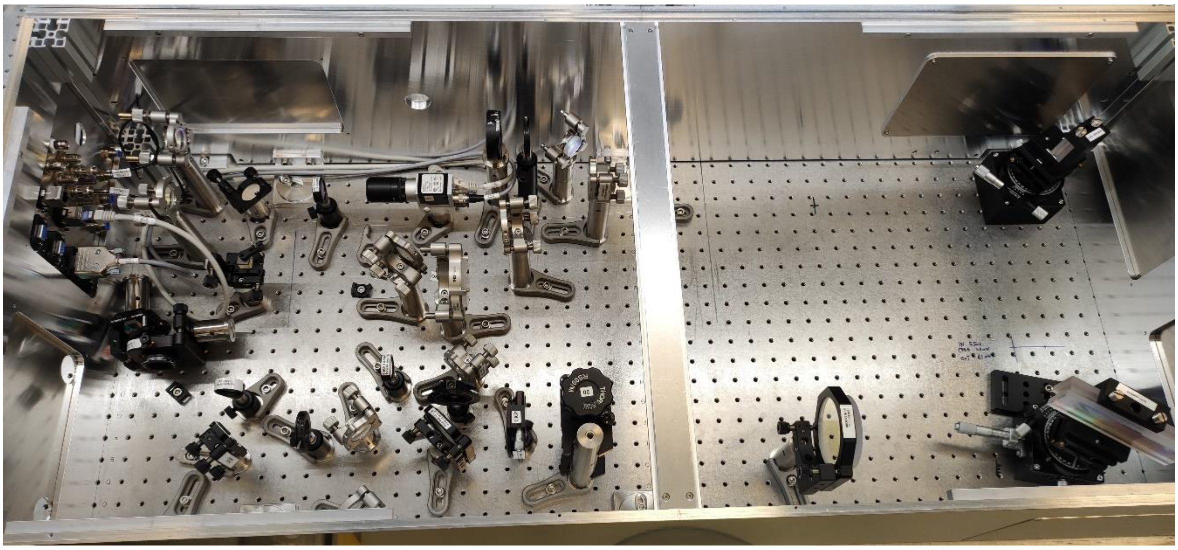

Figure 23: Photo of Treacy grating compressor placed after regenerative amplifier.

The pulses are first resized with a telescope using 3 curved mirrors to a diameter of 7 mm to match the target fluence desired on the SHG crystal placed after compressor. The beam passes through a λ/2 waveplate to ensure the correct polarization, before getting diffracted by the first grating. A folding mirror is placed between the first and second grating to decrease the footprint of compressor. A back reflecting mirror is placed after the second grating which reflects the beam back but at a small angle downward, allowing us to decouple the reflected beam from the input beam. The Fourier transform limit of the incoming pulse is 1.2 ps, however we intentionally over-compress it to obtain a 3 ps long negatively chirped pump pulse.

2.4 Stabilization mechanisms

The long term and short term stability of pump pulses is a very important factor in supercontinuum generation, especially if the SC is used as a seed pulse for OPCPA. Any change in the parameters of the pump beam significantly changes multiple parameters of the generated SC, for example a change in pump energy will not only change the energy of SC but also shift the position of the focus inside crystal, changing the chirp and collimation of the generated SC, which affects OPCPA greatly. For this reason, we implemented multiple active stabilization mechanisms.

2.4.1 Cavity stabilization

A cavity pointing stabilization loop stabilizes the energy of the laser by maintaining proper overlap of the laser cavity mode and the pumped region of the gain medium. The concept of energy stabilisation through active cavity alignment is shown in Figure 24. The thin disk in the amplifier is monitored by a camera (CAM 1 in Figure 17). When the amplifier is pumped but not seeded, photons are spontaneously emitted from regions with excited laser atoms. This light is imaged onto the camera and an image of the pump spot is produced. When the amplifier is seeded, much of the energy from the pump is extracted by the laser pulse circulating in the cavity. Because the inversion is depleted by amplification, the overlap of the amplified pulse and the pump spot is visible as a darker region as shown in Figure 24 (a, b), which corresponds to the position of the cavity mode on the disc.

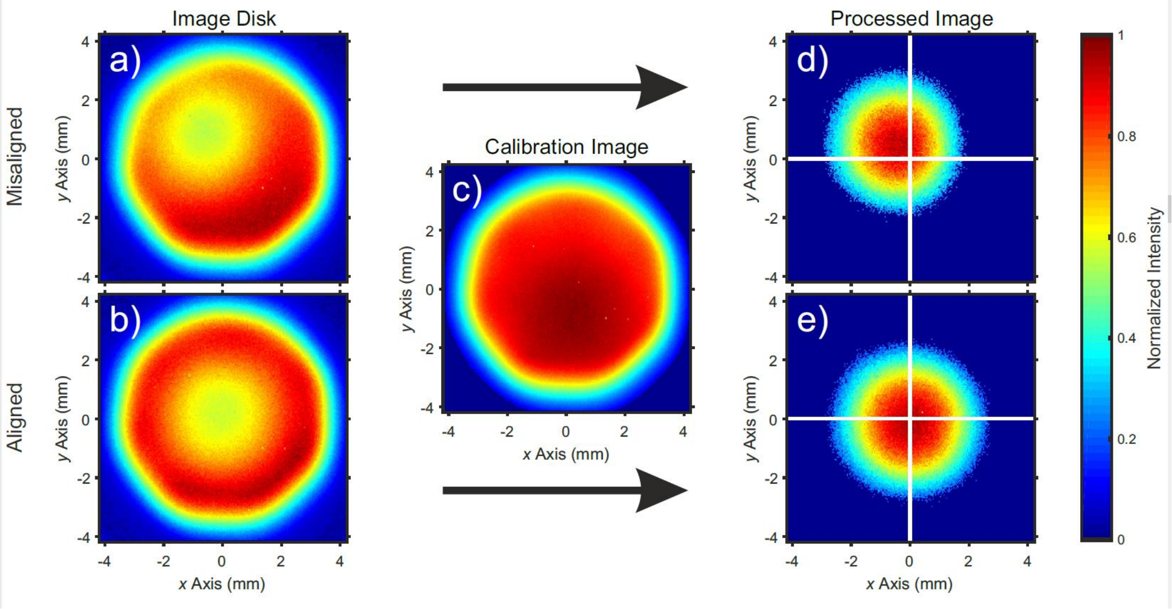

Figure 24: Concept for energy stabilization through active cavity alignment. The raw image of the depleted pump spot for the misaligned and aligned cases is shown in a) an b). This raw image is subtracted from image c), which is the pump spot with the cavity blocked and no depletion present. The resulting difference is a simple circular profile corresponding to the position of cavity mode shown in d) and e) for misaligned and aligned cases. This circular profile is actively centered on the pump profile using a piezo actuated cavity end mirror [65].

The optimum position for this mode is in the center of the pump spot. A cavity misalignment manifests itself as a shift in position of the cavity mode on the disc and often leads to a decrease in efficiency. The energy stabilization loop can be described as follows. The image of the undepleted pump spot on the camera is saved by the camera software as a calibration image and subsequent acquired images are subtracted from this calibration image. After subtracting (a) or (b) from the calibration image (c), the depletion appears as a beam on the camera whose location corresponds to the position of the cavity mode (d), (e). The position of the mode is controlled with a piezo-actuated cavity mirror (PM 1 in Figure 17). The centroid of the depletion is calculated and a feedback loop centres the cavity mode on the centre of the pump spot [65].

2.4.2 Pointing stabilization

With the energy stabilization loop running, the residual pointing error of the output beam is corrected by an external pointing stabilization loop. This 4D pointing loop consists of two piezo actuated mirrors and two cameras (PM 2, PM 3, CAM 2, CAM 3 in Figures 17 and 22). The first piezo actuated mirror (PM 2) is placed at the output of regenerative amplifier. CAM 2 is placed behind PM 3 (at the input to the compressor) looking at leakage through this mirror and beam on mirror is imaged onto camera using telescope consisting of two lenses. The second camera (CAM 3) is located after the compressor.

The centroid of the beam is calculated from camera images and when the beam moves from its designated spot, its position is corrected using the piezo actuated mirrors. This setup ensures that the pointing of the beam coming through grating compressor remains same even after prolonged operation of laser. The repetition rate of this loop is 10 Hz, meaning that while this stabilization works well for slow thermal drifts of beam pointing, it can’t compensate for fast pulse to pulse jumps.

2.4.3 Grating temperature stabilization

The compression of the beam can be adjusted not only by changing the position of gratings inside of compressor but also by changing the temperature and especially temperature gradient of CFBG as mentioned in chapter 2.1. This allows us to change the pulse length of our pump beam without having to physically touch any of the optics. To prevent any random changes in beam compression, due to temperature change of CFBG, an active temperature stabilization loop is enabled. This setup can be potentially improved into active stabilization of pulse compression by adjusting the temperature of CFBG accordingly to changes in pulse length, however this does not seem to be necessary as the pulse length is stable enough simply with temperature stabilization.

These stabilization mechanisms allow us to operate the pump laser for long periods of time without having to do any manual adjustments to the setup, but also significantly improve the ramp up time of system. High power laser system often need a long time to reach a stable operation regime, mainly due the long thermalization of system. In our case this time is significantly shortened, because active stabilization allows us to operate system properly even when warming up.

2.5 Pump laser parameters

Arguably the most important parameters of the pump beam for supercontinuum generation are energy stability, beam spatial profile, spectrum, temporal profile and phase. These final parameters are summarized in this section.

2.5.1 Energy stability

The maximum power output of the regenerative amplifier is around 80W, which at a 2 kHz repetition rate, corresponds to energy of 40 mJ. After passing through the grating compressor which has approximately 10% losses we are left with 72 W. However, for supercontinuum generation we need only small portion of this power, typically around 200 mW (100 µJ). Maximal power is therefore not required for supercontinuum generation, but becomes relevant later for amplification using OPCPA. We are interested mainly in short term (pulse-to-pulse) and long term energy stability.

The long term pulse to pulse measurement of the output energy of the regenerative amplifier is shown in Figure 25. The measurement was taken over a period of 50 minutes on small portion of beam in order to measure every single pulse using pyroelectric energy sensor (PE10-C OPHIR). The energy stability over the entire measurement was 1.0 % RMS, while the short term energy measurement over time a period of 1 minute shown in Figure 25 inset achieved the stability of 0.79 % RMS.

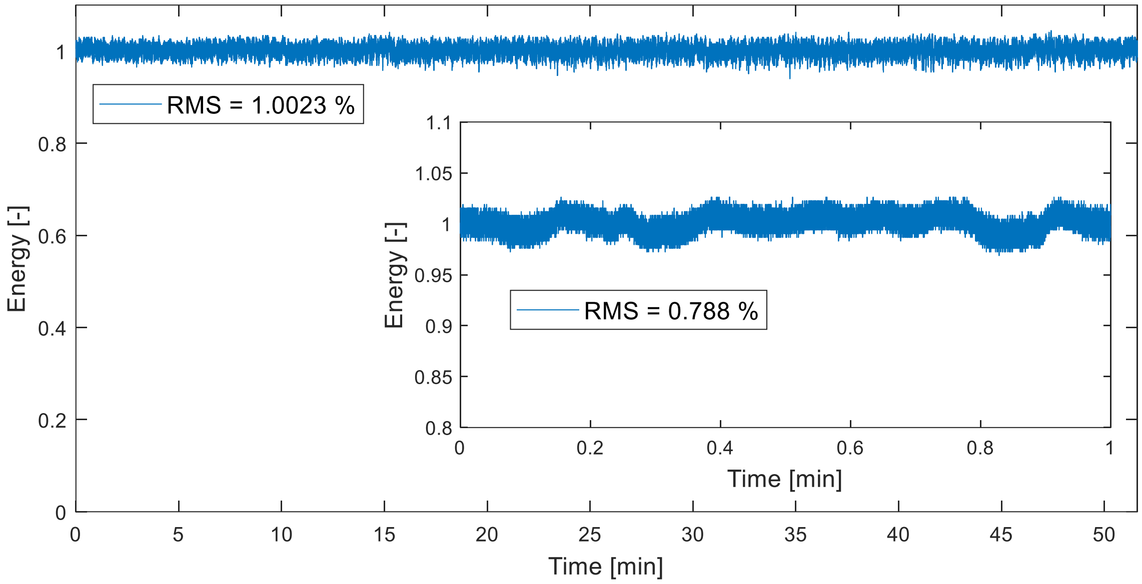

Figure 25: Normalized pulse to pulse measurement of output energy of the regenerative amplifier over period of 50 minutes with the RMS of 1.0 %. Graph inlet shows the pulse to pulse energy stability over period of 1 minute achieving the RMS of 0.79 %.

2.5.2 Temporal profile and spectrum

The temporal profile of the compressed pulses was measured using commercial single-shot Fast FROG from company FemtoEasy. The retrieved temporal and spectral profile with corresponding phases are shown in Figure 26. The spectra width at FWHM is 1.24 nm, which corresponds to Fourier transform limit of 1.26 ps. The pulse is intentionally overcompressed and the temporal profile measured to be 3.58 ps. The pulse temporal shape is not perfect and may be improved in the future by fine temperature tuning of CFBG.

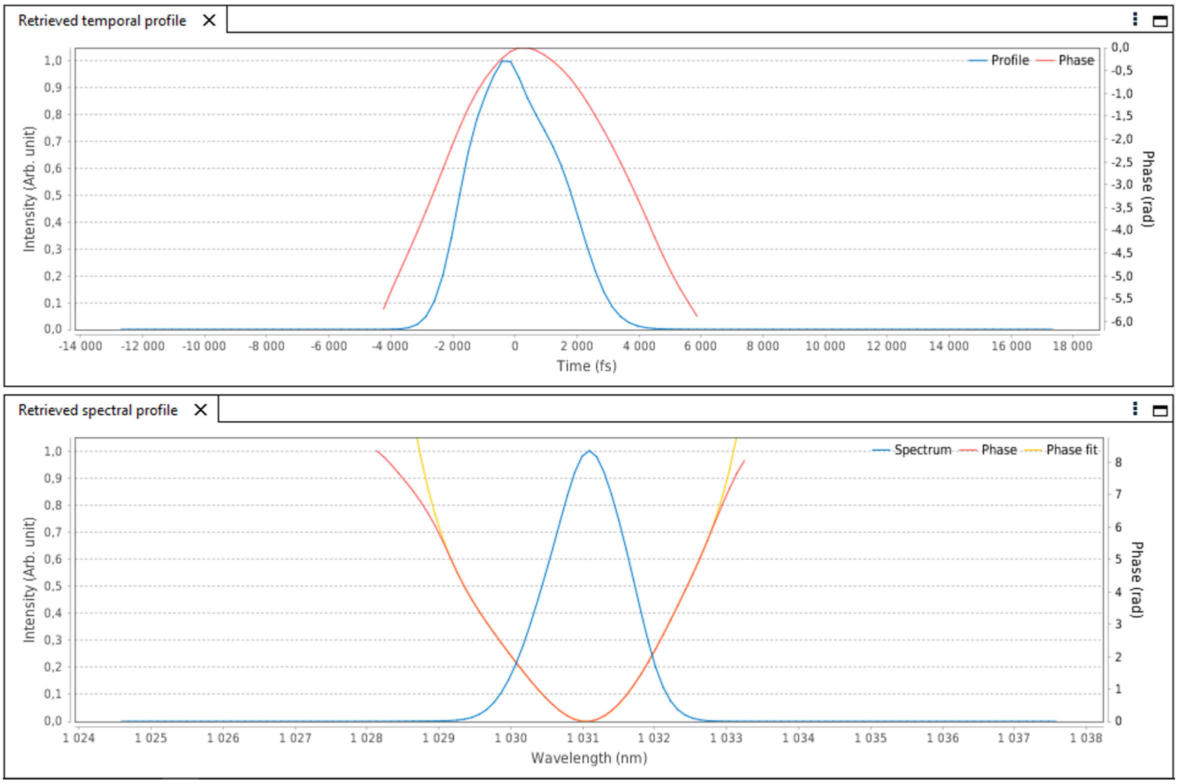

Figure 26: Retrieved temporal (up) and spectral (bottom) profile and their phase.

2.5.3 Beam profile

The beam profile of the compressed pulse was measured with a Camera-based beam profiler SP620 from Ophir company. The beam immediately after the grating compressor is too large to fit onto the CCD of camera, so it was demagnified using a two lens telescope by 50%. The beam profile is shown in Figure 27, the profiles in x and y axis are shown in Figure 28. The diameter of beam at $1/e^2$ is 3.6 mm in x axis and 3.8 mm in y axis, beam is therefore slightly elliptical. This exact beam profile is used as pump for supercontinuum.

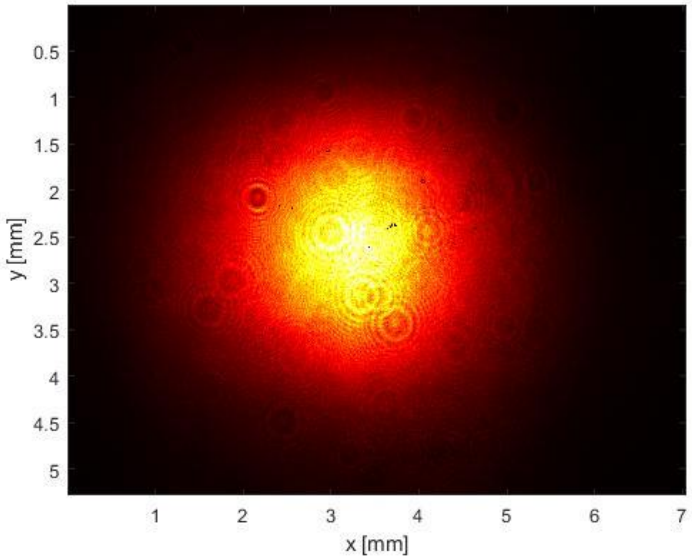

Figure 27: 2D beam profile of pump pulse generated by regenerative amplifier after grating compressor.

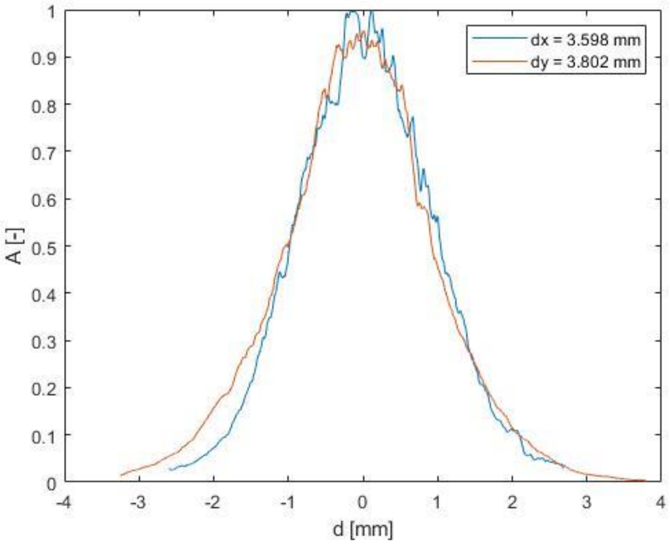

Figure 28: Profile of the beam in *x* (blue) and *y* (red) axis.

3 Supercontinuum generation

In this section supercontinuum generation will be described in detail. While the experimental setup for SC generation is not complex, a variety of parameters can make it difficult to achieve the desired result. The generated supercontinuum is affected by the parameters of the pump beam (pulse energy, length, chirp, spectrum, profile, etc…) and by the geometry of the experimental setup (aperture size, focal length of the focusing lens, position of the crystal) and the effects of these parameters on SC generation will be studied in this chapter. The goal is to find a set of parameters at which the supercontinuum can be reliably generated with sufficient energy and spectral stability, while obtaining as much energy and as broad a spectrum as possible.

3.1 Experimental setup

The general scheme of the experimental setup used for supercontinuum generation is shown in Figure 29. A small portion of the regenerative amplifier output pulse was used as a pump for the supercontinuum as described in previous section (1030 nm, 3 ps, 2kHz), which was picked from main beam with tfp (thin film polarizer). The power of picked beam was about 300 mW which was afterwards attenuated even more using λ/2 waveplate and polarizer. This attenuator allows us to smoothly change pump power going to the supercontinuum crystal, which is very useful when looking for the “stable regime” of SC generation.

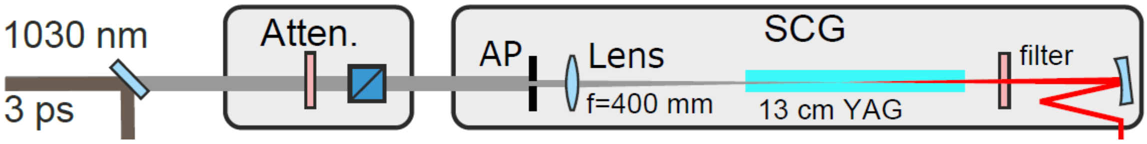

Figure 29: Scheme of experimental setup used for supercontinuum generation, Atten.: attenuator (λ/2 waveplate and polarizer), AP: aperture.

Afterwards the pump beam goes through an adjustable iris aperture which allows us to adjust numerical aperture of the beam. A lens is placed immediately after the aperture which focuses the beam inside or in front of a 13 cm long YAG crystal which serves as the medium for supercontinuum generation. A shortpass spectral filter (Asahi Spectra XIS0960-Shortpass) is placed after the YAG crystal which filters out the pump beam and IR part of supercontinuum and spherical mirror collimating the generated supercontinuum.

A PD-pJ-v2 (Ophir) photodiode-based energy detector capable of measuring single pulses at 2 kHz was used for precise measurement of the generated supercontinuum. A small portion of the generated SC was divided using a splitter for the spectrum measurement using a spectrometer (USB4000-UV-VIS, Ocean Optics). We are also interested in relative stability of the SC in comparison to pump, which means that the energy stability of the pump laser needs to be measured simultaneously. For this, another splitter was placed between the attenuator and aperture and the reflected part of beam was measured using a pyroelectric sensor PE9 (Ophir), also capable of single pulse measurement.

With this setup we can correlate the energy of the supercontinuum and pump laser. The effect of optical splitters was taken into account and correct values of pump and generated light were always calculated afterwards with help of calibration measurements. The pump energy measurement had to be re-calibrated after every change in aperture diameter. Also, every pointing instability of pump laser was translated into energy instability after passing through aperture, but these instabilities were not measured by the pyroelectric sensor placed before aperture. The pointing instability can be possibly taken into account during the measurement if the sensor was placed between aperture and iris, but we want the aperture and focusing lens to be as close together as possible to prevent change in beam shape by propagating over long distances after diffraction on aperture.

3.2 Results interpretation

When trying to achieve a stable supercontinuum we can adjust the parameters of the pump laser (pulse energy, temporal and spatial profile, chirp, *B*-Integral) and the geometrical setup (size of aperture, focal length of lens, position of crystal in relation to position of focus). However, these parameters are not independent, meaning that we can’t easily find ideal set of parameters by adjusting one after another to optimal values. Arguably the most important parameter is pump energy, whenever any of the other values are changed, the optimal enery for stable generation will change and must be adjusted.

Because finding the ideal energy after every change in geometrical setup or pump beam is not trivial, we performed an energy scan which can be done by continuously rotating the waveplate in front of the polarizer. If the energy of pump and generated supercontinuum is measured simultaneously during this scan it is possible to plot energy of SC as the function of pump energy. The “ideal” energy scan of the supercontinuum energy is shown in Figure 30 b) and a) shows photo of filament generated inside YAG crystal during SCG.

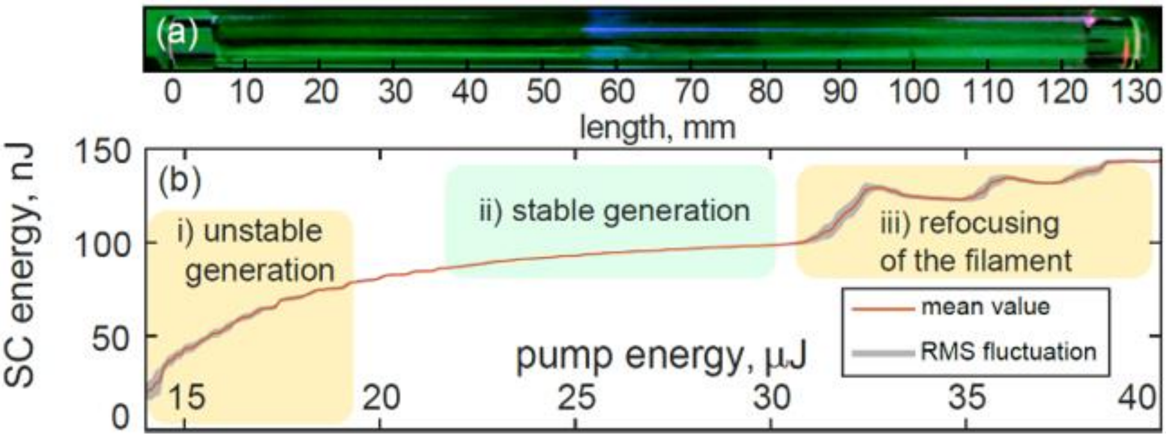

Figure 30: a) photo of YAG crystal with visible filament, b) Dependence of supercontinum energy on pump energy in ideal situation [66].

In the energy scan graph, the slope of the line shows how much the supercontinuum energy changes with pump energy and the width of the line corresponds to pulse to pulse energy stability of SC. The best possible location for SC generation is the area where the line has the smallest possible slope and lowest fluctuation. In this regime, the fluctuations of pump energy do not affect SC generation very much and we can even obtain a SC with better stability than the pump itself.

As shown in Figure 30 b), the energy scan graph can be split into three regions. The first region (*unstable generation*) is right after the threshold for supercontinuum generation, the energy of the SC is increasing quickly with pump energy, pulse to pulse stability is bad and the position of the filament inside crystal is fluctuating quickly. By increasing pump energy further, we enter the *stable generation* regime, where the SC energy and filament position does not change very much with pump energy. In the last regime, a second filament is formed after the first as described in section 1.4. When the formation of the second filament occurs a significant jump in SC power can be observed and sometimes the second filament can be directly visible inside the crystal. In this regime, the pulse to pulse stability of the supercontinuum is very bad, the SC energy jumps up whenever new refocusing occurs and filament is usually visibly moving inside crystal at a constant pump power.

It is clear that we want to always generate supercontinuum inside the stable regime; however, it is important to note that the existence of stable regime is not guaranteed. Often the stable regime is not present and, instead the energy of the SC grows linearly growing until it reaches the refocusing regime. Sometimes the stable regime may have small range, or pulse to pulse stability which is significantly worse than that of the pump energy. The following chapters are devoted to finding the parameters of the pump and an experimental setup leading to the generation of a proper stable regime and the best possible supercontinuum.

3.3 Dependence on crystal position

While it seems natural to place the crystal such that the focal spot of the pump beam is located right at the front surface of rod or right after it, it is interesting to observe the behaviour when the focal spot is moved further inside the crystal or in front of the crystal face. In this chapter we investigate how supercontinuum generation behaves when we change the distance of the YAG crystal front surface from the focal spot of the lens with 400 mm focal length. For each position we performed an energy scan as described in Section 3.2, while maintaining all the other parameters unchanged. The set of energy scans performed with the position of the focal spot of pump beam ranging from 11 cm inside the crystal to 4 cm in front of the crystal is shown in Figure 31.

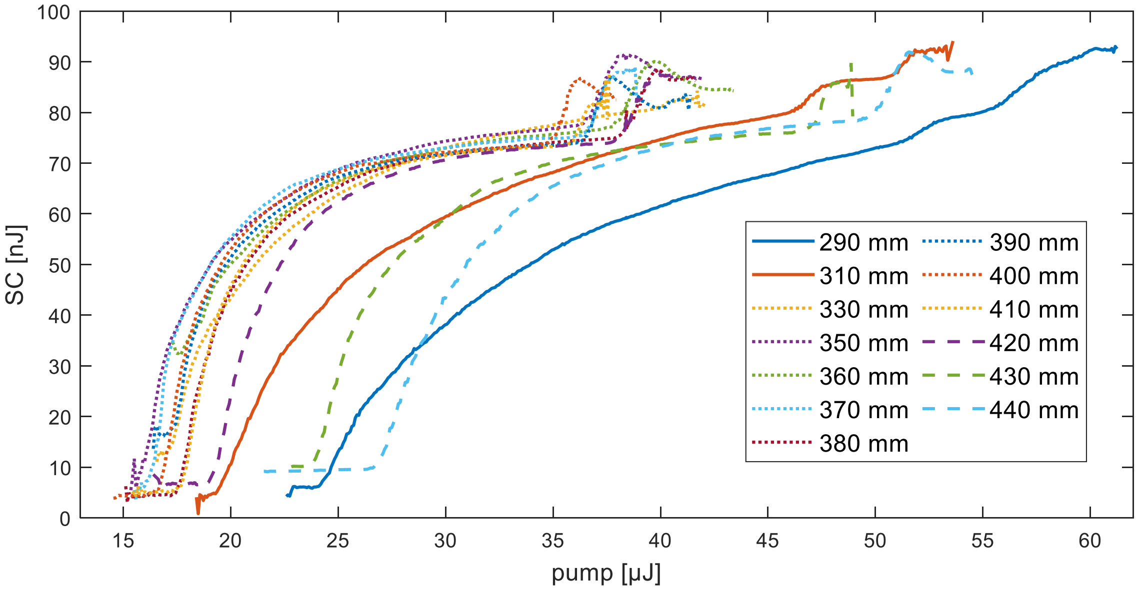

Figure 31: Energy scan of the dependence of the supercontinuum energy on pump energy for different distances of the YAG crystal front surface from the 400 mm focal length focusing lens.

The legend in Figure 31 shows the distance of the front surface of crystal from the lens and we can see that scans ranging from 330 mm (7 cm inside of crystal) to 410 mm distance (1 cm in front of the crystal), shown in graph as dotted lines, are very similar. The scans indicated by dashed lines between 420 mm and 440 mm (2 and 4 cm in front of the crystal) are similar in shape, but are shifted to the right side of the graph, which means that to generate supercontinuum in this arrangement requires more pump power. This is expected, because the beam entering the crystal is divergent, has larger diameter and hence requires more power to get self-focused.

The energy scans for distances of 310 mm and 290 mm (9 and 11 cm inside of crystal), presented with solid lines, have their generation threshold increased as well. In this case it is caused by lack of material after the focal point. Normally, when the threshold for supercontinuum generation is reached, the filament is observed multiple centimetres behind the focal point of the lens and then moves closer to it with an increase in pump power. However, in this case, the focal point is close to the end surface of crystal (just 2 cm for most extreme case) and the beam does not have enough material in front of it to get self-focused and generate SC. In these cases, stronger self-focusing is needed to generate the continuum before the end of the crystal, increasing the SC threshold. These two scans also have a different shape than others, lacking the desired stable region of generation, and instead just steadily increasing with pump power. We believe this is the result of the full filament not fitting within the crystal. Even with enough pump power to generate SC, the filament (which is generally multiple cm long) does not fit inside the crystal and is abruptly cut by the end surface, instead of ending naturally due to plasma defocusing and diffraction.

This actually provides important information about the smallest possible length of crystal which can be used in this particular configuration with 3 ps pulses. It seems that crystals with a length of 4 cm and less will be too short, because there will be not enough distance for entire filament to evolve even while focusing the pump beam directly on the front surface. This is case only for these specific parameters, for example, a supercontinuum generated using femtosecond pulses requires much less pump power and can be focused using lenses with much shorter focal lengths. In these conditions, the YAG crystals can have lengths of only few millimetres.

Another interesting observation which can be made from Figure 31 is that changing the position of focal spot inside the crystal over quite a long distance (around 5 cm in this case) affects the SC generation only slightly. This means that the only parameter of the generated SC we change by moving the crystal along the z axis is the pulse duration due to dispersion in the material after the filament. In practice this is quite a useful tool if we want to amplify the generated SC with OPCPA. The temporal length of the seed pulse can be continuously adjusted by just shifting position of the crystal along the z axis, in our case removing the need for a tuneable picosecond pulse stretcher. This method also changes the delay between OPCPA pump and seed, because supercontinuum gather different group delay in YAG crystal than 1030 nm beam. This potential use of excess crystal length might be another factor to consider when designing a setup for supercontinuum generation.

To determine which focal spot position is most desirable the best achieved energy stability was calculated. This was done by splitting each of the energy scans into multiple shorter regions, calculating their respective RMS, and then picking the best of them. The best achievable short term energy stability for different position of focal spot are shown in Figure 32. The best RMS of 0.39 % was obtained with a focal spot positioned 1 cm and 2 cm in front of the front surface of crystal. However, the energy stability in other positions is still under 0.5 % with the exception of the last two positions close to the end surface of the crystal. It seems that the generation of stable SC is possible with the focal spot in front of the crystal as well as inside as long as there is enough material after the focus for the filament to fully evolve.

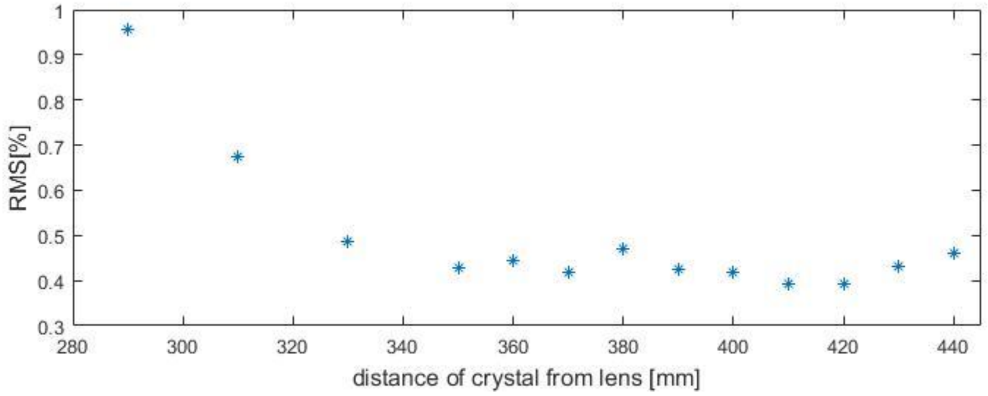

Figure 32: Best achieved supercontinuum stability at given distance between the front face of the YAG crystal and the 400mm focal length focusing lens.

Figure 33 shows how the threshold for supercontinuum generation changes for different positions of focal spot. With enough pump power, the SC can be generated even when the focal spot is as far as 10 cm in front of the crystal or even when completely behind the crystal, although these are certainly not ideal positions for generation.

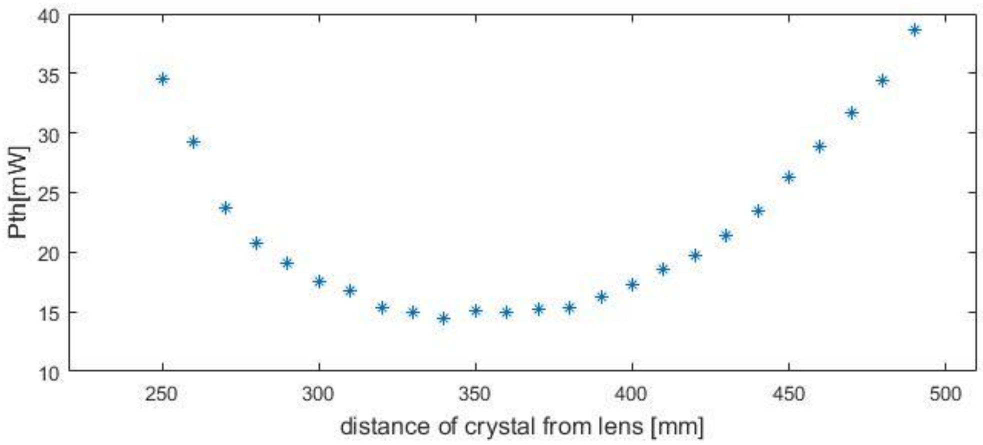

Figure 33: Dependence of supercontinuum generation threshold on YAG crystal front surface distance from a focusing lens with 400 mm focal length.

3.4 Dependence on focal length of the lens

The spatial profile is heavily affecting process of supercontinuum generation. The focal length of used focusing lens is directly affecting the size of beam in the focal spot as well as Rayleigh length. These two important parameters are also affected by the size of collimated beam passing through the lens. The size of the beam in the focal spot decreases with increasing size of the beam which is getting focused and on other hand is increasing with larger focal lengths of the lens.

In this case the pump beam with diameter of 3.7 mm was focused in front of the YAG crystal by lenses with focal lengths of 300 mm, 400 mm, 500 mm and 750 mm. The calculated Rayleigh lengths and diameters of the beam at focus for all used lenses considering $M^2 = 1.1$ is summarized in Table 2. The Pumping of the YAG crystal with diverging beam was chosen on purpose to decrease the likelihood of causing the laser induced damage during the SC generation with short focusing lens. The measured energy scans of generated supercontinuum with different focusing lenses are shown in Figure 34.

Focal length [mm]	Beam diameter at focus [µm]	Rayleigh length [mm]
300	117	10
400	156	19
500	195	30
750	292	65

Table 2: Calculated Rayleigh length and diameter of the beam at focus for used lenses.

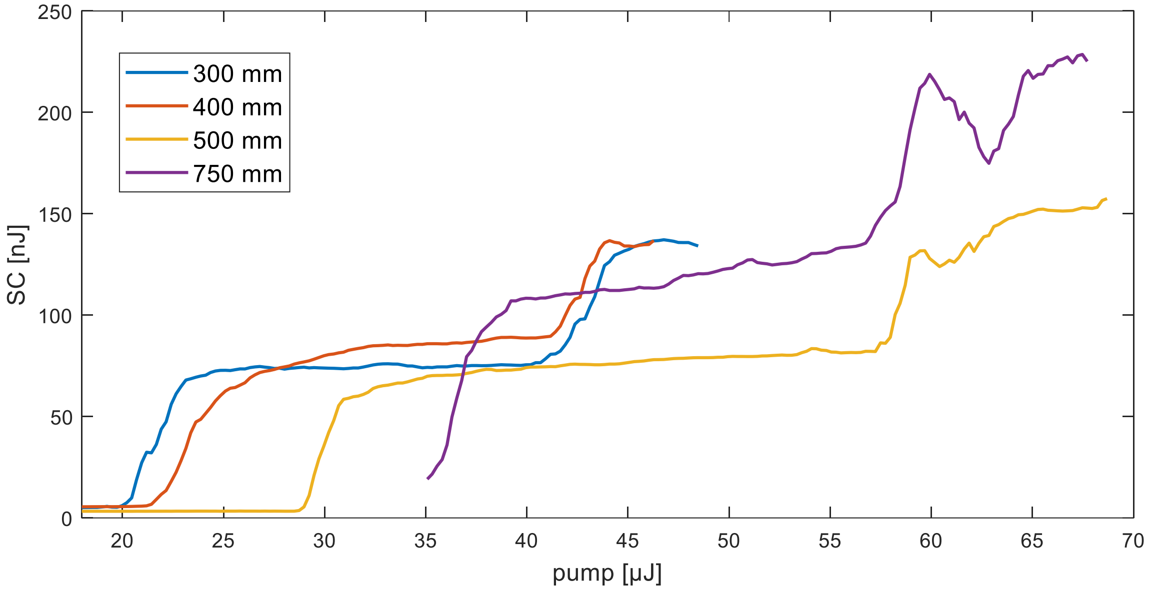

Figure 34: The Energy scans of the generated supercontinuum using different focusing lenses.

The best energy stability of the generated supercontinuum of 0.71 % RMS was achieved with lens with 400 mm focal length narrowly surpassing the stability of pump laser (0.77 % RMS). The stability of SC generated with 500 mm lens was 0.75 % RMS, being slightly worse that the SC obtained with 400 mm lens, but generating noticeably longer stable regime. The stable regime of the supercontinuum generated with 300 mm lens was very “flat”, seemingly not affected by increase in the pump energy at all, however the pulse to pulse energy stability was significantly worse than in previous cases. Stability of SC generated with 300 mm lens as well as 750 mm lens was worse than 1 % RMS, being worse than stability of pump laser. The focusing lens needs to be chosen while taking the size of the pump beam into account. The larger pump beam will require focusing lens with longer focal length and vice versa. The size of pump beam can be also adjusted either by telescope or by clipping off small portion of beam by an aperture.

3.5 Dependence on input aperture

Focus of Gaussian beam diffracted by a circular aperture deviates from Gaussian focus and the far field begins to approach that of a circular beam with an Airy disk. Even in the case of negligible power losses through the aperture, the diffracted beam characteristics may appreciably differ from those of the incident beam [67], [68], [69]. Supercontinuum generation is significantly influenced by the size and spatial profile of the pump beam, so a change in the generated SC beam is expected when the diameter of input aperture is changed.

Supercontinuum energy scans for different input apertures are shown in Figure 35. The size of the pump beam before the iris aperture is 3.2 mm and the measured energy scans are with iris diameters of 1.7 mm, 2.2 mm, 2.6 mm, 2.9 mm and fully open iris, not restricting beam at all. An aperture diameter of 2.9 mm results in the best stability of 0.47 %. By further decreasing the diameter of the aperture, the stable regime of generated supercontinuum shortens and best obtained stability gets significantly worse. The shape of a beam passing through an aperture significantly smaller than its diameter cannot be considered Gaussian anymore and the stability of the supercontinuum generated with such is significantly worse. This trend of generated SC getting worse with aperture significantly than the beam size is consistent and can be observed for pump beam with any parameters. The shift in threshold energy visible in Figure 35 is expected, since focusing a beam with smaller diameter leads to larger focal spot, which needs more energy for self-focusing.

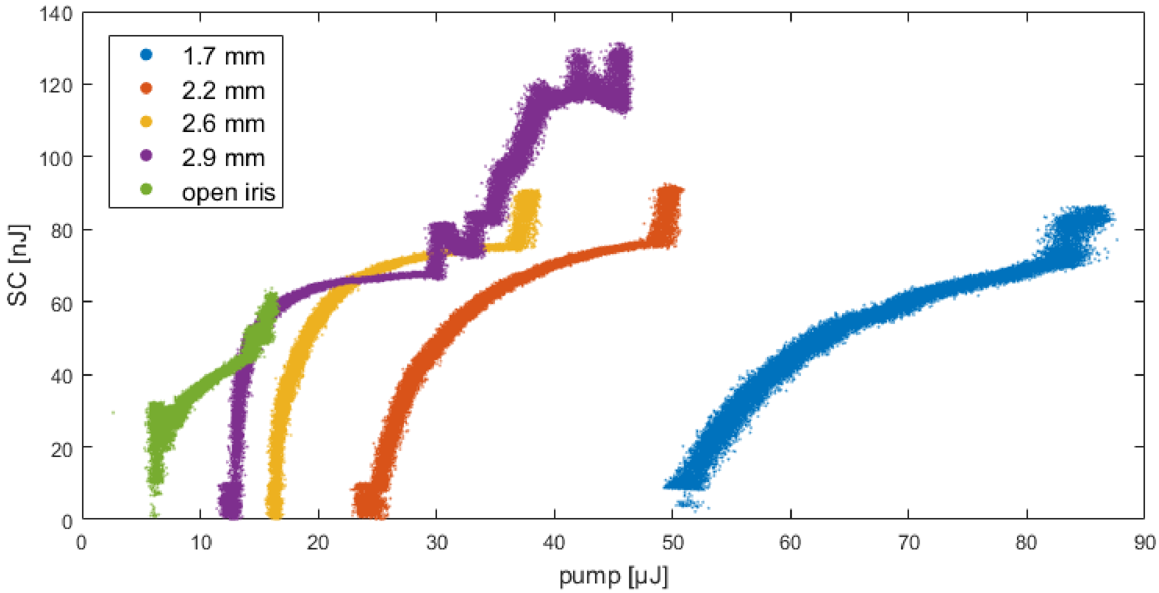

Figure 35: Energy scans of supercontinuum generated with different aperture sizes.

In this measurement the worst energy scan was clearly obtained with open aperture. However, this result is not consistent at all and varies heavily with the pump beam being used, sometimes, even getting better results than with aperture. The reason for this is that aperture can cut off an imperfect outer parts of Gaussian beam which might be disturbing SC generation inside the crystal. The SC is very sensitive the spatial profile of the beam and spotting these imperfections can be difficult even when looking at the near field and far field of pump beam with a camera. However, if a “nice” Gaussian beam is used as a pump, the aperture does not add any extra value. This situation is shown in Figure 36, the 25 minutes long pulse-to-pulse energy measurement of supercontinuum and pump beam was obtained with different pump laser (part of F-SYNC system described in chapter 5.2) providing 4 ps long pulses with maximum energy of 112 mJ at 1 kHz repetition rate. The supercontinuum was generated with an open aperture and YAG crystal was placed 420 mm after focusing lens with 400 mm focal length. The measurement shows, that in the right conditions, very stable supercontinuum (0.35 % RMS), can be generated even without an aperture.

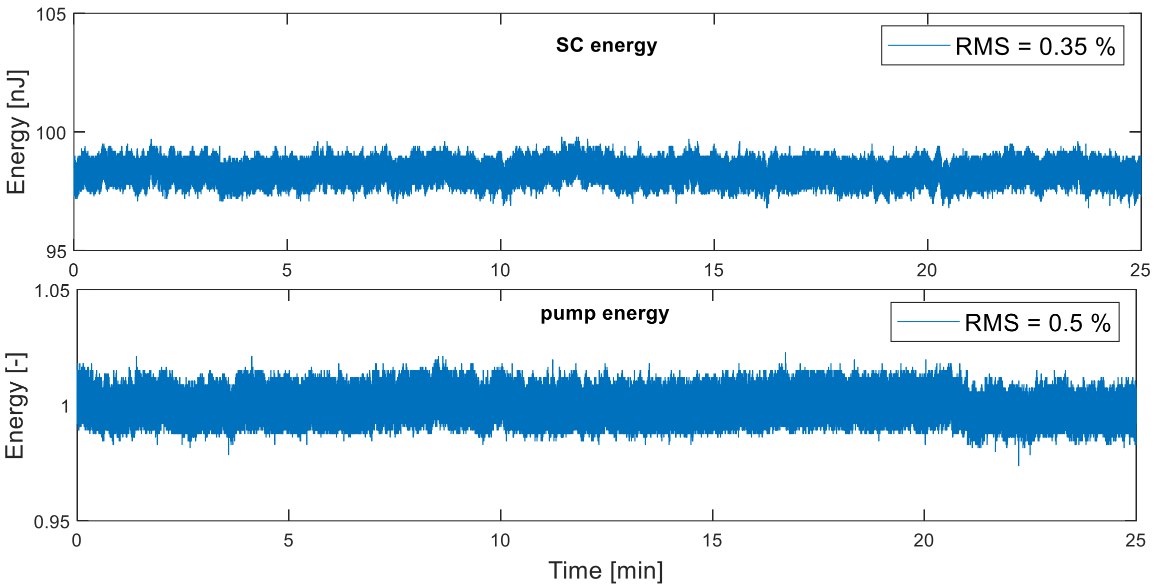

Figure 36: The measured pulse-to-pulse energy stability of supercontinuum generated with an open aperture (top), and coresponding pulse-to-pulse energy stability of pump beam (bottom). This measurement was obtained with F-SYNC pump laser.

The aperture also increases the dependence of the generated supercontinuum on the pointing stability of the pump beam. If changing beam pointing moves the pump beam on the aperture, the energy and profile of the focused pump beam will change as well, decreasing the stability of the SC. For this reason, it is actually better to generate SC without using an aperture if possible. In the case that it is not possible to properly generate a SC (such as in Figure 35) and improving the spatial profile of the beam is also not feasible, an aperture slightly smaller than the diameter of the beam can help significantly, but the pointing stability of the pump laser has to be ensured.

3.6 Filament diameter and length

The supercontinuum generated inside the crystal is naturally divergent, therefore the diameter of the output beam at the output face of the crystal is dependent on the position where the supercontinuum is generated inside the crystal. This position can be approximately determined by observing the position of the filament, which is visible when observing the crystal from the side. We assume that the supercontinuum begins to diverge at the end of the filament, so the measured filament position is taken at end of visible part of the filament. If we measure the size of the beam at the output of the crystal for different positions of the filament inside of the crystal, we can determine the divergence of the beam and its size at the position where it was generated, which should be same as the filament diameter. The scheme of experimental setup for this measurement is shown in Figure 37.

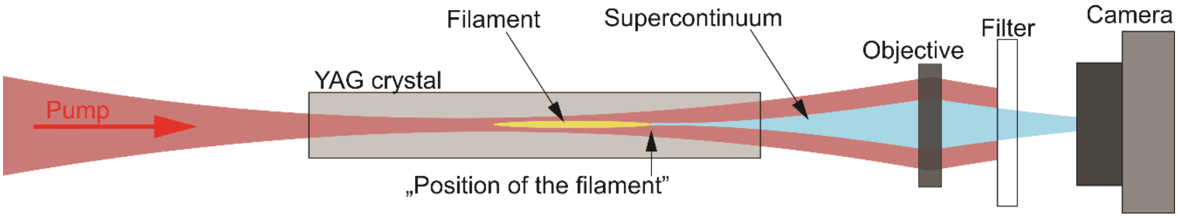

Figure 37: Experimental setup for measurement of filament diameter.

The output face of the YAG crystal was imaged on a beam profiler (SP620, Ophir) with 10x microscopic objective. The 1030 nm pump beam was filtered with 950 nm lowpass spectral filter and the size of the beam measured with the beam profiler was calibrated using the microscopic calibration test placed at the output face of YAG crystal. The filament position inside the crystal was changed by adjusting the energy of the pump pulses and position of the YAG crystal; with an increase in pump energy, the position of the filament moves closer to the front face of crystal, which is expected because self-focusing of pump beam happens sooner and faster. The diameter of the measured supercontinuum beam profile at $1/e^2$ in x and y axis for different filament positions is shown in Figure 38. By extrapolating measured data (considering Gaussian propagation at 800 nm) we can estimate the size of filament to be around 8 µm. While this measurement is not very precise, especially because the visible filament is quite long and we don't know where exactly the supercontinuum beam is generated, the estimated size corresponds well with previously modelled [44] and measured [43] values.

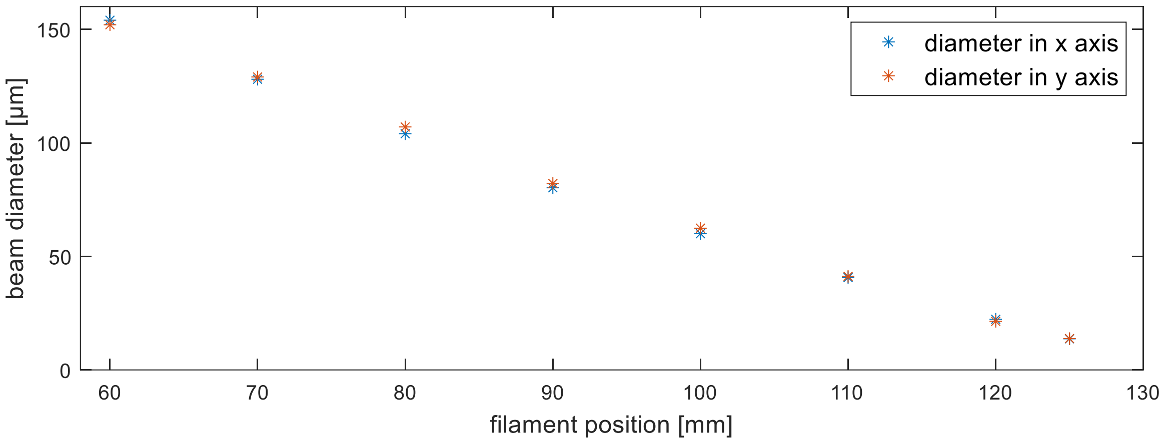

Figure 38: Dependence of SC beam diameter on the exit face of the YAG crystal on the filament position inside the crystal.

When shifting the position of the filament inside the crystal by changing the pump energy we can also observe a significant change in length of visible portion of the filament. Increasing the pump energy not only moves the filament closer to the front face of the crystal, but also increases its length. The dependence of length of the visible portion of the filament, observed from the side of the crystal, on filament position inside the crystal is shown in Figure 39.

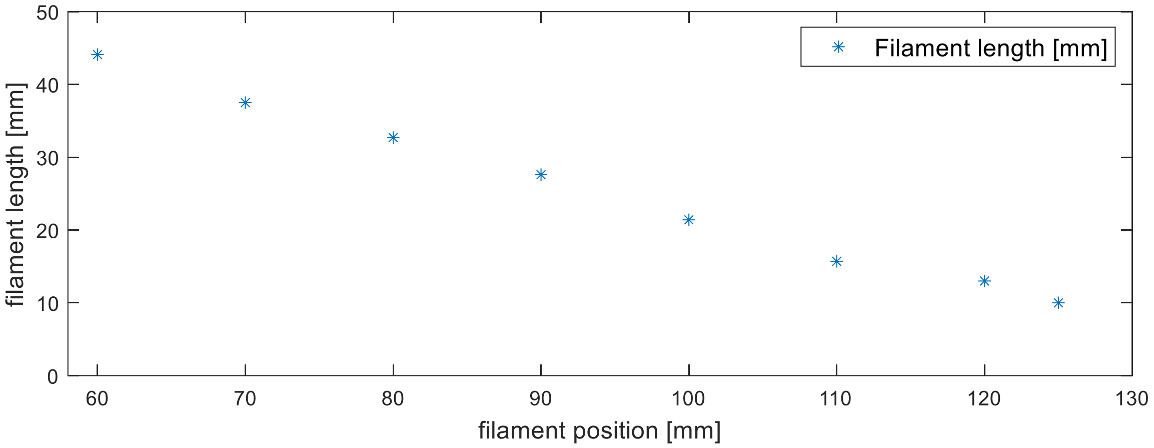

Figure 39: Dependence of the observable filament length on filament position inside crystal.

3.7 Spatial coherence

Since the spectrum of the supercontinuum is extremely broad, its coherence length can be rather short, ~ 1.6 µm [70]. The coherence properties of the supercontinuum are important for many applications: OCT (Optical Coherence Tomography), frequency combs, generation of intense pulses, stabilization of a pulse-to-pulse phase relationship, attosecond jitter, and control of quantum states; to name a few important ones. In our case, the coherence is mainly important to ensure the possibility of pulse compression.

The spatial and temporal coherence of a supercontinuum generated in various materials was numerically [71] and experimentally [72], [73], [74] studied mostly for femtosecond pulses. The coherence of our supercontinuum generated with picosecond pulses was experimentally verified using Young's double hole interference experiment. The theoretical and practical implementation of the method used here is described in detail in: [75].

A simplified scheme of the experimental setup used to measure spatial and temporal coherence of the generated supercontinuum is shown in Figure 40, where r_1 is the filament diameter, f_1 the focal length of lens, $2a$ the diameter of the circular apertures, $2h$ the separation of apertures and l is the distance of apertures from the camera. The supercontinuum is collimated by lens, passes through two circular apertures and creates an interference pattern which is recorded by the camera (Figure 41).

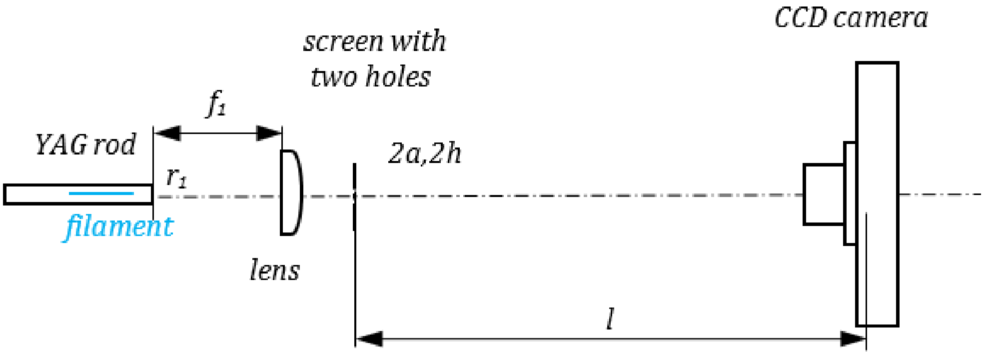

Figure 40: A simplified scheme of the experimental setup used to demonstrate supercontinuum coherence using Young's double hole interference experiment; r_1: filament diameter, f_1: focal length of lens, $2a$: diameter of circular apertures, $2h$: separation of apertures, l: distance of apertures from camera.

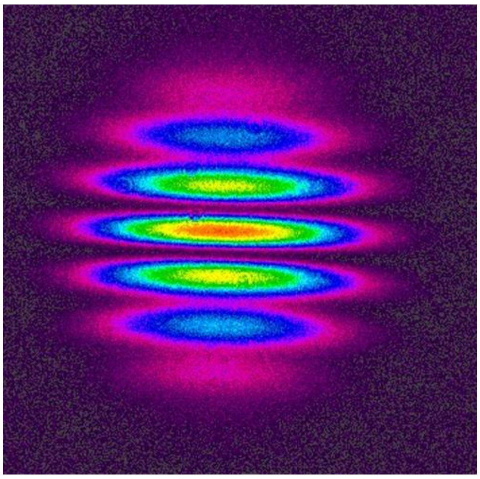

Figure 41: Interference pattern created by supercontinuum diffracted on two circular holes recorded by a CCD camera.

To obtain an information about the coherence of supercontinuum from the measured interference pattern it needs to be fitted by a function describing the theoretical spatial intensity distribution of an interference pattern obtained by Young's experiment [75]:

$$I = 2\left(2\frac{J_1(v)}{v}\right)^2 \left(1 + f(x, l_{coh})\left|2\frac{J_1(u)}{u}\right| \cos(-\delta)\right), \tag{15}$$

Where J is a Bessel function and $\delta = Cuv$. Parameters C, u and v are given as:

$$u = \frac{2\pi}{\lambda}\frac{2h}{f_1} r_1, \tag{16}$$

$$v = \frac{2\pi}{\lambda} a \sin\left(\tan^{-1}\left(\frac{x}{l}\right)\right), \tag{17}$$

$$C = \frac{\lambda f_1}{2\pi r_1 a}. \tag{18}$$

For continuous laser radiation with a long coherent length the function $f(x, l_{coh}) = 1$, while for pulsed laser with coherent length l_{coh} function is defined as:

$$\begin{aligned} f(x, l_{coh}) = \exp\Big[\big(\{[(x_0 - h) - x)]^2 + l^2\}^{1/2} \\ - \{[(x_0 + h) - x)]^2 + l^2\}^{1/2}\big)/l_{coh}\Big]^2. \end{aligned} \tag{19}$$

The function $f(x, l_{coh})$ is entirely dependent on the experimental setup which is schematically shown in Figure 42.

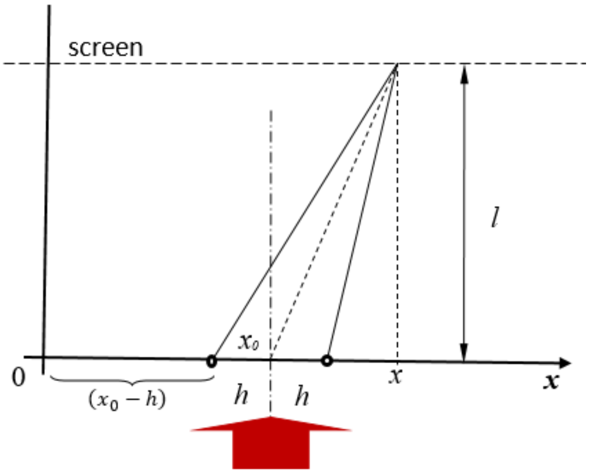

Figure 42: Scheme of Young's interference experiment where beam coming from bottom passes through two aperture separated by distance 2*h* and arrives at CCD screen.

The 2D graph of the spatial intensity distribution in the *y* axis of measured interference pattern shown in Figure 41 is plotted and fitted by function (15) in Figure 43. The theoretical function fits well with measured experimental data and provides us with the coherence length of the generated supercontinuum $l_{\mathrm{coh}} = 2.14\ \mu\mathrm{m}$.

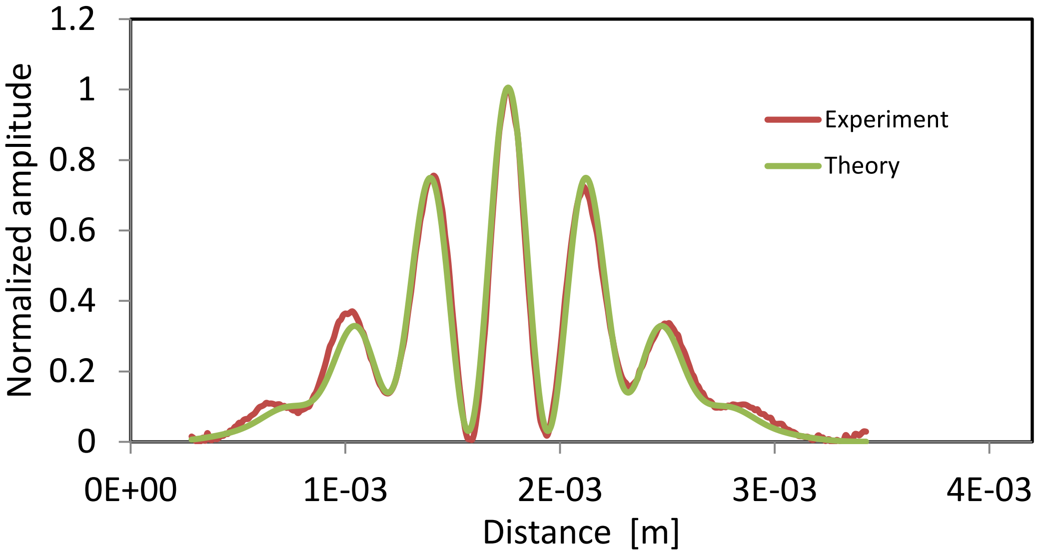

Figure 43: Experimentally measured spatial intensity distribution of the interference pattern obtained by Young's experiment the fitted by function (15) to obtain the coherence length of the generated supercontinuum.

3.8 Spectral range and shape

The spectral range and shape of the supercontinuum are very important parameters for our application, which is seeding a short pulse laser amplifier. The spectrum needs to be wide enough to enable compression to the target pulse length, which is usually not problem as the generated SC is usually very broad, but it also has to be reasonably "uniform" in the desired spectral region to be useable for amplification. The phase of the spectrum also needs to be "well-behaved" in order to be compressible to its Fourier limit using the tools for dispersion control at our disposal which will be verified in section 4.

Figure 44 b) shows the development of the supercontinuum spectra with increasing energy from the generation threshold up to the filament refocusing regime. The corresponding energy scan is shown in Figure 44 a). The SC spectrum starts around 700 nm and broadens very fast with increasing energy. The lower wavelength limit for the spectral broadening is determined by the material properties of YAG crystal which gets increasingly absorptive around 515 nm and lower [76]. Before the light is measured by a spectrometer it passes through lowpass filter which cuts of everything above 950 nm, however it seems like the spectrum naturally ends just before reaching this value. This is surprising since intuition and simulations shows that upper spectrum limit should span all the way towards the wavelength of pump laser which is 1030 nm in this case.

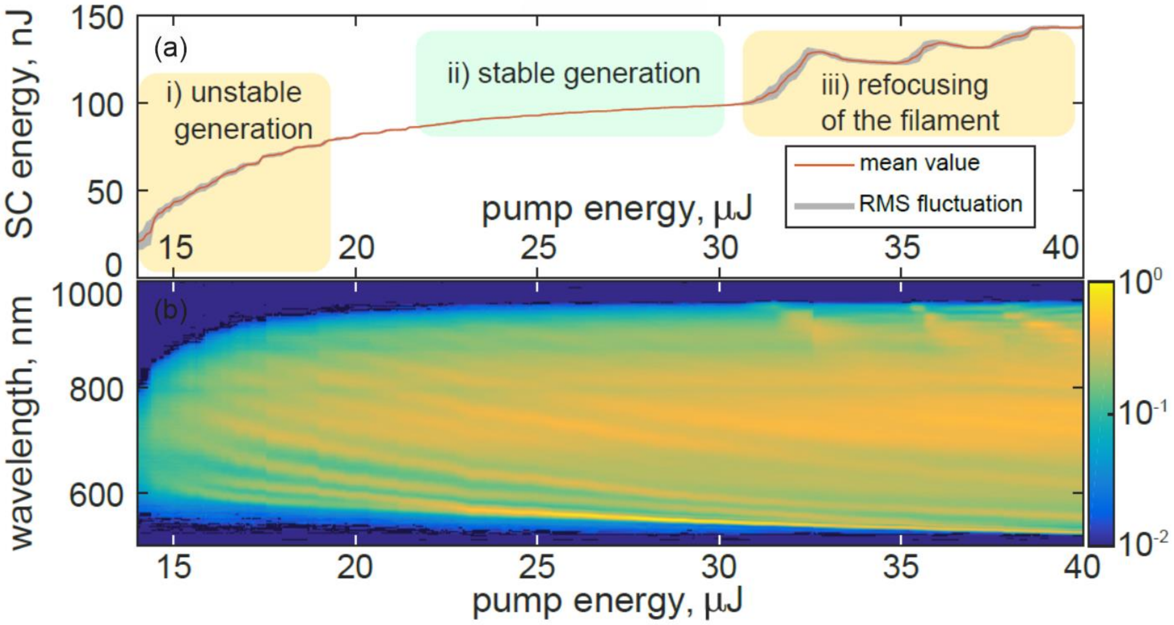

Figure 44: b) The development of spectrum range and shape with increasing energy of pump laser. a) Corresponding energy scan of supercontinuum [66].

For better visualization, the chosen spectra close to threshold (E_p = 15 μJ), in the stable regime (E_p = 25 μJ) and with filament refocusing (E_p = 35 μJ) from Figure 44 b) are plotted in Figure 45. With increasing energy of the pump laser, the spectrum broadens, is more modulated and a characteristic sharp peak appears on the lower wavelength side of the spectrum. This peak moves closer to lower wavelength limit of spectrum with increasing pump energy. When the pump energy exceeds the value for filament refocusing, high frequency modulations appear on the longer wavelength side of the spectrum. These are caused by interference between the two filaments generated in the crystal and are the most sensitive indicator of multifilamentation.

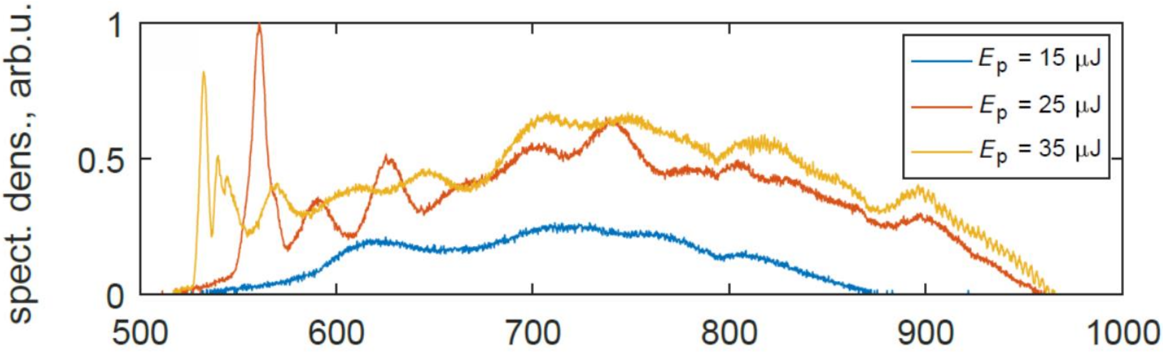

Figure 45: Plotted normalized spectra of generated supercontinuum for different energy of pump laser; close to threshold (E_p = 15 µJ), in stable regime (E_p = 25 µJ) and with filament refocusing (E_p = 35 µJ) [66].

The spectrum in the stable regime spans from 515 nm to 950 nm which, in theory, allows for compression up to 1.66 fs. When looking at Figure 45, the blue line corresponding to the SC just above threshold might seem to be the most suitable spectrum for most applications thanks to its smoothness. However, in this regime, the energy stability of the SC is significantly worse than in the stable regime which needs to be considered when stability is important for the application.

3.9 Dependence on pulse chirp

The behaviour of supercontinuua generated with differently chirped pump pulses is studied in this section. The supercontinuum was initially generated and optimized with the positively chirped, 5 ps long pump pulses. Afterwards the length of the pump pulses was changed by moving the second grating inside the compressor further away, making distance between the gratings longer and thus increasing the pulse compression (Figure 22). The pulse length was adjusted from 5 ps positively chirped to 4.7 ps negatively chirped. The shortest pulse duration was 1.3 ps which is close to Fourier transform limit (1.26 ps).

In order to assure that all measurements are comparable, the initial SC setup was not adjusted during entire measurement, which means that following energy scans do not necessarily represent the best achievable performance for a given pulse chirp. In this measurement we used a 400mm focal length lens, the distance between the crystal and lens was 420 mm and the aperture was completely open in order to diminish the effect of possible pointing changes introduced during compressor adjustments. A frog trace of the pump pulse was taken after every grating movement, to measure the pulse length and to ensure that the pulse was properly compressed, and its temporal profile was as close to Gaussian as possible. To make the final representation of the obtained data more clear, the measured data was split into two graphs: the supercontinuum energy scans for positively chirped pump pulses are shown in Figure 46, while negatively chirped are in Figure 47.

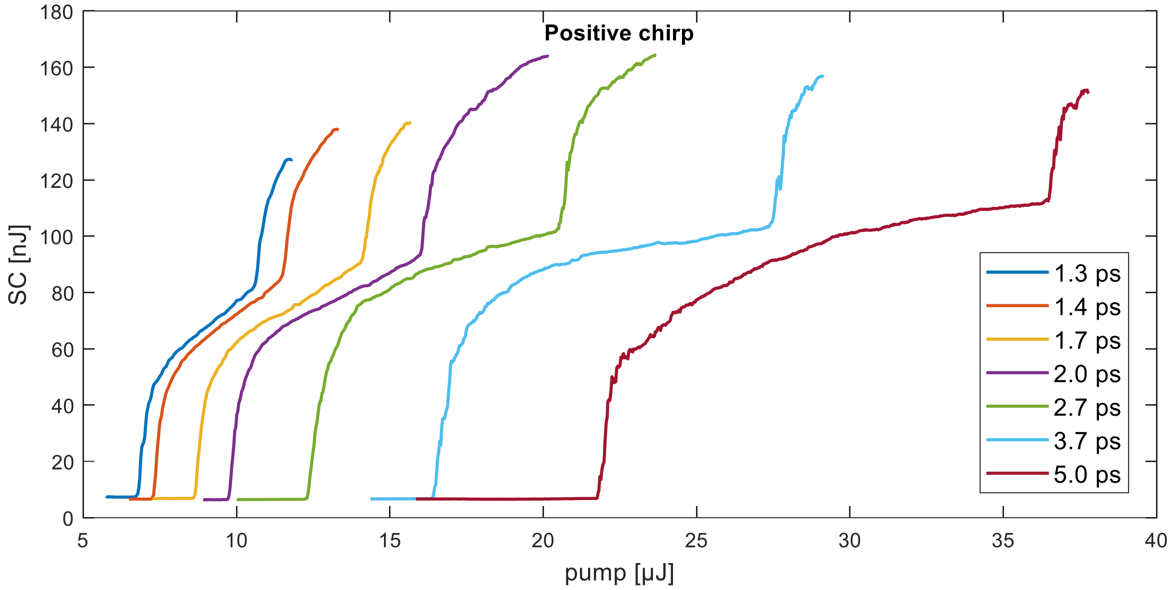

Figure 46: Set of supercontinuum energy scans for different length of pump pulse durations when the pulse is positively chirped.

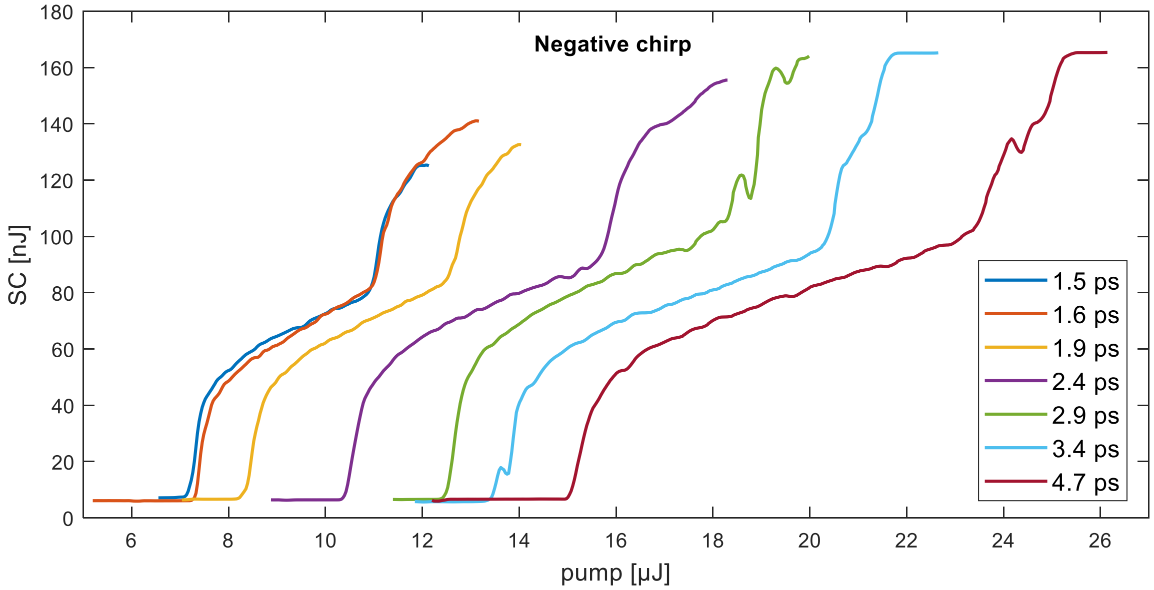

Figure 47: Set of supercontinuum energy scans for different length of pump pulse durations when the pulse is negatively chirped.

The most noticeable effect of the increased pump pulse duration on the generated supercontinuum was the increased threshold for SCG, which is expected, as the longer pulses require higher energy to reach powers sufficient for self-focusing. However, this also ultimately leads to an increase in supercontinuum energy in the stable regime. The maximum energy in the stable regime (right before filament refocusing which can be clearly identified by the steep energy increase in graphs above) of the SC for 1.3 ps pulses is ≈ 80 nJ but reaches ≈ 110 nJ for 5 ps long pulses. This represents 37.5 % increase in the obtainable energy by increasing the pulse length from 1.3 ps to 5 ps which can be useful for some applications for both positively and negatively chirped pulses.

By looking at the above graphs it might seem like the SC generated with longer pump pulses takes longer to reach the filament refocusing regime, but this it is not the case. The relative distance between the threshold for supercontinuum generation and filament refocusing is same for every measurement, in this case, the energy needed for filament refocusing (E_{fr}) is approximately 1.7 times higher than the threshold energy (E_{tr}) $E_{fr} \approx 1.7 * E_{tr}$. This value changes with pump beam diameter and aperture size, but seems to be independent of pulse length or crystal position, unless the second filament is generated prematurely, typically by a non-Gaussian temporal or spatial profile of pump beam containing multiple local maxima. Another difference is increase of threshold energy for positively chirped pulses, which needs more energy to initiate the supercontinuum generation compared to negatively chirped pulses of same length. This is potentially caused by competition between negative chirp and self-phase modulation, where the self-phase modulation first compensates negative chirp, compressing pulse to its Fourier limit, increasing its intensity significantly, which leads to faster SC generation. This happens only with negatively chirped pulses, the self-phase modulation affecting positively chirped pulses does not cause this effect, explaining the increased threshold in comparison to negatively chirped pulses.

The Figures 48 and 49 show the development of spectra for positively and negatively chirped pulses, respectively. The spectrum of the generated supercontinuum was always measured in the stable regime, approximately 10 % under the threshold for filament refocusing. In all cases, the spectrum spans from 515 nm to 950 nm, and, while the shape of the spectrum changes with the length of the pump pulse, it is difficult to define an ideal shape. The only significant difference is the rise of the sharp peak between 500 nm and 600 nm for the positively chirped case, however, this is not exclusive for this special case of pulse chirp and can be commonly observed for differently chirped pulses as well.

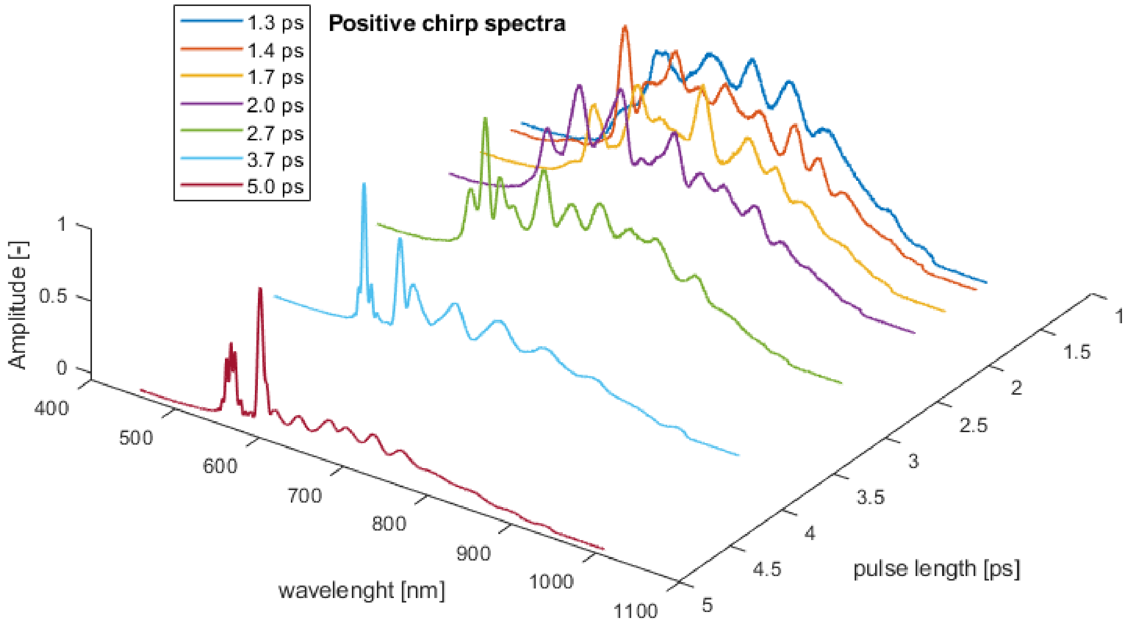

Figure 48: Spectra of generated supercontinuum for different pulse durations of positively chirped pump pulse.

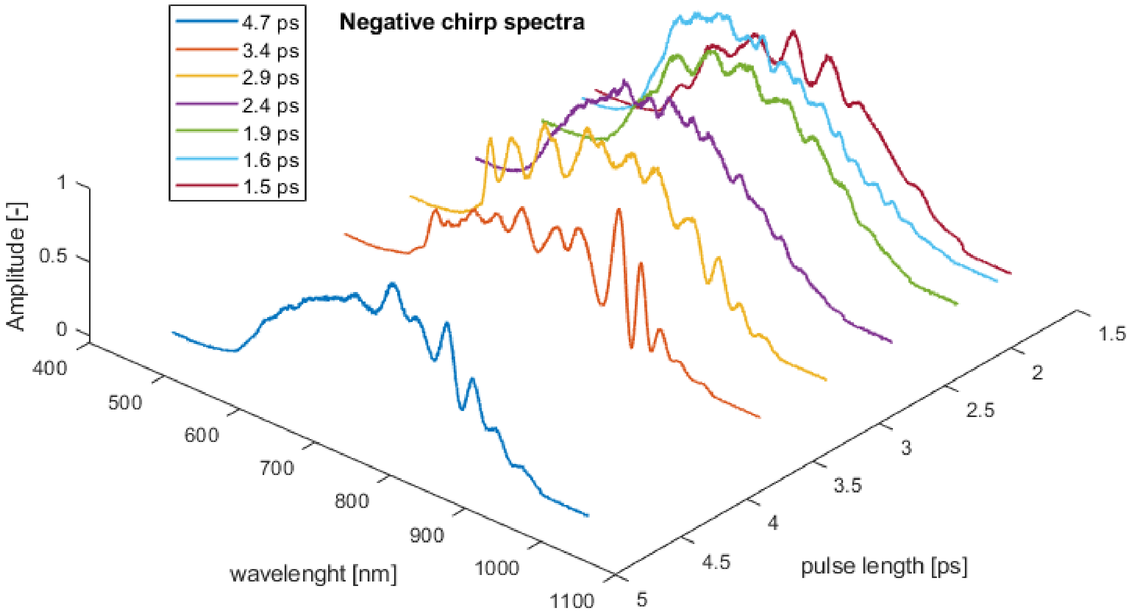

Figure 49: Spectra of generated supercontinuum for different pulse durations of negatively chirped pump pulse.

3.10 Dependence on *B*-integral

The effect of the *B*-integral accumulated by the pump beam before entering the YAG crystal on supercontinuum generation is studied in this section. The *B*-integral is defined as:

$$B = \frac{2\pi}{\lambda} \int n_2 I(z) dz, \tag{20}$$

where $I(z)$ is the optical intensity along the beam axis, z is the position in beam direction, and n_2 is the nonlinear refractive index. As $n_2 I$ is the nonlinear change in the refractive index, the B integral represents the total on-axis nonlinear phase shift accumulated over a given distance in a nonlinear medium. [77].

In our case, the vast majority of *B*-integral is accumulated during pump beam amplification inside regenerative amplifier, especially inside the Pockels cell crystal through which the beam passes two times during each round-trip. We adjust the initial B-integral on the pulse by changing the number of round-trips in the amplifier. During standard operation of the regenerative amplifier, the number of round-trips is chosen such that the amplification just reaches saturation, the maximum energy in the amplified pulse, while keeping the *B*-integral and average optical power inside the resonator as low as possible.

Increasing the number of round-trips above that needed to reach saturation will no longer increase the energy of the amplified pulse, but will introduce an additional nonlinear phase accumulated during these extra passes. Starting at initial value of 31 round-trips (RT), we increase them by one all the way up to 42 RT, performing the supercontinuum energy scan for each value. Because the nonlinear phase accumulation is intensity dependent, only the final few passes in the cavity significantly contribute to the B-integral. For this reason, an increase from 31RT to 42RT significantly increases the B-integral.

The supercontinuum was generated with 400 mm lens, an open aperture to mitigate the potential difference in pointing instability during measurement and the YAG crystal placed 420 mm after the focusing lens, generating the SC with a diverging beam. A SC scan was performed after every RT increase, and after reaching 42 RT, the YAG crystal was moved closer to the lens (370 mm) to generate SC with converging pump beam. The measurement was then repeated in the opposite direction, decreasing by one RT each step to 31RT. The measured data for SC generated with diverging and converging pump beam are shown in Figures 50 and 51 respectively.

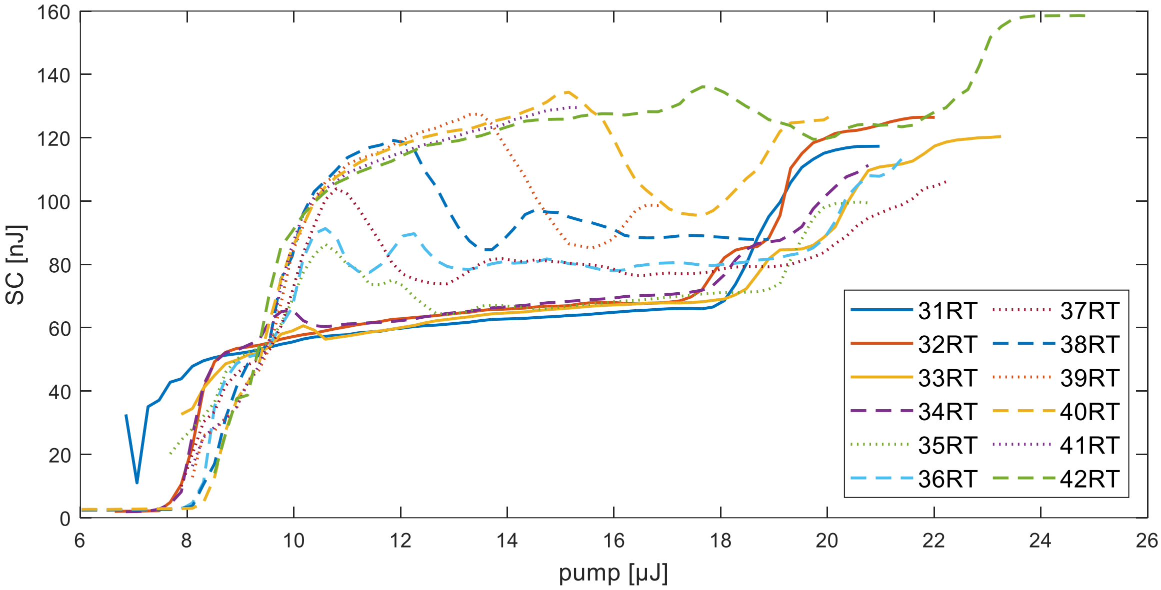

Figure 50: Supercontinuum energy scans for different number of roundrips inside regenerative amplifier, introducing different amount of *B*-integral, with YAG crystal placed 420 mm after focusing lens.

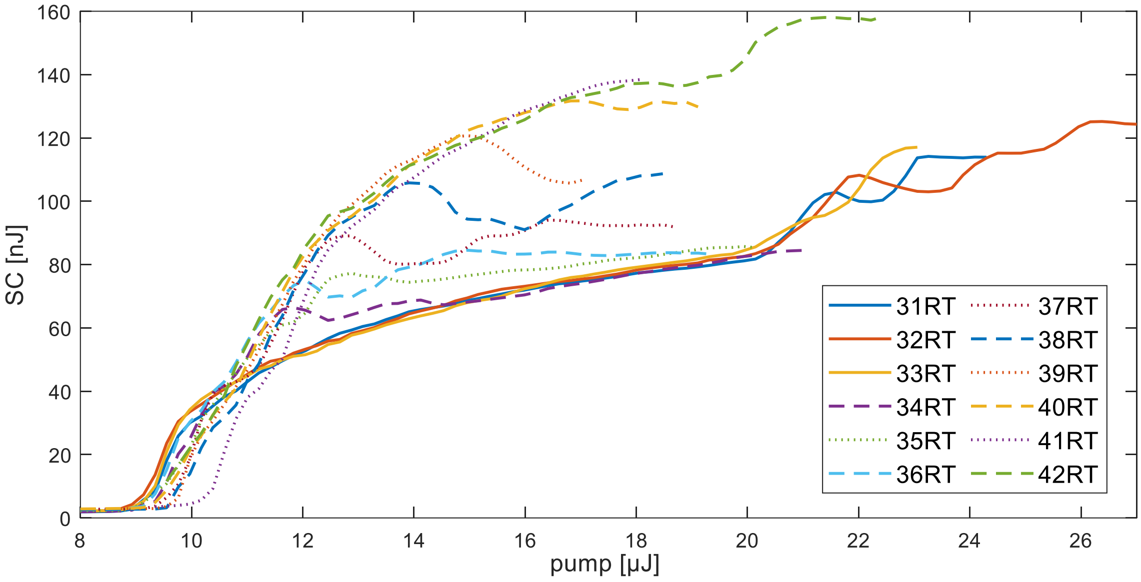

Figure 51: Supercontinuum energy scans for different number of roundrips inside regenerative amplifier, introducing different amount of *B*-integral, with YAG crystal placed 370 mm after focusing lens.

As seen in Figures 50 and 51, supercontinuum generation with fewer round-trips behaved in the expected way (energy scans indicated with solid lines): after the threshold for generation SC energy grows to around 60 nJ, creating long stable region before reaching the energy needed for refocusing. However, as the amount of round-trips increases, the behaviour changes. The energy of the generated supercontinuum increases immediately above the level corresponding to the stable generation regime and further increases with pump energy. The energy of the SC drops down close to the stable regime, but the measured pulse to pulse stability is significantly worse. With higher pump pulse *B*-integral this drop occurs at higher SC energies.

The physical explanation for this behaviour of supercontinuum generation with pump pulses with increased amount of *B*-integral is unclear, one possible cause can be an extra phase distortion of the pump pulse. However, it is clear that large amounts of accumulated nonlinearity in the pump pulses clearly affects the SC generation negatively and should be taken into consideration.

3.11 Spatial profile

The spatial profile of the generated supercontinuum is an important characteristic for further amplification in the OPCPA amplification chain. The spatial profile of the SC for different values of pump energy was measured using a beam profiler SP620 (OPHIR). The supercontinuum was generated in YAG crystal, with an open aperture and a 400 mm lens placed 420 mm before the crystal. The pump beam was filtered using a shortpass filter. The measured spatial profile of the supercontinuum for various pump energies is shown in Figure 52. Figure 53 indicates where on the energy scan curve were individual beam profiles measured.

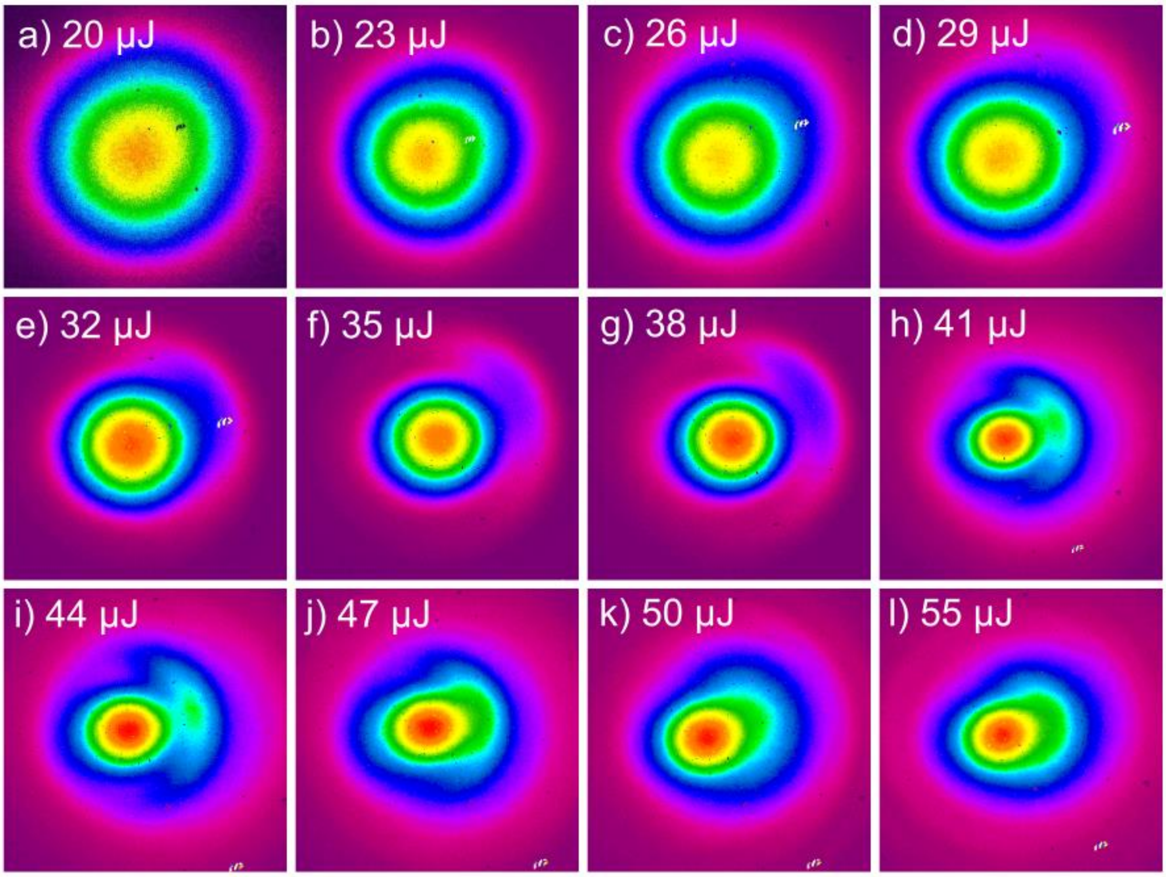

Figure 52: The spatial profile of supercontinuum generated in YAG crystal for different energy of pump beam.

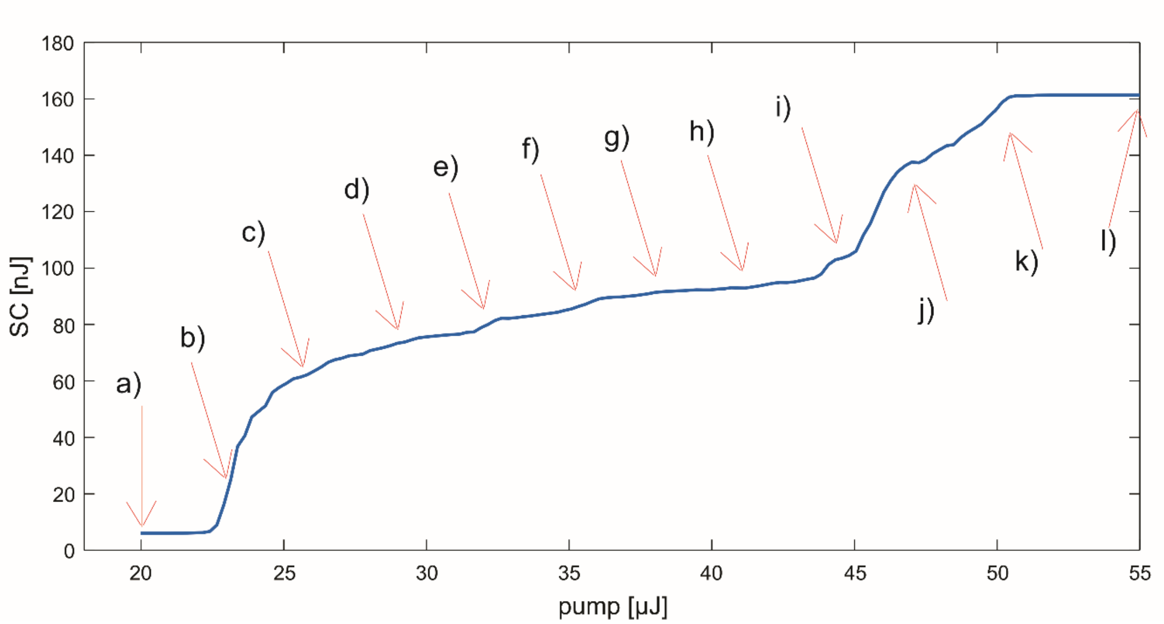

Figure 53: The energy scan of supercontinuum for which the spatial profiles shown in Figure 52 were measured with indicated location of individual profiles on energy curve.

The initially generated supercontinuum profile is nearly Gaussian. With an increase in pump energy a characteristic supercontinuum "halo" starts to appear surrounding the Gaussian beam in the centre. This conical emission appearing as a halo around main beam has higher divergence and is typically caused by refocusing of the filament inside the crystal [78]. As the pump energy increased, the beam shape gets more distorted, especially when generating in unstable regime where the refocusing of the filament occurs.

The Gaussian shape of the generated supercontinuum is important and always needs to be verified. Even in this case, the significant beam distortion can be observed while still generating in stable regime. Another potential issue can be the fluctuation of the size of the collimated or focused supercontinuum. This is caused by change in position of the filament inside the crystal, which than cannot be properly collimated by curved mirror placed after the YAG crystal. This can be sometimes observed even during otherwise stable generation and can cause significant problems during the OPCPA amplification.

3.12 Infrared portion of SC

The supercontinuum generated with 1030 nm pump pulses has a visible portion, containing shorter wavelengths and also infrared part with wavelengths longer than 1030 nm. So far, in this work, only the visible portion of the supercontinuum spectrum was discussed because it is the only part relevant for the OPCPA amplification in our system and the rest of the generated spectra was always removed with shortpass spectral filter. However, the infrared portion of the supercontinuum is always generated and its basic characteristics were measured.

The experimental setup for measuring the infrared portion of the supercontinuum was not different from standard setup (400 mm focusing lens, 3.5 mm aperture, YAG crystal placed 420 mm from focusing lens), only the 950 nm shortpass filter at the output was replaced with 1050 nm longpass reflective spectral filter to remove the remainder of the pump beam as well as a visible portion of the generated supercontinua. The spectrum of the supercontinuum generated in the stable region was measured with a fiber spectrometer (NIRQUEST512-2.5, Ocean Insight) and is shown in Figure 54. The spectrum starts with a sharp edge at 1050 nm caused by the spectral filter and spans all the way to 2500 nm (which is also detection limit of our spectrometer). The spectrum of the infrared portion typically consists of two peaks centred around 1150 nm and 1900 nm with a very weak area around 1500 nm. This measured spectral shape correlates well with numerical simulations performed by Alexandr Špaček shown in Figure 55 [44].

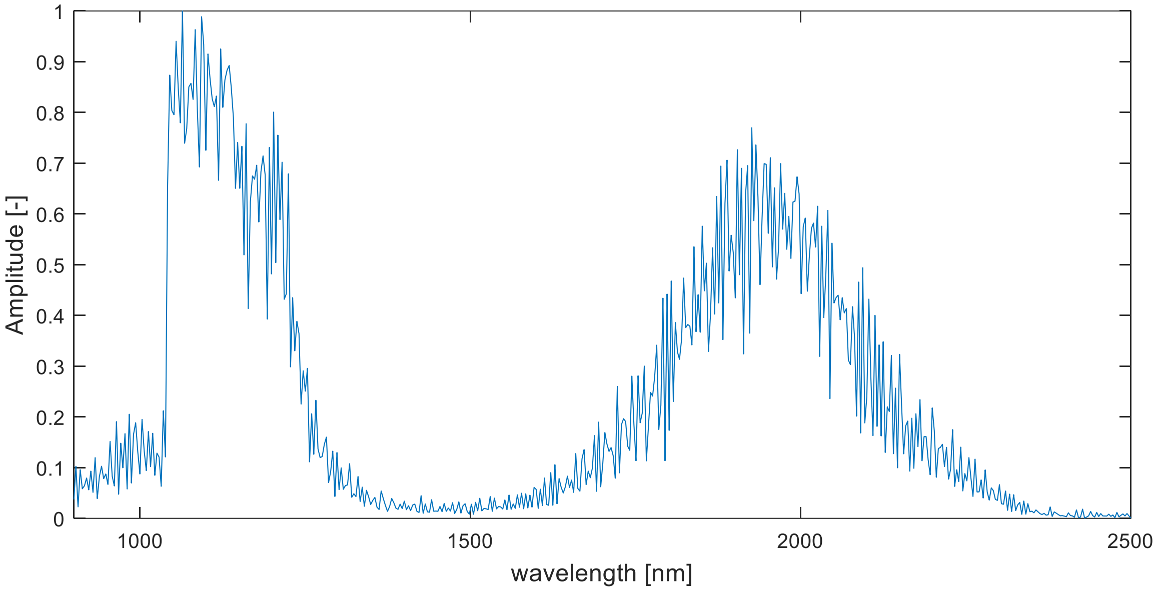

Figure 54: Measured normalized spectrum of the infrared portion of the generated supercontinuum.

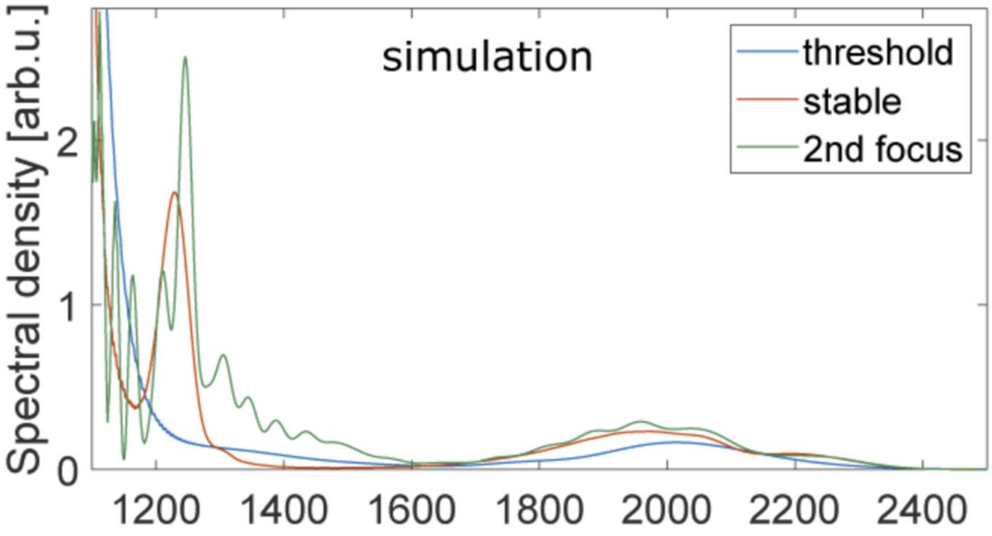

Figure 55: Numerically simulated infrared portion of spectra of supercontinuum generated in 13 cm long YAG with 3 ps pulses. The simulated spectrum of „stable“ regime corresponds well with measured spectrum [44].

Figure 56 shows a measured energy scan for the infrared portion of the generated supercontinua. The energy of each single pulse at 2 kHz was measured using a pyroelectric sensor (PE9-ES-C, Ophir). The shape of the energy scan is similar to the visible part of the SC with characteristic stable region present before filament refocusing occurs. The infrared portion of the SC contains significantly more power than the visible part. While the typical energy of visible part of the SC in stable region is between 70-100 nJ, the infrared portion reaches up to 700 nJ in stable region. However, the pulse-to-pulse stability is worse, in this case the best obtained short term stability was 1.82 % RMS.

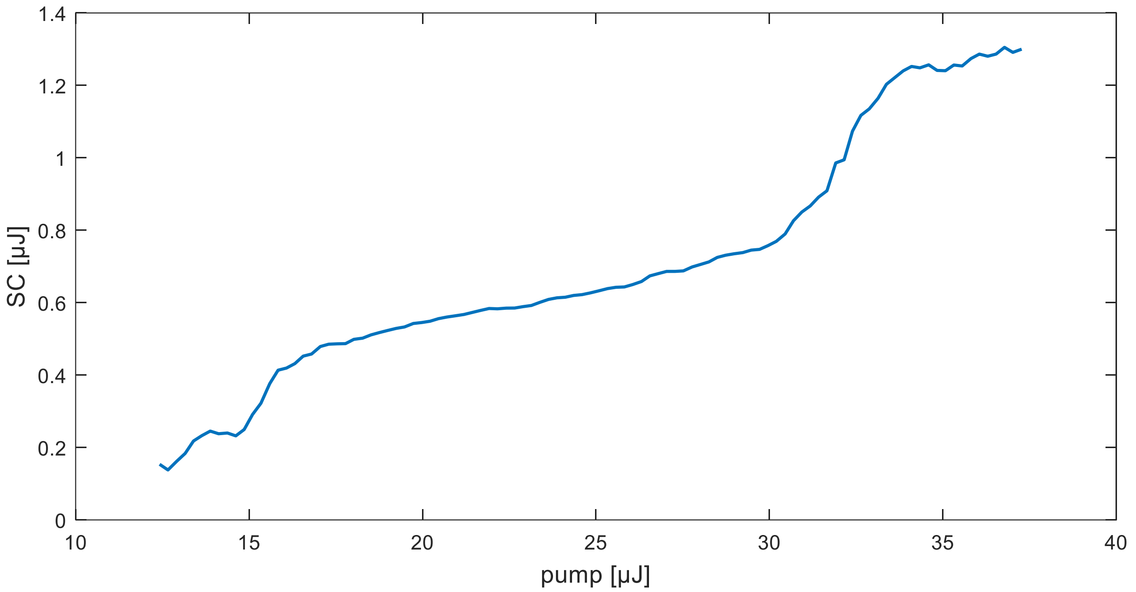

Figure 56: A measured energy scan of infrared portion of the generated supercontinuum.

3.13 Best results

The best supercontinuum generation results achieved by tuning the experimental setup and parameters of pump beam are summarized in this section. They were obtained with negatively chirped 3 ps long pump pulses with a 3.5 mm in diameter at a 1 kHz repetition rate. The pump beam was limited by a circular aperture with 2.7 mm diameter before being focused by a lens with a 400 mm focal length. The distance between the lens and the 130 mm long YAG rod was 370 mm, meaning that the geometrical focus of the lens was located 30 mm inside the crystal.

The pulse to pulse energy measurements of the pump laser and the generated supercontinuum over period 1000 s are shown in Figure 57. The relative RMS fluctuations of the supercontinuum are 0.3 % which is a significant improvement to the stability of the pump beam (0.8 %). The average energy of the generated SC is 93.8 nJ, the efficiency of this process is 0.39 %.

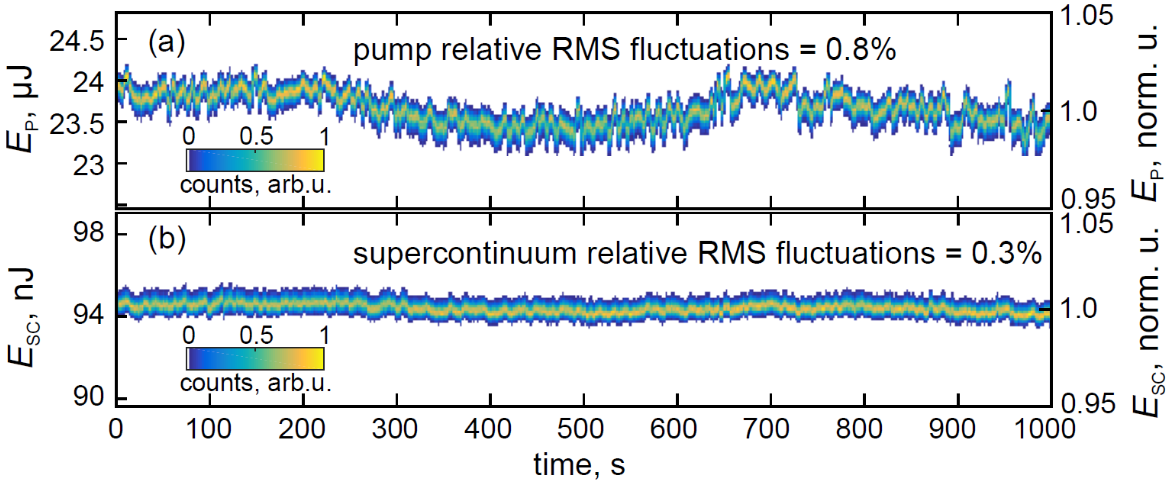

Figure 57: Pulse to pulse energy measurement of a) pump laser b) generated supercontinuum, with calculated corresponding RMS fluctuations.

The spectral shape and stability measured with repetition rate of 10 Hz over long period of time is shown in Figure 58 a). The spectral profile of the generated SC in time is very stable and, as shown in Figure 58 b) which shows the development of the spectral shape in time does not seem to change in time. The spatial profile shown in Figure 58 c) is Gaussian and very smooth.

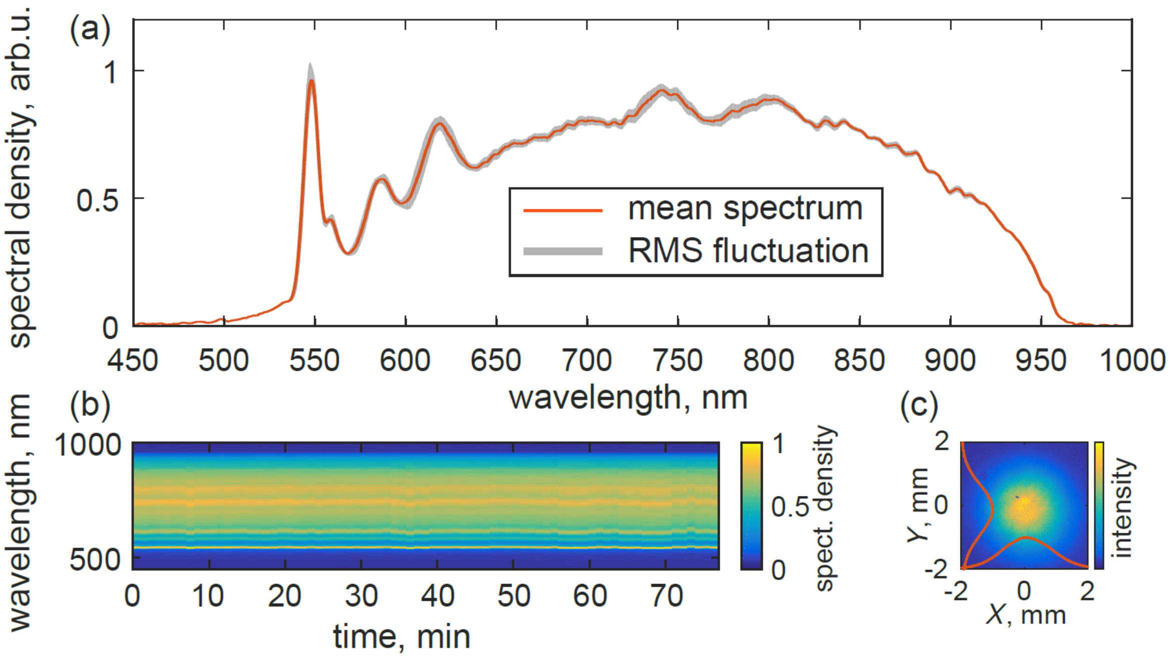

Figure 58: a) Spectral stability of generated supercontinuum over period of 77 minutes. b) Development of spectral shape of supercontinuum in time. c) Spatial profile of generated SC.

4 Amplification and compression

In the previous chapter it was shown that it is possible to generate a coherent supercontinuum with good short and long term energy and spectral stability. Before planning implementation in high power OPCPA systems it is necessary to show in practice that the generated SC can be used as a reliable seed for OPA and can be compressed after amplification. An experimental setup consisting of two OPA stages and a prism compressor was built as proof of a concept and will be presented in this chapter.

4.1 OPCPA amplification

A simplified experimental scheme for supercontinuum generation, its amplification and compression using a single picosecond pump source is shown in Figure 59. A small fraction of the pump beam is used for the supercontinuum which is built to generate as stable SC as possible, as described in section 3.13. The remaining pump passing through the YAG crystal is filtered using a 950 nm shortpass filter and collimated by a focusing silver mirror ($f = 200$ mm). Prior to the OPCPA, an acousto-optic programmable dispersive filter (Dazzler, Fastlite) adjusts the duration of the SC seed, which was stretched by dispersion in the YAG crystal to match the duration of the OPCPA pump. Additionally, it allows for compensation of higher order dispersion. The throughput of the Dazzler is > 30%.

Afterwards, the supercontinuum is amplified in two consecutive OPCPA stages using BBO crystals. The OPCPA is pumped by a 515 nm beam, which is the second harmonic of the 1030 nm pump laser output. The OPCPA stages are intentionally operated well below saturation to avoid the OPCPA-induced modification of the signal phase; therefore, the full energy of the pump is not used in the OPCPA. The output energy after the OPCPA is 120 μJ, which is sufficient for the temporal pulse diagnostics (Spider and Wizzler).

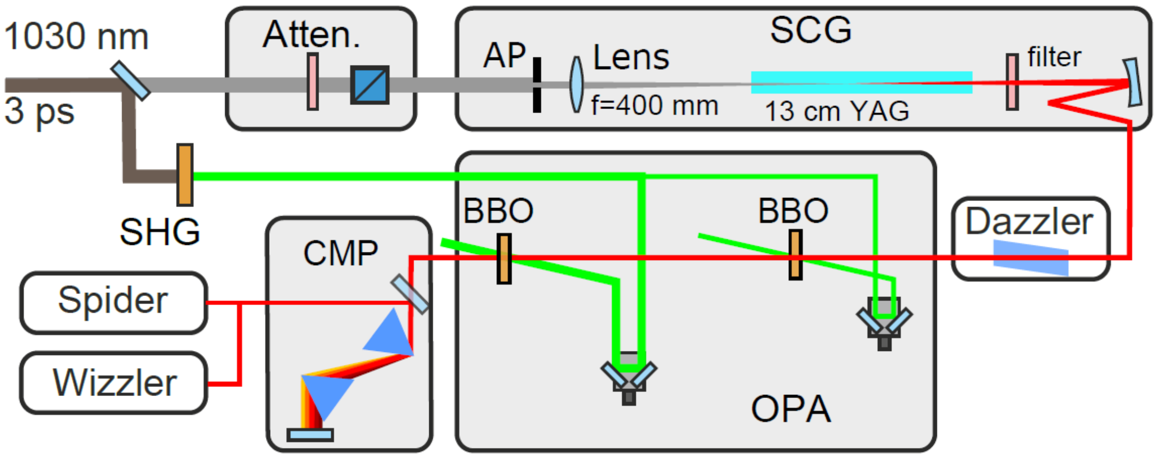

Figure 59: Simplified experimental scheme for generation, amplification and compression of supercontinuum. Atten.: variable attenuator (λ/2 waveplate and polarizer), AP: iris aperture, SCG: second harmonic generation, Dazzler: acousto-optic programable dispersive filter, OPA: optical parametrical amplification, BBO: β - barium borate crystal, CMP: SF11 prism compressor.

4.2 Compression

After amplification, the supercontinuum is compressed using an SF11 prism pair with ≈ 40 cm separation. In order to get as close to the Fourier limit as possible, the higher order dispersion, which cannot be fully compensated with the prism compressor, are adjusted with Dazzler. The temporal shape of the pulse is retrieved using an FC Spider (APE). However, the maximum spectral width supported by the Dazzler is 200 nm with bottom limit of 650 nm, which means that the entire generated supercontinuum (550 nm – 950 nm) cannot be amplified, compressed and measured at once. For this reason, the supercontinuum was divided into two spectral regions, each amplified, compressed and measured separately. The spectrum and achieved compression of both regions measured with Spider is shown in Figure 60.

The first spectral region, 100 nm bandwidth centered at 750 nm, is shown in Figure 60 (a), with a dotted line and was compressed to 22.2 fs (Figure 60 (b)). The second region shown in Figure 60 (a) was centred around 850 nm, 180 nm wide and compressed to 12.7 fs (Figure 60 (c)). Both spectral regions are compressible close to their respective Fourier limits. The total dispersion, which was compensated for by the Dazzler and the prism compressor, is estimated to be GDD = 8250 fs^2, TOD = 4800 fs^3 (at 800 nm). This mainly corresponds to the material dispersion of YAG (GDD = 7380 fs^2, TOD = 4220 fs^3 after propagating through 75 mm of material).

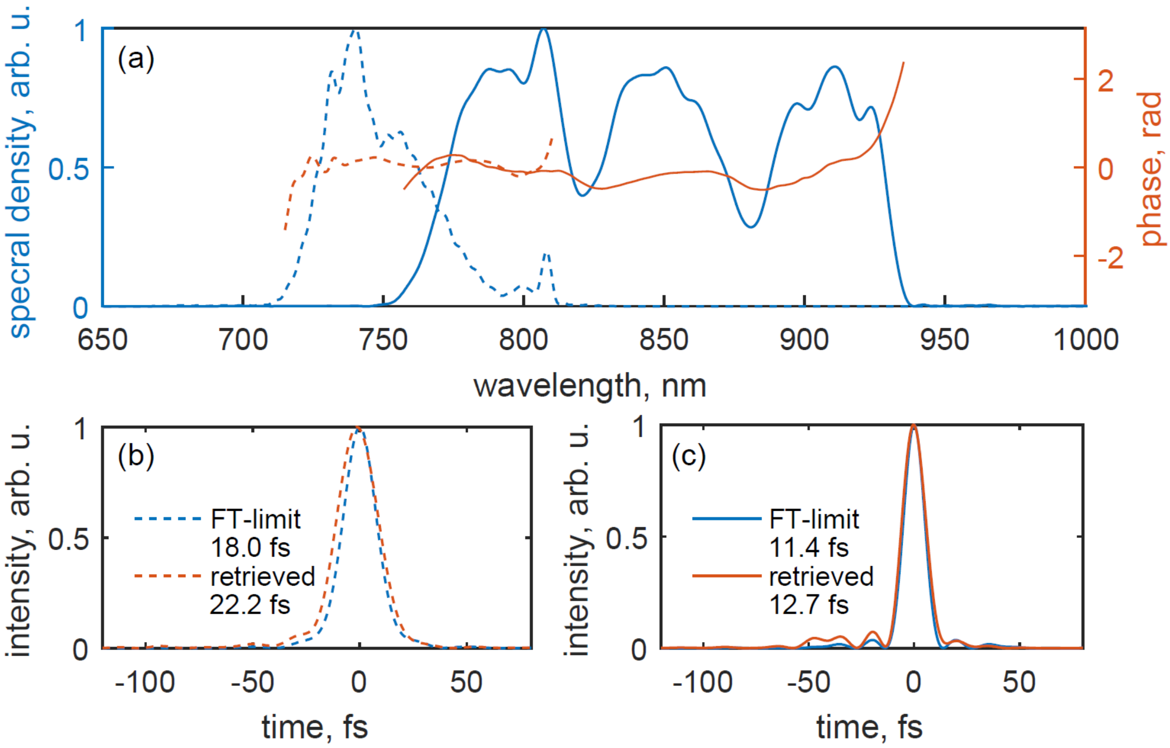

Figure 60: (a) Spectrum and phase of the compressed pulses in both measured regions. Temporal pulse reconstruction corresponding to the spectrum centred at (b) 750 nm (c) 850 nm

Although the pump laser is highly stable, a small change in the starting position of the filament depending on the pump energy can be observed. This in turn could cause a dispersion fluctuation, observable as a fluctuation of the compressed pulse duration, which is highly undesirable for a broadband seed pulse. To confirm the stability of the dispersion, the stability of the compressed pulse duration was investigated using a Wizzler (Fastlite), which allows for a single shot measurement of pulse temporal profile at a high repetition rate.

Figure 61 (a) shows single-shot measurements taken at a repetition rate of 10 Hz for 1000 pulses. No dispersion tuning was performed during the measurement. From a sample of 1000 pulses, the FWHM duration was calculated to be 13,8 ± 0,2 fs with RMS GDD fluctuations of 45 fs^2 (calculated at the corresponding central wavelength). The temporal evolution and the spectrum of a typical pulse, as retrieved by the Wizzler, are shown in Figure 61 (b) and 61 (c). Based on these results, showing good compressibility and temporal stability of amplified pulses, the supercontinuum seems to be an excellent candidate for seeding femtosecond OPCPA systems.

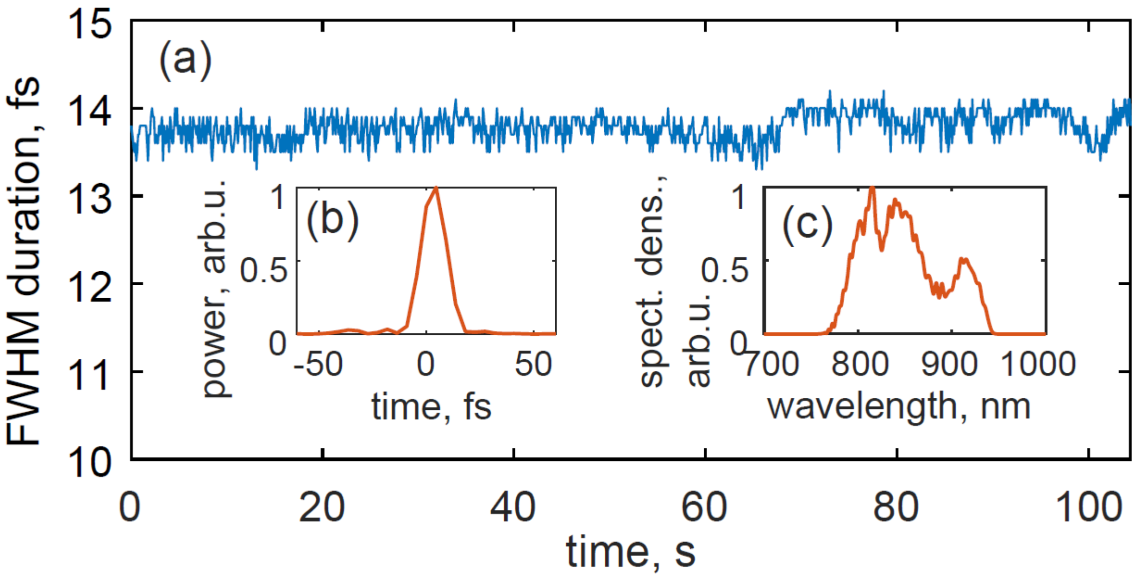

Figure 61: (a) Single-shot measurement of the pulse duration for 1000 pulses at 10 Hz repetition rate, measured using the Wizzler (Fastlite). (b) Typical reconstructed temporal profile and (c) typical fundamental spectrum.

5 Implementation

Based on the results of our tests evaluating the suitability of supercontinuum for seeding high power laser systems such supercontinuum seeders have been deployed in two new high power OPCPA systems which are under development at ELI-Beamlines. Work on both systems started in 2019 as part of the ADONIS project. In both cases the regenerative amplifier generating picosecond pulses serves as a pump for SC and pump for a OPCPA which is seeded by SC, eliminating the need for any complicated active synchronization systems. These systems will be described in this section with emphasis on front end of L2 laser system (DUHA) where the author is primarily involved.

5.1 L2 laser system (DUHA)

L2-DUHA is intended to be a high repetition rate, 100 TW-class laser system whose primary purpose is to serve as a driver for a laser wakefeeld acceleration (LWFA)-based X-ray free electron laser (XFEL). In order to provide a solid foundation for such an LWFA-based XFEL, the driving laser must be a 100 TW-class laser with a high repetition rate of over 25 Hz and exceptional energy and pointing stability. Rather than target high energy or high peak power, the emphasis of the L2-DUHA laser is on increased repetition rate with high stability in the 100 TW regime. The key technology used in the L2-DUHA laser is diode pumped solid state laser (DPSSL)-pumped OPCPA. In addition to the primary near infrared 100 TW output of the laser, L2-DUHA has an auxiliary 5 mJ, 30 fs, 2 kHz mid-IR output which can be used for generating high harmonics passively synchronized to the main beamline output.

The L2-DUHA OPCPA is divided into 2 sections, simplified scheme of laser system is shown in Figure 62. The first section is a picosecond broadband front end (BBFE), which generates the seed pulses via supercontinuum generation and amplifies 820 nm-centred broadband pulses up to mJ-level. In addition to the 1 mJ, 820 nm near-IR pulse train, the BBFE also produces a mid-IR auxiliary output which is synchronized to the near-IR pulse train. The near-IR pulses are stretched to 1.5 ns and sent to the second section of the laser which is the high energy OPCPA. It is pumped by a cryogenically cooled, diode-pumped Yb:YAG amplifier operating at 50 Hz with a 1030 nm output energy of 12 J, and an expected frequency doubled energy of 8.5 J. According to simulations output energy of 4 J should be possible and after compression will exceed 100 TW.

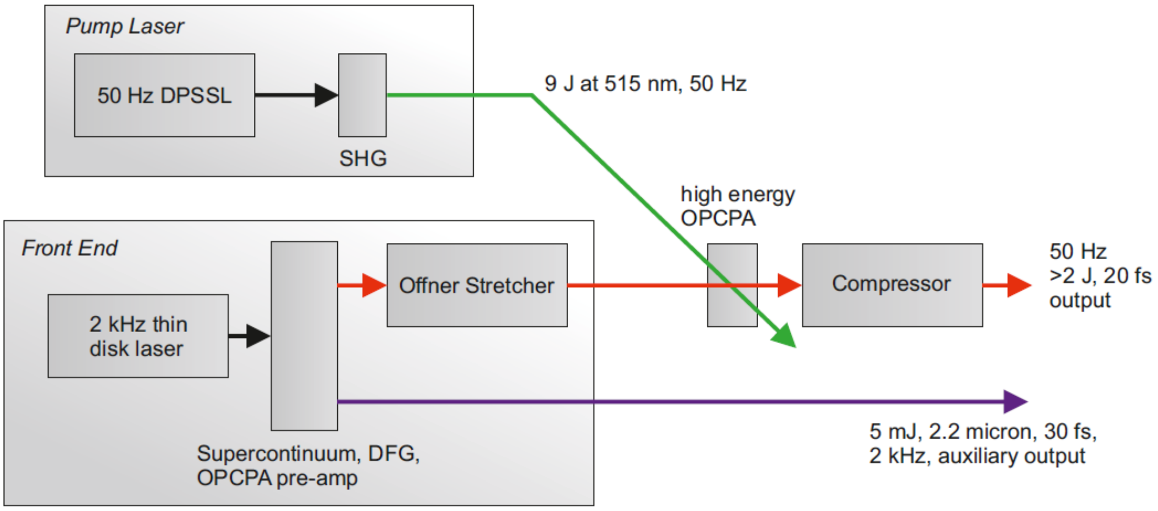

Figure 62: The simplified scheme of L2-DUHA laser system which will be providing 100 TW level near-IR output and synchronized 5 mJ, 30 fs, 2 kHz auxiliary output at 2.2 µm.

5.1.1 Broadband front end

The broadband front end is the source for both the mid-IR auxiliary pulse train and the NIR seed for the 100 TW amplifier. Both outputs are generated via nonlinear frequency conversion of a narrowband laser source and subsequent picosecond OPCPA. Picosecond OPCPA is chosen as the method of amplification in the BBFE to ensure excellent contrast. Because the pulses themselves originate from a supercontinuum and the amplification is gated by the picosecond pump pulse, there is no mechanism for generating noise photons outside this picosecond window in the front end. The general scheme is shown schematically in Figure 63. The entire front end system is pumped by single regenerative amplifier, which is in detail described in section 2, including seeding oscillator and grating compressor.

A small portion of the energy (2x 150 µJ) of the 1030 nm picosecond pulse train is diverted using 2 beam splitters and drives two parallel supercontinua in YAG crystals (one is used to seed the near-IR OPCPA and the other to seed the mid-IR OPCPA). The geometrical setup for both of the supercontinua generation is identical and set up in a way which is described in section 3.13 to achieve the best possible energy and spectral stability of generated broadband supercontinuum. A Dazzler is installed on each branch to have fine control over the dispersion for the near-IR and mid-IR branches.

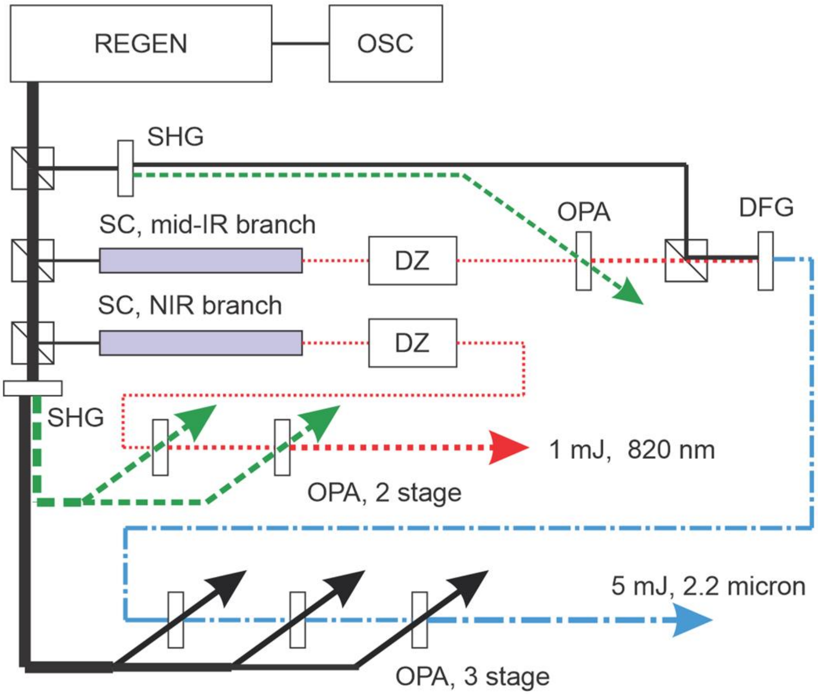

Figure 63: The simplified scheme of dual output BBFE. The red dotted lines indicate NIR pulses, black solid lines indicate 1030 nm, green dashed lines indicate 515 nm, and blue dot-dashed lines indicate 2.2 µm. DZ, Dazzler; SC, supercontinuum; OPA, optical parametric amplification; DFG, difference frequency generation; REGEN, Yb:YAG thin disk amplifier; OSC, modelocked oscillator including stretcher; SHG, second harmonic [79].

The remainder of the regenerative amplifier output passes through an LBO crystal and 10 mJ of the pulse is frequency doubled in a 2 mm length LBO crystal to 515 nm to pump the 820 nm near-IR picosecond OPCPA pre-amplifier. The unconverted 1030 nm pulses (approximately 25 mJ) will be used to pump the mid-IR chain. The conversion efficiency is intentionally lowered to around 25% in order to have more power in the mid-IR section while also having a more top-hat beam profile.

The 800 nm portion of the spectrum from the near-IR supercontinuum is sent on to the near-IR picosecond OPCPA amplifier. For 100 nJ pulses after Dazzler losses we are left with roughly 20 nJ to seed the OPCPA amplifier. The OPCPA will closely resemble the first 2 stages of OPCPA in the L1-Allegra laser [29]. BBO will be used as the amplification crystal in these stages because of the high d_{eff} and the large non-collinear angle. The length of the crystals is 2 mm and, with 10 mJ at 515 nm for the pump, it is expected that 1 mJ will be achieved in after two stages of OPCPA.

The 1 mJ energy is taken as the seed energy to the stretcher and will be used as the seed in the subsequent nanosecond OPCPA design. A photo of the assembled and pre-aligned stretcher is shown in Figure 64. The pulse duration of the stretched pulse has to match the

τ_s = 1.5 ns duration of the pump pulses. This is accomplished by an Öffner stretcher. A pre-compressor is added before the stretcher to fine tune the chirp of the output pulse, without the need to adjust the final compressor. So far, the amplification of the generated supercontinuum with the first OPCPA stage and following alignment through the prepared pre-compressor and stretcher has been demonstrated. The implementation of the second OPCPA stage, amplifying the near-IR branch to full power and stretcher optimization should be finalized by end of March 2023.

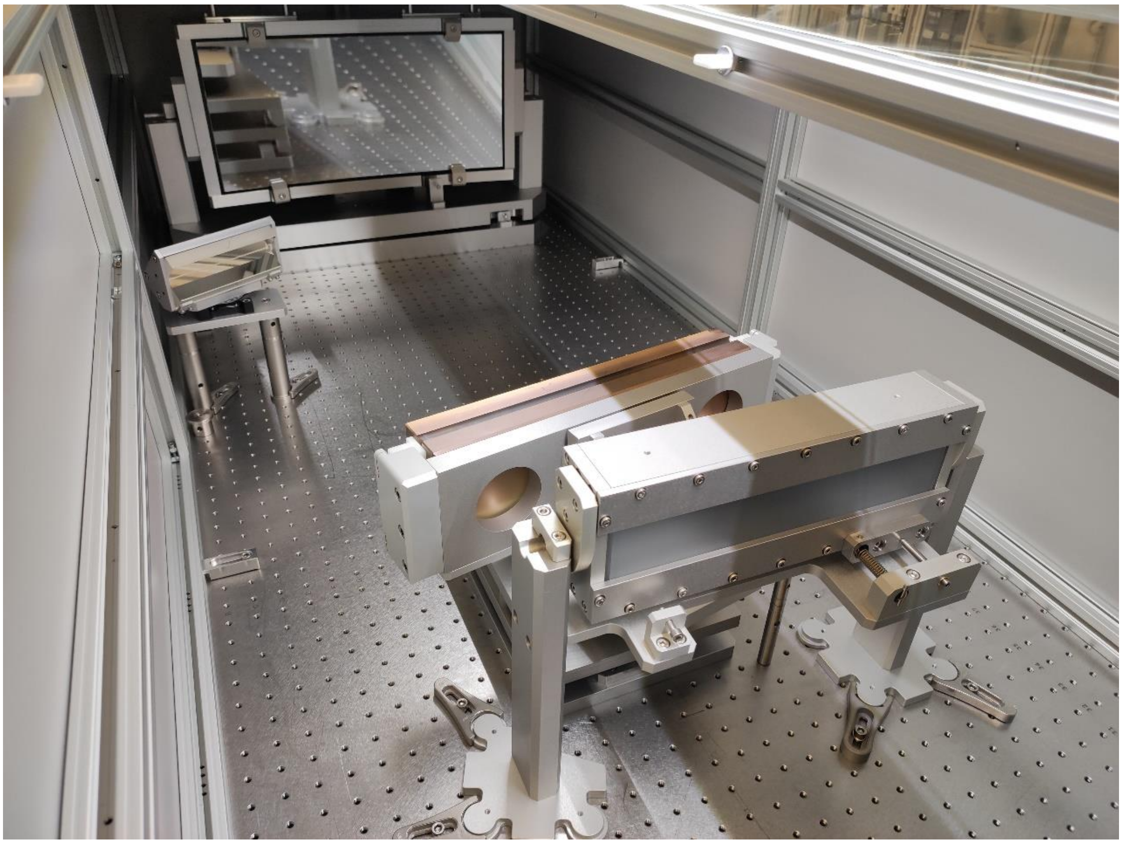

Figure 64: Photo of nanosecond stretcher, showing large curved and flat folding mirrors, back reflecting mirror and second grating.

The output of the second supercontinuum is used to seed the mid-IR amplifier. The Dazzler is set such that the diffracted spectrum covers 650 – 750 nm (corresponding to 1.8 – 2.8 µm after DFG). This supercontinuum is pre-amplified via OPCPA in a 1.3 mm long BBO crystal using an 80 µJ, 515 nm pump pulse. The energy of pre-amplified near-IR signal pulse is around 20 µJ. After pre-amplification, the broadband beam is collinearly combined with the 1030 nm beam on a polarizing beam splitter and sent into another BBO crystal cut for a broadband difference frequency generation (DFG). The DFG crystal is a BBO cut at 22.8° with a 5 mm × 5 mm aperture and a 1.5 mm length, the OPA geometry is collinear. Achieved mid-IR output is 0.5-1 µJ with spectrum ranging from 1800 to 2600 nm. The experimentally achieved results of mid-IR generation using DFG are shown in Figure 65.

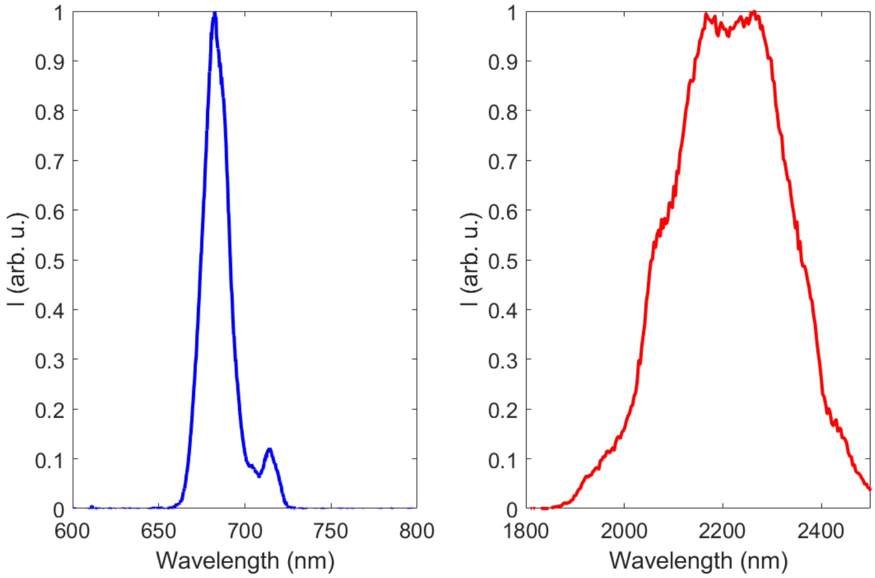

Figure 65: The left curve shows the spectrum of the NIR pulse used for pumping the DFG stage. After DFG in BBO with a 1030 nm pulse, the mid-IR spectrum on the right is generated and will be used as the signal in the subsequent auxiliary output mid-IR OPCPA stages.

Because the temporal coherence of the 1030 nm driving pulses is preserved in the generation of the supercontinuum the broadband 700 nm-centred pump pulses have a fixed phase relationship with respect to the 1030 nm idler pulses. This fixed phase relationship ensures a passively stable carrier-envelope phase (CEP) of the generated mid-IR idler pulse. In the event that the laser will suffer long term drifts, the CEP can be stabilized by actively controlling the relative phase of the 1030 nm signal pulse and the 700 nm-centred pump with a motorized delay stage on the 1030 nm branch.

After this, the mid-IR pulse will be amplified in 3 more stages of OPCPA pumped by residual 1030 nm passing through the SHG crystal. The first 2 stages will be BBO and the final stage will be BiBO, all in non-collinear geometry. The energy of the mid-IR should be 70 µJ after first OPCPA stage, 800 µJ after the second stage and reach 5 mJ after the final stage. After the OPCPA pre-amplifier, the mid-IR pulses are compressed using a 150 mm long suprasil rod together with Dazzler optimization for higher-order dispersion. Figure 66 shows the measured autocorrelation trace at the output of the bulk compressor. The ability to generate a broadband mid-IR spectrum using amplified supercontinuum in DFG crystal was demonstrated as well as amplification in first two OPCPA stages and compression in bulk to under 50 fs. The mid-IR branch of front end should be finalized by implementing the last OPCPA stage and optimizing pulse compression till by the end of 2023.

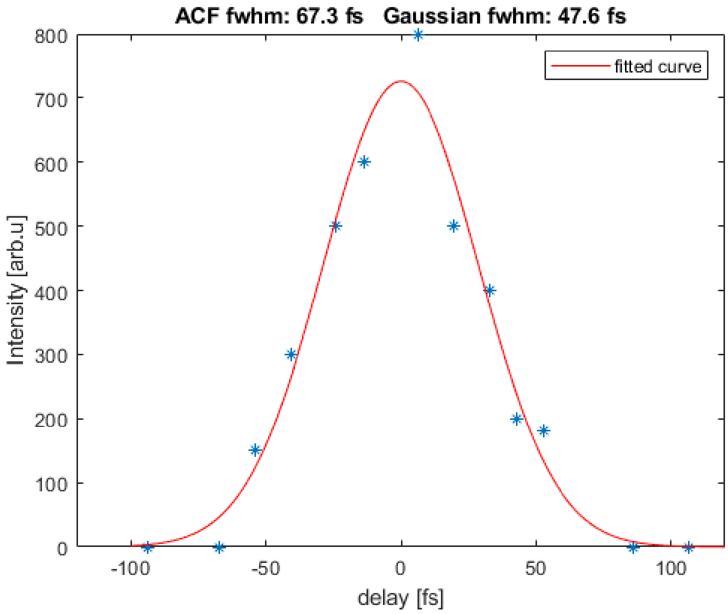

Figure 66: Measured pulse duration of compressed mid-IR pulses using scanning autocorrelator.

5.1.2 High energy OPCPA

The pump for the high energy OPCPA section is a cryogenically cooled, diode-pumped Yb:YAG multi-slab amplifier. This Yb:YAG multi-slab architecture was pioneered at Rutherford Appleton Lab with the DiPOLE project [80] and is currently utilized in the BIVOJ laser at HiLase [81]. The Yb:YAG slabs are cooled by flow of cryogenic helium (≈150 K), which allows operation at significantly higher average powers and also increases the thermal conductivity of the crystal [63]. Operation of this high energy pump DPSSL was demonstrated for 10 J, 10 Hz and square shaped beam. The laser is currently being upgraded to increase the repetition rate from 10 Hz to 50 Hz and the output energy from 10 J to 12 J at 1030 nm which will be converted to 515 nm via second harmonic generation. The shape of the beam will also be changed from a square to a circle due to experimental requirements. In the final form, this system will be able to provide 8.5 J of pump light at 515 nm at 50 Hz repetition rate which will be divided into two 3 ns pulses.

The nanosecond high energy OPCPA will be done in 4 stages. The pump will be split into two branches by a beam splitter after SHG. The weaker double pulse (0.25 J per pulse) will pump 2 stages of OPCPA in BBO and stronger double pulse (4 J per pulse) will pump the remaining 2 stages in LBO as shown in Figure 67. The predicted output energy for this chain is 4.0 J. The target compressed pulse duration for driving the experiment is 25 fs. Assuming 70% loss through the compressor this should give a peak power on the output of 112 TW from the system.

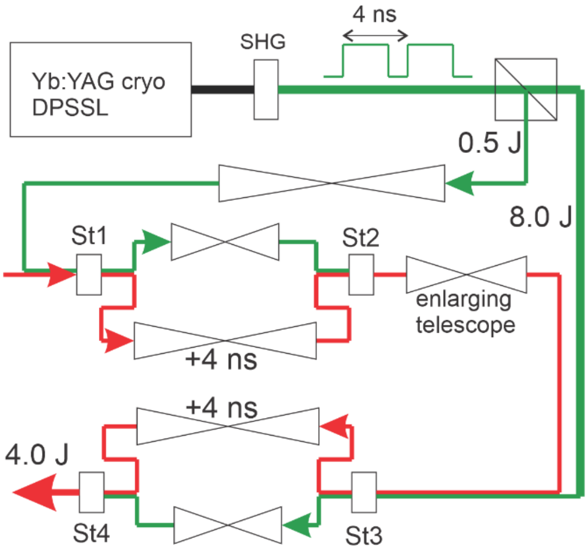

Figure 67: Conceptual scheme of the high energy OPCPA. The double pulses from the amplifier are separated by 4 ns, so the signal is delayed by 4 ns relative to the pump between each pair of crystals. Stage 1 and 2 share 0.5 J of pump energy in 2 pump pulses, while stages 3 and 4 share 8 J in 2 pump pulses. The pump and signal beams are imaged onto each crystal [79].

5.2 F-SYNC

The goal of the Femtosecond Synchronization project (F-SYNC) is to provide a synchronized auxiliary 1 kHz, 10 mJ femtosecond pulse train to the existing 1 kHz L1-Allegra laser [26]. This auxiliary laser system will serve as a high energy probe pulse for the main L1-Allegra output with arbitrary relative delay and femtosecond precision. This system will also serve as a high energy channel to investigate methods of high energy, ultra-fast coherent combination [82].

L1-Allegra is seeded by a broadband Ti:sapphire oscillator (80 MHz, central wavelength 810 nm) and its repetition rate is locked to a RF master clock. The F-SYNC laser is seeded by an 80 MHz, 1030 nm modelocked fiber laser which is synchronized to the same RF clock. Electronically locking the two oscillators referenced to the same clock provides optical synchronization on the level of 100 fs. Reducing the timing jitter further to the level of 10 fs will be assured by two balanced optical cross-correlators. A portion of the F-SYNC fiber oscillator output is cross-correlated with a portion of the output of the L1-Allegra Ti:sapphire oscillator. The generated error signal is then fed to fiber delay line 1 which compensates the timing jitter with a fast piezo element as shown in Figure 68. The second cross-correlator in the system corrects for jitter originating from the regenerative amplifier using delay line 2 down to 10 fs precision [83].

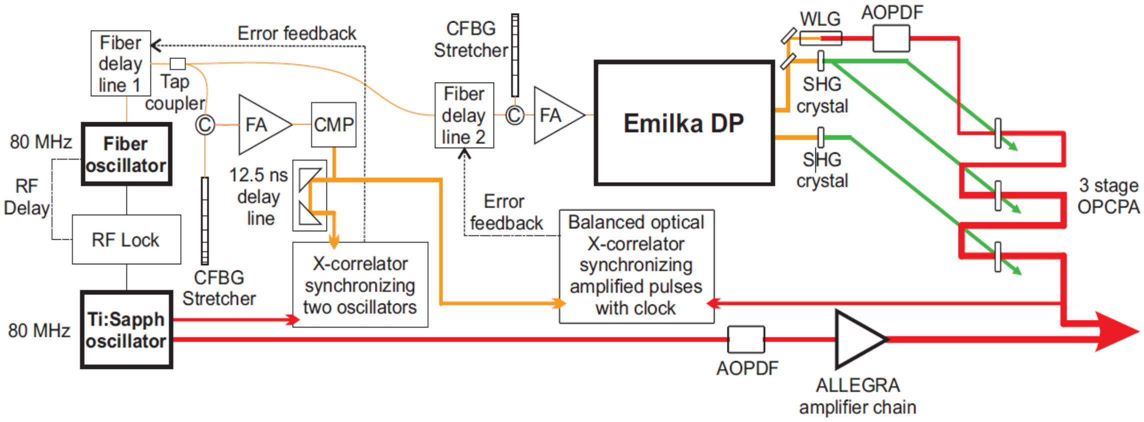

Figure 68: Schematics of F-SYNC synchronized with L1-Allegra: FA - fiber amplifier, CMP - compressor, C - circulator, CFBG - chirped fiber Bragg grating, AOPDF - acousto-optical dispersive filter (Dazzler), WLG - white light generation, SHG - second harmonic generation, OPCPA – optical parametric chirped pulse amplifier Emilka DP - 100 W regenerative amplifier for double pulses [83].

F-SYNC consists of a master oscillator, a seed distribution system completely in fiber, a pump laser with grating compressor, supercontinuum (SC) seed, and 3 stages of optical parametric chirped pulse amplification (OPCPA). The pump laser for the F-SYNC OPCPA chain is a diode-pumped Yb:YAG thin disk regenerative amplifier. This pump laser is in principle very similar to the regenerative amplifier described in section 2. A key different feature of this laser is that it amplifies two adjacent pulses from the 80MHz train separated by 12.5 ns originating in the fiber oscillator. At the output of the amplifier, 112 mJ is extracted and divided into two pulses. Afterwards, the amplified double pulses are spatially separated by a fast Pockels cell into two individual beams, each containing one pulse. After the spatial separation, these two parallel beams are compressed in one common compressor to a pulse length of a few picoseconds [84]. Figure 69 shows F-SYNC pump pulse generation system.

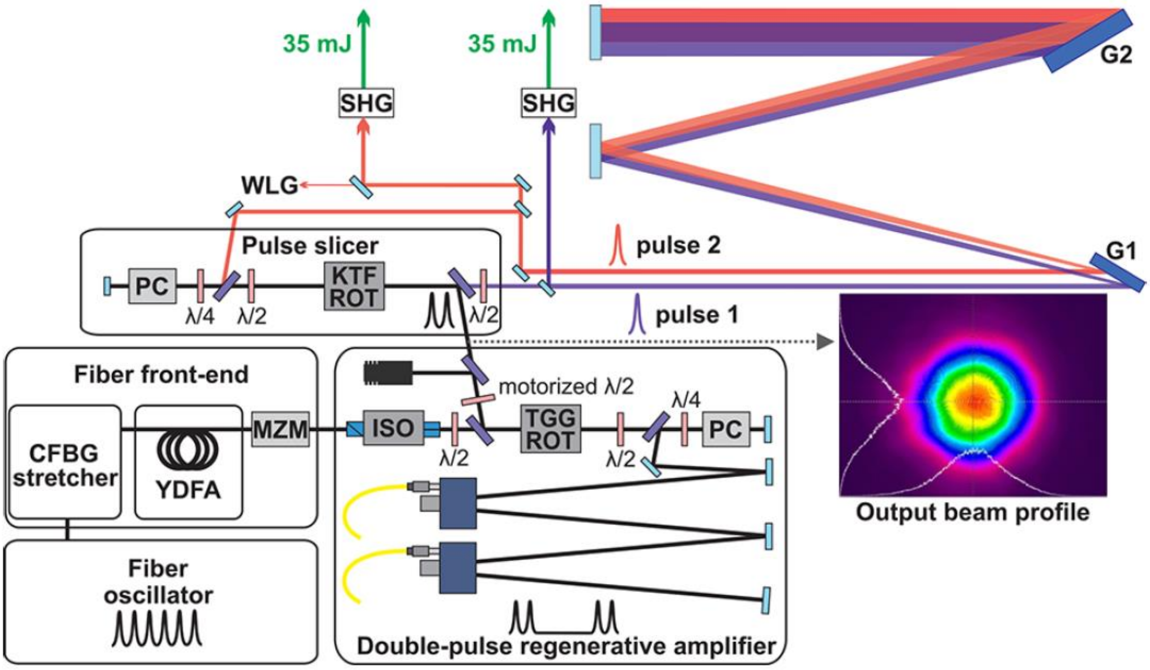

Figure 69: F-SYNC pump pulse generation. CFBG, chirped fiber Bragg grating; PC, Pockels cell; YDFA, Yb-doped fiber amplifier; MZM, Mach–Zehnder modulator; ISO, isolator; ROT, rotator; SHG, second-harmonic generation; WLG, white light generation [84].

A small leakage of pulse 2 is focused through a 13 cm long YAG rod generating a supercontinuum stretching from 550 to 950 nm where is cut by a short-pass filter. The experimental setup for supercontinuum generation is very similar to the setup described in section 3.13. The difference is that the YAG crystal is positioned behind the focal point of the lens, which leads to increased energy of the generated supercontinuum which is desired effect for better performance of the first OPCPA stage. The supercontinuum stability exceeds that of the driving laser and does not degrade even after extended period of use. The measured long term stability of the generated supercontinuua (0.35 % RMS) can be seen in

Figure 36. The generated broadband signal then passes through an acousto-optical dispersive filter (Dazzler) to adjust dispersion and is used as a seed for the three following OPCPA stages. Because the supercontinuum seed and OPCPA pump pulses are generated from the same laser there is no need for a pump/seed jitter stabilization system.

Both pump pulses are converted to the second harmonic in 2mm LBO crystals with a conversion efficiency reaching 80%. The first pump pulse is split and used to amplify the broadband signal in the first two stages. The second pump pulse is entirely used for pumping the third stage. All three stages utilize 2mm thick BBO crystals. Amplification in the OPCPA chain has been demonstrated in two distinct regimes which can be smoothly transitioned by a Dazzler settings. In the first case, 16 mJ pulse energy with a bandwidth supporting 20 fs pulse duration was achieved. In the second case, pulse energy is 8 mJ with a bandwidth supporting 11 fs pulse duration [83].

6 Conclusion

The OPCPA is currently frequently used technology for reaching high powers with laser pulses, these systems typically require separate laser source for seeding the OPCPA and another one for pumping. Synchronization of two separate laser sources with sufficient precision is a challenging task and it also increases the complexity of the system. This can be avoided by generating the seed for the OPCPA by a pump laser via supercontinuum generation. This method is already being used when supercontinuum is generated with femtosecond pulses, but is still considered to be a difficult task when generated with picosecond pulses. This thesis investigated the possibility to generate stable SC using picosecond pulses, so it can be used as a seed source for a high power OPCPA systems at ELI-Beamlines.

6.1 Summary of achieved results

To ensure a stable pump beam for supercontinuum generation as well as for further amplification, the regenerative amplifier was built and optimized. The seed for regenerative the amplifier is provided by a commercial fiber oscillator (Origami, NKT Photonics) at 80 Mhz. The seed is stretched by CFBG, amplified by a fiber amplifier and the repetition rate is reduced to 2 kHz with a pulse picker. The regenerative amplifier uses Yb:YAG as the active medium for amplification and can achieve 85 W (42,5 mJ) of power at the output. The pulses are afterwards compressed in a grating compressor to negatively chirped 3 ps long pulses. The energy, pointing and temporal stability of pump beam is ensured by implementation of cavity pointing stabilization, output beam pointing stabilization and CFBG temperature stabilization. After the grating compressor, we obtain 76 W (33.5 mJ) of output power with ≈ 1 % RMS long term pulse-to-pulse stability.

The main goal of this work was to generate the supercontinuum using the 3 ps long pump pulses with sufficient spectral and energy stability, so it can be used as a seed for OPCPA. While the experimental setup for supercontinuum generation is very simple it requires just focusing of the pump beam into the nonlinear medium it is still challenging to achieve the desired results. One of the main problems when generating the supercontinuum with picosecond pulses is a high chance of optical degradation, damage or permanent modification of the material. As a solution to this issue, we decided to generate the supercontinuum in loose focus setup inside long (13 cm) YAG crystal using the lens with long focal length.

The wide variety of the pump beam parameters, as well as different experimental setups were investigated in order to achieve the optimal supercontinuum generation. The supercontinuum is heavily dependent on size and shape of the pump beam and focal length of the focusing lens. Change in the length of pump pulses by introducing positive or negative chirp leads to increase of required pump energy but also increases energy of generated supercontinuum in the stable regime. The stable supercontinuum was generated in the region from 5 ps positively chirped pulse to 4.5 ps negatively chirped pulse with minimum length of 1.3 ps when compressed to Fourier limit. The stable supercontinuum can be generated with different positions of YAG crystal with respect to the lens focal point, even in the case of diverging pump beam. Changing the position of focal spot inside the crystal has only small effect on SC generation, allowing for continuous adjustment of the pulse length of generated supercontinuum.

When the parameters of the pump beam and experimental setup are chosen properly, the generated supercontinuum has pulse to pulse energy stability exceeding the stability of the pump pulse. Typical energy of the supercontinuum generated in the stable regime is 70 – 100 nJ with stable and continuous spectrum ranging from 515 nm to 950 nm [A2], [A3]. The generated supercontinuum is coherent and has a Gaussian beam profile. The infrared portion of the supercontinuum contains significantly more energy (≈ 0.7 µJ), spans from 1050 nm to 2500 nm, but measurements indicate that it is less stable.

The generated stable supercontinuum was amplified in two stages of OPCPA to demonstrate its possible usage as a seed for the high power OPCPA. The supercontinuum was amplified in two spectral regions, with 100 nm bandwidth centered at 750 nm and 180 nm bandwidth centered around 850 nm. Amplified SC was compressed close to its Fourier limit in both of these region using a prism compressor and Dazzler. The great energy stability of supercontinuum, together with compressibility and good temporal stability shows that the picosecond supercontinuum can be used as a seed for high power OPCPA [A1].

Based on these results, the supercontinuum have been deployed in two new high power OPCPA systems which are under development at ELI-Beamline to generate the seed for the OPCPA. Work on both systems started in 2019 as part of the ADONIS project. In both cases the regenerative amplifier providing picosecond pulses serves as a pump for SC and pump for a OPCPA which is seeded by SC, eliminating the need for any complicated active synchronization systems.

Authors primary involvement is in the development of the broadband front end for L2 laser system (DUHA). One of the frond end outputs will be seeding high energy nanosecond OPCPA of L2 laser. The initial seed is generated by the supercontinuum generation, which is amplified in two OPCPA stages and afterwards stretched by grating stretcher. The second branch of the front end will be providing 5 mJ, 30 fs auxiliary output at 2300 nm. This branch starts with supercontinuum generation as well, which is then amplified in single OPCPA stage. The mid IR beam is generated by combining an amplified supercontinuum with 1030 nm beam in DFG crystal. This beam will be amplified in 3 OPCPA stages and compressed in bulk. In the F-SYNC project, author was responsible for generation of stable supercontinuum, which is currently being used as seed for OPCPA, which will provide auxiliary beam to L1 Allegra laser.

6.2 Contribution to knowledge and practice

The generation of stable supercontinuum with picosecond pulses provides the picosecond OPCPA system with a simplified alternative to seeding with separate sources of broadband light. To our knowledge, we were the first to generate the stable picosecond supercontinuum with a long YAG crystal and published these results in 2017. Afterwards the generation of stable broadband supercontinuum with picosecond pulses used for seeding OPCPA, was reported by multiple research groups, confirming our research results [85], [86], [87], [88], [89].

The main practical impact of achieved results with picosecond supercontinuum generation was implementation of this technology into two new laser systems at ELI-Beamlines: F-SYNC and L2 laser DUHA. While both systems are still under development, the F-SYNC laser has already incorporated permanent supercontinuum setup for OPCPA seeding and L2 DUHA front end successfully demonstrated supercontinuum amplification in both near IR and MID IR branches.

References

1. **M. Balu, J. Hales, D.J. Hagan, and E.W. Van.** White-light continuum Z-scan technique for nonlinear materials characterization. *Opt. Express 12, 3820–3826 (2004).*

2. **L. De Boni, A.A. Andrade, L. Misoguti, C. Mendonça, and S.C. Zilio.** Z-scan measurements using femtosecond continuum generation. *Opt. Express 12, 3921–3927 (2004).*

3. **Xu, H.L., Daigle, J.F., Luo, Q., Chin, S.L.** Femtosecond laser-induced nonlinear spectroscopy for remote sensing of methane. *Appl. Phys. B 82, 655–658.*

4. **O. Mouawad, P. Béjot, F. Billard, P. Mathey, B. Kibler, F. Désévédavy, G. Gadret, J.-C. Jules, O. Faucher, F. Smektala.** Filament-induced visible-to-mid-IR supercontinuum in a ZnSe crystal: Towards multi-octave supercontinuum absorption spectroscopy. *Optical Materials, Vol. 60, P. 355-358, (2016).*

5. **Udem, T., Reichert, J., Haensch, T. & Kourogi, M.** Accuracy of optical frequency comb generators and optical frequency interval divider chains. *Opt. Lett. 23, 1387–1389 (1998).*

6. **C. Calabrese, A.M. Stingel, L. Shen, and P.B. Petersen.** Ultrafast continuum mid-infrared spectroscopy: probing the entire vibrational spectrum in a single laser shot with femtosecond time resolution. *Opt. Lett. 37, 2265–2267 (2012).*

7. **U. Megerle, I. Pugliesi, C. Schriever, C.F. Sailer, and E. Riedle.** Sub-50 fs broadband absorption spectroscopy with tunable excitation: putting the analysis of ultrafast molecular dynamics on solid ground. *Appl. Phys. B 96, 215–231 (2009).*

8. **R.R. Alfano and L. Shapiro.** Emission in the region 4000 to 7000 A via four photon coupling in glass. *Phys. Rev. Lett. 24.* 1970, pp. 584-587.

9. **R. R. Alfano, S. L. Shapiro.** Observation of self-phase modulation and small-scale filaments in crystals and glasses. *Phys. Rev. Lett. 24.* 1970, pp. 592-594.

10. **Chinlon Lin, R. H. Stolen.** New nanosecond continuum for excited-state spectroscopy. *Appl. Phys. Lett. 28, 216 (1976).*

11. **Lin Chinlon, Nguyen V.T., French W.G.** Wideband near-i.r. continuum (0.7–2.1 μm) generated in low-loss optical fibres. *Electronics Letters. Institution of Engineering and Technology (IET). (1978), 14(25), 822-823.*

12. **R.L. Fork, C.V. Shank, C. Hirlimann, R. Yen, and W.J. Tomlinson.** Femtosecond white-light continuum pulses. *Opt. Lett. 8, 1–3 (1983).*

13. **Gross Barry, Manassah Jamal T.** Supercontinuum in the anomalous group-velocity dispersion region. *Journal of the Optical Society of America B. The Optical Society. 9 (10): 1813-1818. (1992).*

14. **A. Brodeur, S.L. Chin.** Ultrafast white-light continuum generation and self-focusing in trans-parent condensed media. *J. Opt. Soc. Am. B 16, 637–650 (1999).*

15. **A.K. Dharmadhikari, F.A. Rajgara, and D. Mathur.** Systematic study of highly efficient white-light generation in transparent materials using intense femtosecond pulses. *Appl. Phys. B 80, 61-66 (2005).*

16. **A. Saliminia, S.L. Chin, and R. Vallée.** Ultra-broad and coherent white light generation in sili-ca glass by focused femtosecond pulses at 1.5 μm. *Opt. Express 13, 5731–5738 (2005).*

17. **J. Darginavičius, D. Majus, V. Jukna, N. Garejev, G. Valiulis, A. Couairon, and A. Dubietis.** Ultra-broadband supercontinuum and third-harmonic generation in bulk solids with two optical-cycle carrier-envelope phase-stable pulses at 2 μm. *Opt. Express 21, 25210–25220 (2013).*

18. **I. Gražulevičiūtė, M. Skeivytė, E. Keblytė, J. Galinis, G. Tamošauskas, and A. Dubietis.** Supercontinuum generation in YAG and sapphire with picosecond laser pulses. *Lithuanian Journal of Physics, Vol. 55, No. 2, pp. 110–116 (2015).*

19. **Chihiro Nagura, Akira Suda, Hiroyuki Kawano, Minoru Obara, Katsumi Midorikawa.** Generation and characterization of ultrafast white-light continuum in condensed media. *Appl Opt. 2002 Jun 20;41(18):3735-42.*

20. **A. Marcinkevičiūtė, V. Jukna, R. Šuminas, N. Garejev, G. Tamošauskas, A. Dubietis.** Supercontinuum generation in the absence and in the presence of color centers in NaCl and KBr. *Results in Physics, Volume 14, September 2019, 102396.*

21. **F. Silva, D.R. Austin, A. Thai, M. Baudisch, M. Hemmer, D. Faccio, A. Couairon, J. Biegert.** Multi-octave supercontinuum generation from mid-infrared filamentation in a bulk crystal. *Nature Communications volume 3, (2012).*

22. **N. Garejev, G. Tamošauskas, A. Dubietis.** Comparative study of multioctave supercontinuum generation in fused silica, YAG, and LiF in the range of anomalous group velocity dispersion. *J. Opt. Soc. Am. B 34, 88–94 (2017).*

23. **R.R. Alfano.** *The Supercontinuum Laser Source.* s.l. : Springer, 2006.

24. **Audrius Dubietis, G. Tamošauskas, R. Šuminas, Vytautas Jukna, Arnaud Couairon.** Ultrafast supercontinuum generation in bulk condensed media. *Lithuanian Journal of Physics.* 2017, 57, pp. 113-157.

25. **Hanieh Fattahi, Haochuan Wang, Ayman Alismail, Gunnar Arisholm, Vladimir Pervak, Abdallah M. Azzeer, and Ferenc Krausz.** Near-PHz-bandwidth, phase-stable continua generated from a Yb:YAG thin-disk amplifier. *Optics Express.* 2016, 24.

26. **P. Bakule, R. Antipenkov, J. Novák, and et al.** Readiness of L1 allegra laser system for user operation at eli beamlines. *in OSA High-brightness Sources and Light-driven Interactions Congress 2020, (2020), p. HF1B.7.*

27. **František Batysta, Roman Antipenkov, Jonathan T Green, Jack A Naylon, Jakub Novák, Tomáš Mazanec, Petr Hříbek, Charalampos Zervos, Pavel Bakule, Bedřich Rus.** Pulse synchronization system for picosecond pulse-pumped OPCPA with femtosecond-level relative timing jitter. *Optics express, 2014, 22 (24), 30281-30286.*

28. **J. Ahrens, O. Prochnow, T. Binhammer, T. Lang, B. Schulz, M. Frede, and U. Morgner.** Multipass OPCPA system at 100 kHz pumped by a CPA-free solid-state amplifier. *Optics Express Vol. 24, Issue 8, pp. 8074-8080 (2016).*

29. **Batysta František, Antipenkov Roman, Novák Jakub, Gree, Jonathan T, Naylon Jack A, Horáček Jakub, Horáček Martin, Hubka, Zbyněk, Boge Robert, Mazanec Tomáš, Himmel Bedrich, Bakule Pavel, Rus, Bedrich.** Broadband OPCPA system with 11 mJ output at 1 kHz, compressible to 12 fs. *Optics Express.* 2016, p. 17843.

30. **František Batysta, Roman Antipenkov, Jonathan T. Green, Jack A. Naylon, Jakub Novák, Tomáš Mazanec, Petr Hříbek, Charalampos Zervos, Pavel Bakule, and Bedřich**

Rus. Pulse synchronization system for picosecond pulse-pumped OPCPA with femtosecond-level relative timing jitter. *Optics Express Vol. 22, Issue 24, pp. 30281-30286 (2014).*

31. **R. Riedel, A. Stephanides, M. J. Prandolini, B. Gronloh, B. Jungbluth, T. Mans, and F. Tavella.** Power scaling of supercontinuum seeded megahertz-repetition rate optical parametric chirped pulse amplifiers. *Optics Letters Vol. 39, Issue 6, pp. 1422-1424 (2014).*

32. **Jakub Novák, Jonathan T. Green, Thomas Metzger, Tomáš Mazanec, Bedřich Himmel, Martin Horáček, Zbyněk Hubka, Robert Boge, Roman Antipenkov, František Batysta, Jack A. Naylon, Pavel Bakule, and Bedřich Rus.** Thin disk amplifier-based 40 mJ, 1 kHz, picosecond laser at 515 nm. *Optics Express Vol. 24, Issue 6, pp. 5728-5733 (2016).*

33. **Zbyněk Hubka, Roman Antipenkov, Robert Boge, Emily Erdman, Michael Greco, Jonathan T. Green, Martin Horáček, Karel Majer, Tomáš Mazanec, Petr Mazůrek, Jack A. Naylon, Jakub Novák, Václav Šobr, Petr Strkula, Murat Torun, Boguslaw Tykalewicz, Pavel Bakule.** 120 mJ, 1 kHz, picosecond laser at 515 nm. *Optics Letters Vol. 46, Issue 22, pp. 5655-5658 (2021).*

34. **A. Couairona, A. Mysyrowiczb.** Femtosecond filamentation in transparent media. *PhysicsReports.* 2007, 441, pp. 47-190.

35. **Marburger, J. H.** Self-focusing: Theory. *Progress in Quantum Electronics.* April 1975, 4, pp. 35-110.

36. **Chiao, R.Y., Garmire, E., Townes, C.H.** Self-trapping of optical beams. *Phys. Rev. Lett.* 1964, 13, pp. 479-482.

37. **Fibich, G., Gaeta, A.L.** Critical power for self-focusing in bulk media and in hollow waveguides. *Opt. Lett.* 2000, 25, pp. 335-337.

38. **Polyanskiy, Mikhail.** *refractiveindex.info.* [Online] https://refractiveindex.info.

39. **Piotr Kabaciński, Tomasz M. Kardaś, Yuriy Stepanenko, and Czesław Radzewicz.** Nonlinear refractive index measurement by SPM-induced phase regression. *Opt. Express 27, 11018-11028.* 2019, 8.

40. **Dawes, E.L., Marburger, J.H.** Computer studies in self-focusing. *Phys. Rev.* 1969, 3, pp. 862-868.

41. **M. Sheik-Bahae, D. J. Hagan, and E. W. Van Stryland.** Dispersion and band-gap scaling of the electronic Kerr effect in solids associated with two-photon absorption. *Phys. Rev. Lett. 65, 96 – Published 2 July 1990.*

42. **Lim, Khan.** Laser Filamentation - Beyond Self-focusing and Plasma Defocusing. *Electronic Theses and Dissertations.* 2014.

43. **S. Tzortzakis, L. Sudrie, M. Franco, B. Prade, and A. Mysyrowicz.** Self-Guided Propagation of Ultrashort IR Laser Pulses in Fused Silica. *Physical Review Letters, Volume 87, Number 21, (2001).*

44. **Alexandr Špaček, Lukáš Indra, František Batysta, Petr Hříbek, Jonathan T. Green, Jakub Novák, Roman Antipenkov, Pavel Bakule, and Bedřich Rus.** Stability mechanism of picosecond supercontinuum in YAG. *Optics Express.* Vol. 28, Issue 14, pp. 20205-20214 (2020).

45. **Run Wang, Qingbin Zhang, Dan Li, Shengliang Xu, Pengkun Cao, Yueming Zhou, Wei Cao, Peixiang Lu.** Identification of tunneling and multiphoton ionization in intermediate Keldysh parameter regime. *Opt. Express.* 2019 Mar 4;27(5):6471-6482.

46. **M. Kolesik, G. Katona, J.V. Moloney, E.M. Wright.** Theory and simulation of supercontinuum generation in transparent bulk media. *Appl. Phys. B.* 77, 185–195 (2003).

47. **Keldysh, L. V.** Ionization in the field of a strong electromagnetic wave. *J. Exptl. Theoret. Phys.* (U.S.S.R.) 47, 1945-1957 (November, 1964).

48. **M. D. Feit, J. A. Fleck.** *Effect of refraction on spot-size dependence of laser-induced breakdown.* Appl. Phys. Lett. 24, 169 (1974).

49. **Yablonovitch, Eli.** *Self-phase modulation and short-pulse generation from laser-breakdown plasmas.* Physical rewiev A, volume 10, number 6 (1974).

50. **Koprinkov, I.G.** *Ionization variation of the group velocity dispersion by high-intensity optical pulses.* Applied Physics B volume 79, pages 359–361 (2004).

51. **M. Kolesik, G. Katona, J.V. Moloney.** Physical factors limiting the spectral extent and band gap dependence of supercontinuum generation. *Phys. Rev. Lett. 91, 043905.*

52. **S. Skupin, L. Bergé.** Self-guiding of femtosecond light pulses in condensed media: Plasma generation versus chromatic dispersion. *Physica D 220, 14–30 (2006).*

53. **Joshua E. Rothenberg.** Pulse splitting during self-focusing in normally dispersive media. *Opt. Lett.* 17(8), 583–585 (1992).

54. **Jinendra K. Ranka, Robert W. Schirmer, and Alexander L. Gaeta.** Observation of Pulse Splitting in Nonlinear Dispersive Media. *Physical Review Letters.* Vol. 77, N. 18, 28 October 1996.

55. **Luc Bergé, Jens Juul Rasmussen, Evgenii A. Kuznetsov, Elena G. Shapiro, and Sergei K. Turitsyn.** Self-focusing of chirped optical pulses in media with normal dispersion. *Journal of the Optical Society of America B.* Vol. 13, Issue 9, pp. 1879-1891 (1996).

56. **Silberberg, Yaron.** Collapse of optical pulses. *Optics Letters Vol. 15, Issue 22, pp. 1282-1284 (1990).*

57. **I Gražulevičiūtė, N Garejev, D Majus, V Jukna, G Tamošauskas and A Dubietis.** Filamentation and light bullet formation dynamics in solid-state dielectric media with weak, moderate and strong anomalous group velocity dispersion. *Journal of Optics, 18 (2016) 025502 (7pp).*

58. **J. R. de Oliveira, Marco A. de Moura, J. Miguel Hickmann, and A. S. L. Gomes.** Self-steepening of optical pulses in dispersive media. *Opt. Soc. Am. B.* 11 November 1992, 9.

59. **F. DeMartini, C. H. Townes, T. K. Gustafson, P. L. Kelley.** Self-Steepening of Light Pulses. *Physical review, Vol. 164, No. 2, (1967).*

60. **Ranka, J.K., Gaeta, A.L.** Breakdown of the slowly varying envelope approximation in the self-focusing of ultrashort pulses. *Opt. Lett.* 1998, 23, pp. 534-536.

61. **Joshua E. Rothenberg.** Space-time focusing: breakdown of the slowly varying envelope approximation in the self-focusing of femtosecond pulses. *Optics Letters, Vol. 17, No. 19, October 1, 1992.*

62. **Julijanas Želudevičius, Rokas Danilevičius, and Kęstutis Regelskis.** Optimization of pulse compression in a fiber chirped pulse amplification system by adjusting dispersion parameters of a temperature-tuned chirped fiber Bragg grating stretcher. *J. Opt. Soc. Am. B 32, 812-817 (2015).*

63. **Jonathan T. Green, Jack A. Naylon, Lukaš Indra, František Batysta, Martin Horáček, Boguslaw Tykalewicz, Roman Antipenkov, Jakub Novák, Zbyněk Hubka, Robert Boge, Pavel Bakule, Bedřich Rus.** Fiber-based front ends for extreme light applications. *Proc. SPIE 10683, Fiber Lasers and Glass Photonics: Materials through Applications, 1068312 (17 May 2018).*

64. **J. Novák, J. T. Green, T. Metzger, T. Mazanec, B. Himmel, M. Horácek, Z. Hubka, R. Boge,.** Thin disk amplifier-based 40 mJ, 1kHz, picosecond laser at 515 nm. *Opt. Express.* vol. 24, pp. 5728–5733, Mar 2016.

65. **Robert Boge, Jakub Horáček, Petr Mazůrek, Jack Alexander Naylon, Jonathan T. Green, Zbyněk Hubka, Václav Šobr, Jakub Novák, František Batysta, Roman Antipenkov, Pavel Bakule, and Bedřich Rus.** Robust method for long-term energy and pointing stabilization of high energy, high average power solid state lasers. *Review of Scientific Instruments 89, 023113 (2018); https://doi.org/10.1063/1.5018713.*

66. **Lukáš Indra, František Batysta, Petr Hříbek, Jakub Novák, Zbyněk Hubka, Jonathan T. Green, Roman Antipenkov, Robert Boge, Jack A. Naylon, Pavel Bakule, and Bedřich Rus.** Picosecond pulse generated supercontinuum as a stable seed for OPCPA. *Optics Letters Vol. 42, Issue 4, pp. 843-846 (2017).*

67. **Crenn, P. Belland and J. P.** Changes in the characteristics of a Gaussian beam weakly diffracted by a circular aperture. *Applied Optics.* Vol. 21, Issue 3, pp. 522-527 (1982).

68. **DeShazer, J. P. Campbell and L. G.** Near Fields of Truncated-Gaussian Apertures. *Journal of the Optical Society of America.* Vol. 59, Issue 11, pp. 1427-1429 (1969).

69. **Rose, H. T. Yura and T. S.** Gaussian beam transfer through hard-aperture optics. *Applied Optics.* Vol. 34, Issue 30, pp. 6826-6828 (1995).

70. **Alfano, R.R.** The Supercontinuum Laser Source. New York : Springer, 2006, pp. 524–527, https://doi.org/10.1007/0-387-25097-2_21.

71. **John M. Dudley, Stéphane Coen.** Coherence properties of supercontinuum spectra generated in photonic crystal and tapered optical fibers. *Optics Letters.* Vol. 27, Issue 13, pp. 1180-1182 (2002).

72. **Chunlei Huang, Meisong Liao, Wanjun Bi, Xia Li, Lili Hu, Long Zhang, Longfei Wang, Guanshi Qin, Tianfeng Xue, Danping Chen, and Weiqing Gao.** Ultraflat, broadband, and highly coherent supercontinuum generation in all-solid microstructured optical fibers with all-normal dispersion. *Photonics Research.* Vol. 6, Issue 6, pp. 601-608 (2018).

73. **Iosif Zeylikovich, Vladimir Kartazaev, and R. R. Alfano.** Spectral, temporal, and coherence properties of supercontinuum generation in microstructure fiber. *Journal of the Optical Society of America B.* Vol. 22, Issue 7, pp. 1453-1460 (2005).

74. **I. Zeylikovich, R.R. Alfano.** Coherence properties of the supercontinuum source. *Appl. Phys. B 77, 265–268 (2003).*

75. **B. J. Thompson, E. Wolf.** Two-Beam Interference with Partially Coherent Light. *Journal of the Optical Society of America.* Vol. 47, Issue 10, pp. 895-902 (1957).

76. **M. E. Innocenzi, R. T. Swimm, M. Bass, et al.** Optical absorption in undoped yttrium. *Journal of Applied Physics.* 68, 1200 (1990).

77. **Paschotta, Rudiger.** Encyclopedia of Laser Physics and Technology. *https://www.rp-photonics.com/b_integral.html.* [Online] 2022.

78. **S. V. Chekalin, V. P. Kandidov.** From self-focusing light beams to femtosecond laser pulse filamentation. *Physics - Uspekhi 56 (2) 123 - 140 (2013).*

79. **Jonathan T. Green, Roman Antipenkov, Pavel Bakule, Jan Bartoníček, Jan Eisenschreiber, Martin Finrich, Michael Greco, Lukáš Indra, Daniel Kramer, Jack A. Naylon, Jakub Novák, Alexandr Špaček, Bedřich Rus.** L2-DUHA 100 TW high repetition rate laser system at ELI-Beamlines: Key design considerations. *Reza Kenkyu, 49(2), 106-109.*

80. **Saumyabrata Banerjee, Klaus Ertel, Paul D. Mason, P. Jonathan Phillips, Mariastefania De Vido, Jodie M. Smith, Thomas J. Butcher, Cristina Hernandez-Gomez, R. Justin S. Greenhalgh, and John L. Collier.** DiPOLE: a 10 J, 10 Hz cryogenic

gas cooled multi-slab nanosecond Yb:YAG laser. *Optics Express Vol. 23, Issue 15, pp. 19542-19551 (2015).*

81. **Paul Mason, Martin Divoký, Klaus Ertel, Jan Pilař, Thomas Butcher, Martin Hanuš, Saumyabrata Banerjee, Jonathan Phillips, Jodie Smith, Mariastefania De Vido, Antonio Lucianetti, Cristina Hernandez-Gomez, Chris Edwards, Tomas Mocek, and John Collier.** Kilowatt average power 100 J-level diode pumped solid state laser. *Optica Vol. 4, Issue 4, pp. 438-439 (2017).*

82. **E. C. Erdman, J. Novák, R. Antipenkov, M. Horáček, L. Indra, B. Tykalewicz, M. Torun, P. Mazůrek, J. A. Naylon, P. Bakule, B. Rus.** 100 W Dual-Output Thin Disk Laser for Picosecond OPCPA Pumping. *in Conference on Lasers and Electro-Optics, Technical Digest Series (Optica Publishing Group, 2022), paper STu4N.2.*

83. **J. Novák, E. Erdman, R. Antipenkov, L. Indra, J. T. Green, B. Tykalewicz, P. Mazůrek, M. Torun, J. A. Naylon, P. Bakule, B. Rus,.** F-SYNC: a 1 kHz high energy OPCPA auxiliary beam synchronizable with fs precision and arbitrary delay to the L1-Allegra laser. *in Conference on Lasers and Electro-Optics, Technical Digest Series (Optica Publishing Group, 2022), paper SF4E.2.*

84. **Jakub Novák, Emily C. Erdman, Roman Antipenkov, Boguslaw Tykalewicz, Martin Horáček, Petr Mazůrek, Murat Torun, Jonathan T. Green, Jack A. Naylon, Pavel Bakule, Bedřich Rus.** Dual-output kilohertz pump laser for high-energy picosecond OPCPA. *Opt. Lett. 47, 4869-4872 (2022).*

85. **Tsuneto Kanai, Yeon Lee, Meenkyo Seo, and Dong Eon Kim.** Supercontinuum-seeded, carrier-envelope phase-stable, 4.5-W, 3.8-μm, 6-cycle, KTA optical parametric amplifier driven by a 1.4-ps Yb:YAG thin-disk amplifier for nonperturbative spectroscopy in solids. *Journal of the Optical Society of America B Vol. 36, Issue 9, pp. 2407-2413 (2019).*

86. **Nicolas Thiré, Raman Maksimenka, Bálint Kiss, Clément Ferchaud, Grégory Gitzinger, Thomas Pinoteau, Hervé Jousselin, Sebastian Jarosch, Pierre Bizouard, Vittorio Di Pietro, Eric Cormier, Károly Osvay, and Nicolas Forget.** Highly stable, 15 W, few-cycle, 65 mrad CEP-noise mid-IR OPCPA for statistical physics. *Optics Express Vol. 26, Issue 21, pp. 26907-26915 (2018).*

87. **Paulius Mackonis, Aleksej M. Rodin.** Laser with 1.2 ps, 20 mJ pulses at 100 Hz based on CPA with a low doping level Yb:YAG rods for seeding and pumping of OPCPA. *Optics Express Vol. 28, Issue 2, pp. 1261-1268 (2020).*

88. **Paulius Mackonis, Aleksej M. Rodin,.** OPCPA investigation with control over the temporal shape of 1.2 ps pump pulses. *Optics Express Vol. 28, Issue 8, pp. 12020-12027 (2020).*

89. **Siqi Cheng, Gourab Chatterjee, Friedjof Tellkamp, Axel Ruehl, and R. J. Dwayne Miller.** Multi-octave supercontinuum generation in YAG pumped by mid-infrared, multi-picosecond pulses. *Optics Letters Vol. 43, Issue 18, pp. 4329-4332 (2018).*

Related publications and conference proceedings

[A1] **Lukáš Indra**, František Batysta, Petr Hříbek, Jakub Novák, Zbyněk Hubka, Jonathan T. Green, Roman Antipenkov, Robert Boge, Jack A. Naylon, Pavel Bakule, and Bedřich Rus. Picosecond pulse generated supercontinuum as a stable seed for OPCPA, Opt. Lett. **42**, 843 (2017).

[A2] **Lukáš Indra**, František Batysta, Petr Hříbek, Jakub Novák, Jonathan T. Green, Roman Antipenkov, Jack A. Naylon, Pavel Bakule, and Bedřich Rus. Stable supercontinuum generation in YAG with picosecond pulses, OSA Technical Digest (online) (Optica Publishing Group, 2017), paper JTh2A.87

[A3] **Lukáš Indra**, František Batysta, Petr Hříbek, Jakub Novák, Jonathan T. Green, Roman Antipenkov, Jack A. Naylon, Pavel Bakule, and Bedřich Rus, Properties of Picosecond Supercontinuum Generated in Long Bulk YAG, OSA Technical Digest (Optica Publishing Group, 2019), paper JTu3A.19

[A4] Jonathan T. Green, Roman Antipenkov, Pavel Bakule, Jan Bartoníček, Jan Eisenschreiber, Martin Finrich, Michael Greco, **Lukáš Indra**, Daniel Kramer, Jack A. Naylon, Jakub Novák, Alexandr Špaček, Bedřich Rus. L2-DUHA 100 TW high repetition rate laser system at ELI-Beamlines: Key design considerations**,** Reza Kenkyu, 49(2), 106-109.

[A5] Alexandr Špaček, **Lukáš Indra**, František Batysta, Petr Hříbek, Jonathan T. Green, Jakub Novák, Roman Antipenkov, Pavel Bakule, and Bedřich Rus, Stability mechanism of picosecond supercontinuum in YAG, *Optics Express Vol. 28, Issue 14, pp. 20205-20214 (2020)*

[A6] Alexandr Špaček, Jonathan T. Green, **Lukáš Indra**, Wojciech Szuba, František Batysta, Jakub Novák, Petr Hříbek, Pavel Bakule, Bedřich Rus, Stable Mid-IR Generation by ps-supercontinuum in YAG, *OSA High-brightness Sources and Light-driven Interactions Congress 2020*

[A7] J. Novák, E. Erdman, R. Antipenkov, **L. Indra**, J. T. Green, B. Tykalewicz, P. Mazůrek, M. Torun, J. A. Naylon, P. Bakule, and B. Rus, F-SYNC: a 1 kHz high energy OPCPA auxiliary beam synchronizable with fs precision and arbitrary delay to the L1-Allegra laser, in *Conference on Lasers and Electro-Optics*, Technical Digest Series (Optica Publishing Group, (2022), paper SF4E.2.

Other publications and conference proceedings

[A8] Martin Horáček, **Lukáš Indra**, Jonathan T Green, Jack A Naylon, Boguslaw Tykalewicz, Jakub Novák, František Batysta, Tomáš Mazanec, Jakub Horáček, Roman Antipenkov, Zbyněk Hubka, Robert Boge, Pavel Bakule, Bedřich Rus, Multi-channel, fiber-based seed pulse distribution system for femtosecond-level synchronized chirped pulse amplifiers Rev. Sci. Instrum. 2017 88, 013109 (2017)

[A9] P. Bakule, R. Antipenkov, J. T. Green, J. Novák, F. Batysta, B. Rus, R. Boge, Hubka, Z., J. A. Naylon, M. Horáček, J. Horáček, P. Strkula, D. Snopek, **L. Indra**, and B. Tykalewicz, “Development of high energy, sub-15 fs OPCPA system operating at 1 kHz repetition rate for ELI-Beamlines facility,” *in Research Using Extreme Light: Entering New Frontiers with Petawatt-Class Lasers III*, International Society for Optics and Photonics, vol. 10241, SPIE, 2017, pp. 21–29.

[A10] Roman Antipenkov, František Batysta, Robert Boge, Emily Erdman, Michael Greco, Jonathan T. Green, Zbyněk Hubka, **Lukáš Indra**, Karel Majer, Tomáš Mazanec, Petr Mazůrek, Jack Naylon, Jakub Novák, Václav Šobr, Alexandr Špaček, Murat Torun, Boguslaw Tykalewicz, Pavel Bakule, and Bedřich Rus, The Current Commissioning Results of the Allegra Kilohertz High-Energy Laser System at ELI-Beamlines, *OSA Technical Digest* (Optica Publishing Group, 2019), paper ATh1A.6

[A11] Hubka, Z., R. Boge, F. Batysta, R. Antipenkov, J. Novak, M. Greco, E. Erdman, A. Spacek, **L. Indra**, K. Majer, J. T. Green, J. A. Naylon, P. Bakule, and B. Rus, “High energy, high average power, nonlinear frequency conversion and parametric amplification of picosecond pulses in vacuum,” *in Nonlinear Optics (NLO), Optical Society of America*, 2019, NTh2B.7.

[A12] Pavel Bakule, Roman Antipenkov, Jakub Novák, František Batysta, Robert Boge, Jonathan Tyler Green, Zbyněk Hubka, Michael Greco, **Lukáš Indra**, Alexandr Špaček, Jack Alexander Naylon, Karel Majer, Petr Mazůrek, Emily Erdman, Václav Šobr, Boguslaw Tykalewicz, Tomáš Mazanec, Petr Strkula, and Bedřich Rus, Readiness of L1 ALLEGRA Laser System for User Operation at ELI Beamlines**,** in *OSA High-brightness Sources and Light-driven Interactions Congress* 2020, (2020), p. HF1B.7.

[A13] Roman Antipenkov, Robert Boge, Emily Erdman, Michael Greco, Jonathan T. Green, Annika Grenfell, Martin Horáček, Zbyněk Hubka, **Lukáš Indra**, Karel Majer, Tomáš Mazanec, Petr Mazůrek, Jack Naylon, Jakub Novák, Václav Šobr, Alexandr Špaček, Petr Strkula, Wojciech Szuba, Boguslaw Tykalewicz, Pavel Bakule, and Bedřich Rus "TW-class Allegra Laser System at ELI-Beamlines", Proc. SPIE 11777, *High Power Lasers and Applications*, 117770E (18 April 2021);

[A14] Roman Antipenkov, R. Boge, E. Erdman, M. Greco, J. T. Green, A. Grenfell, M. Horáček, Z. Hubka, **L. Indra**, K. Majer, T. Mazanec, P. Mazůrek, J. Naylon, J. Novák, V. Šobr, A. Špaček, P. Strkula, W. Szuba, B. Tykalewicz, P. Bakule, and B. Rus, TW-class Allegra Laser System at ELI-Beamlines, SPIE Optics + Optoelectronics, paper 11777-7 (2021)

[A15] Roman Antipenkov, Emily Erdman, Jakub Novák, Robert Boge, Zbyněk Hubka, Jonathan Tyler Green, Alexander Špaček, **Lukáš Indra**, Wojciech Szuba, Annika Grenfell, Boguslaw Tykalewicz, Václav Šobr, Murat Torun, Petr Mazůrek, Jack Naylon, Pavel Bakule and Bedřich Rus, upgrades of L1 - Allegra laser at ELI-Beamlines facility for the extended user experiment capabilities, Laser congress, 11-15 Dec (2022), ASSL AW2A.4

[A16] E. C. Erdman, J. Novák, R. Antipenkov, M. Horáček, **L. Indra**, B. Tykalewicz, M. Torun, P. Mazůrek, J. A. Naylon, P. Bakule, and B. Rus. 100 W Dual-Output Thin Disk Laser for Picosecond OPCPA Pumping, *in Conference on Lasers and Electro-Optics, Technical Digest Series* (Optica Publishing Group, 2022), paper STu4N.2.

List of Figures